RELIABILITY OF PERINEAL COMPLEX STIFFNESS ASSESSED USING ULTRASOUND SHEAR WAVE ELASTOGRAPHY

Talita Martins

Thesis submitted to the University of Ottawa in partial fulfillment of the requirements for the degree of Master of Science in Human Kinetics

School of Human Kinetics
Faculty of Health Sciences
University of Ottawa

© Talita Martins, Ottawa, Canada, 2026

ABSTRACT

The perineal complex (PC) transmits loads across the pelvic floor, stabilizing pelvic organs. Its mechanical properties may inform pelvic floor disorders yet remain unquantified in vivo. This study aimed to determine the analysis-stage intra- and inter-rater reliability of ultrasound-derived shear wave velocity (SWV) across three postures (supine, standing, deep squat) and two imaging planes (sagittal, subdivided into superficial and deep zones; and transverse) in 27 nulliparous females. SWV was extracted offline. Intra-rater reliability was excellent across all postures and images (ICC 0.968–0.995). Inter-rater reliability was excellent in the superficial zone and transverse plane (ICC 0.951–0.989) and good in the deep zone (ICC 0.864–0.882). Deep-zone signal dropout reduced usable trials in standing. Posture modulated stiffness, with deep squat increasing SWV and optimizing deep-zone image quality. Offline SWV analysis of the PC is highly reproducible and potentially sensitive to posture-related differences, though deep-zone acoustic attenuation remains a primary feasibility constraint.

Keywords: perineal complex, perineal body, ultrasound imaging, shear wave elastography, stiffness.

RÉSUMÉ

Le complexe périnéal (CP) transmet les charges à travers le plancher pelvien, stabilisant les organes pelviens. Ses propriétés mécaniques pourraient éclairer les troubles du plancher pelvien, mais demeurent non quantifiées in vivo. Cette étude visait à déterminer la fiabilité intra- et inter-évaluateurs, à l'étape de l'analyse, de la vitesse de l'onde de cisaillement (SWV) obtenue par échographie dans trois postures (décubitus dorsal, station debout, squat profond) et deux plans d'imagerie (sagittal, subdivisé en zones superficielle et profonde; et transverse) chez 27 nullipares. La SWV a été extraite hors ligne. La fiabilité intra-évaluateur était excellente pour toutes les postures et images (ICC 0,968–0,995). La fiabilité inter-évaluateurs était excellente dans la zone superficielle et le plan transverse (ICC 0,951–0,989) et bonne dans la zone profonde (ICC 0,864–0,882). Les pertes de signal dans la zone profonde ont réduit le nombre d'essais utilisables en position debout. La posture modulait la rigidité, le squat profond augmentant la SWV et améliorant la qualité d'image de la zone profonde. L'analyse hors ligne de la SWV du CP est hautement reproductible et potentiellement sensible aux différences liées à la posture, bien que l'atténuation acoustique dans la zone profonde demeure une contrainte majeure de faisabilité.

Mots-clés: complexe périnéal, corps périnéal, imagerie ultrasonore, élastographie par ondes de cisaillement, rigidité.

PREFACE

This thesis is submitted in partial fulfillment of the requirements for the Master of Science in Human Kinetics at the University of Ottawa. The research was approved by the University of Ottawa Research Ethics Board (REB File No. H-05-25-11515).

As the principal investigator, I was responsible for the study design, the development of the imaging and analysis protocol, participant recruitment, data collection, data processing, and preparation of the manuscript. Scientific supervision, methodological guidance, and critical revision of the work were provided by my primary supervisor, Dr. Linda McLean, and by Dr. Sabine Vesting, co-supervisor, both of whom shaped the conceptual foundation of the study and offered expert counsel at every stage of the research.

Several colleagues contributed to specific components of the project. Dr. Caroline Baldini, postdoctoral fellow, assisted in refining the imaging protocol and supported data collection. The protocol itself imposed unusual demands. Because reliable image acquisition required the assessor to hold the transducer with minimal perturbation, at times, while seated on the floor, a second operator was indispensable. Undergraduate student volunteers Tanushir Chahal, Raya Akhavan, Juliana Paul, Leticia Falconni and Salma Faouzi prepared the assessment room, manually operated the ultrasound system during acquisition, and helped position and reassure participants throughout each session, support without which the data collection could not have been completed. Tanushir Chahal additionally served as Rater B in the reliability analysis.

The offline post-processing of the shear wave elastography images relied on custom MATLAB code developed by Layla Mitri, lead engineer, and Lina Bashir, an engineering student, in the Motor Function Measurement Laboratory. Their work was instrumental in streamlining the analysis. No other collaborators participated in data collection, analysis, or interpretation. All work presented in this thesis was carried out during my enrollment in the MSc program in Human Kinetics at the University of Ottawa. An article based on this thesis is in preparation for submission to a peer-reviewed journal in the field of pelvic floor biomechanics and ultrasound imaging.

ACKNOWLEDGEMENTS

This was a demanding road, especially as an international student, and I could not have reached its end on determination alone. What carried me through the longest stretches were the people who refused to let me walk them by myself. To my mother, my sister, my father, and my best friends back in Brazil: distance never loosened your hold on me. From across an ocean, you found countless ways to be present, steadying me when I had little left to give. To the friends who became my family in this country, you turned an unfamiliar place into somewhere I belonged. You made the solitude bearable and, more often, made it disappear altogether. And to the remarkable group of women I have had the privilege of working alongside: my supervisor, my co-supervisor, and every one of my lab-mates from the Motor Function Measurement Lab. You built a space defined by sisterhood and trust, a place where I felt safe, welcomed, loved and never less than supported.

TABLE OF CONTENTS

ABSTRACT ii

RÉSUMÉ iii

PREFACE iv

ACKNOWLEDGEMENTS v

TABLE OF CONTENTS vi

LIST OF FIGURES ix

LIST OF TABLES xii

LIST OF ABBREVIATIONS xiii

1. Chapter 1 – General Introduction 1

1.1. Purpose of the study 3

1.1.1. Research Question 3

1.1.2. Overall Aim 3

1.1.2.1. Specific objectives 3

2. Chapter 2 – Literature Review 4

2.1. Anatomy of the Perineal Complex 4

2.1.1. Definition, Morphology, and Tissue Composition 4

2.1.2. Layered Architecture and Muscle Connectivity 5

2.2. Biomechanical Function of the Perineal Complex 7

2.2.1. Structural Support, Force Transmission, and Pelvic Floor Stability and Coordination 7

2.2.2. Tissue Mechanical Properties 8

2.2.3. Contributions of the PC Beyond Pelvic Organ Support 10

2.3. Perineal Complex Alterations and Pelvic Floor Disorders 10

2.4. Clinical Assessment of the Perineal Complex 13

2.5. Imaging Modalities for Assessing the Perineal Complex 14

2.5.1. Magnetic Resonance Imaging (MRI) 14

2.5.2. Ultrasound imaging..... 15
2.5.3. SWE Physical Principles 16
2.5.4. Why SWE is promising 18
2.5.5. SWE at the Perineal Complex 19
2.6. Gaps in Current Assessment Methods and the Need for the Current Study 21
3. Chapter 3 – Methods..... 23
3.1. Study Design and Participants..... 23
3.2. Instruments/Materials 23
3.3. Image Acquisition..... 24
3.4. Image Analysis 28
3.4.1. Analytical rationale..... 29
3.4.2. Stage 0 — Pre-export elastogram calibration. 30
3.4.3. Stage 1 — Smoothing. 31
3.4.4. Stage 2 — ROI delineation and sequential quality-control gating. 32
3.4.5. Stage 3 — ROI-based SWV extraction. 33
3.4.6. Assessor Training, Independent Assessment, and Bias Mitigation 35
3.4.7. Intra-rater reliability..... 35
3.4.8. Inter-rater reliability..... 36
3.5. Outcome measures..... 36
3.6. Data Analysis..... 36
4. Chapter 4 – Results..... 39
4.1. Reliability of Shear Wave Velocity..... 41
4.2. Reliability of Region-of-Interest Geometry 43
4.3. Trial attrition and deep-zone ROI traceability..... 44
4.4. Comparison of Shear Wave Velocity Among Postures..... 45
5. Chapter 5 – General Discussion 47

5.1. Summary of findings 47

5.2. Reliability of Shear Wave Velocity Determined in the Perineal Complex 48

5.3. Signal Availability and the Reliability of the Shear Wave Velocity Estimate 49

5.4. Postural Modulation of Perineal Complex Stiffness 50

5.5. Strengths and Limitations 52

5.6. Implications and Future Directions 53

6. Conclusion 56

7. References 57

8. Appendix 70

8.1. Appendix A — REB Approval Letter 70

8.2. Appendix B — Participant Consent Form 72

8.3. Appendix C — Participant Questionnaire 79

8.4. Appendix D — Detailed Offline SWE Post-Processing Workflow ... 81

8.5. Appendix E — Supplementary Material 85

LIST OF FIGURES

Figure 1. Three-dimensional model of the female Perineal Complex (PC). (A) Transverse (Caudal) view showing the PC in relation to the bulbospongiosus, superficial transverse perineal (STP) muscles, perineal membrane, and external (EAS) and internal (IAS) anal sphincters. (B) Mid-sagittal view showing the PC (outlined in yellow) between the vaginal canal and the anal canal. (C) Sagittal view showing the pubovisceral components of the levator ani: pubovaginalis, puboperinealis, and puboanalis. Schematic model based on the anatomical descriptions of Larson et al. (2010) and Santoro et al. (2016) (Section 2.1.2). Model created by Lina Bashir (MFM Lab, University of Ottawa); reproduced with permission..... 5

Figure 2. Intravaginal spacer..... 25

Figure 3. Perineal complex (PC) imaged in the sagittal plane. **(A)** B-mode image of the PC. The yellow outline delineates the PC superficial zone (PC-SZ), and the blue outline represents its deep zone (PC-DZ). The vaginal canal, containing the intravaginal spacer (IVS), is outlined in pink, and the anal canal is outlined in green. Depth is indicated by the scale on the right (cm). **(B)** The same unannotated B-mode image. **(C)** Probe positioning over the perineum with a linear transducer in the sagittal plane, demonstrated on a model. 26

Figure 4. Perineal complex (PC) imaged in the transverse plane. **(A)** B-mode image showing the transverse view at the level of the anal sphincter complex. The extreme boundary of the external anal sphincter (EAS) is outlined in green, and the extreme boundary of the internal anal sphincter (IAS) is outlined in blue. The perineal complex (PC) lies superficial to the sphincter complex in this plane, largely corresponding to the superficial transverse perineal muscle. **(B)** The same unannotated B-mode image. **(C)** Probe positioning over the perineum with a linear transducer in the transverse plane, demonstrated on a model. 27

Figure 5. Shear wave elastography (SWE) of the perineal complex in the supine position with the rectangular elastogram field of view indicated. The regions of interest were drawn freehand as indicated in green. **(A)** The sagittal plane view, illustrating two ROIs within the superficial and deep zones of the elastogram field of view. **(B)** Transverse-plane view showing the ROI..... 27

Figure 6. SWE of the PC in sagittal and transverse plane views under three postures. 28

Figure 7. Data collection and image-analysis workflow by operator. Rater A acquired all clips and performed Stages 0–1 once. Quality-control gates were applied to Rater A's first-session ROIs (A1), and the resulting excluded-trial list was applied to Rater A's second session (A2; one week later) and to Rater B's session (B). Each session delineated its own ROIs, in randomized order and blinded to the other sessions. Intra-rater reliability: A1 vs. A2; inter-rater reliability: A1 vs. B. ICC, intraclass correlation coefficient; MDD95, minimal detectable difference (95%); QC, quality control; ROI, region of interest; SEM, standard error of measurement; SWV, shear wave velocity.... 29

Figure 8. Smoothing. (A) Frame selection; (B) Ensemble median and ensemble averaged colour maps. 32

Figure 9. ElastoGUI (MATLAB) interface during region of interest (ROI) delineation of the perineal complex on a sagittal supine trial. Showing the co-registered B-mode image (left) and the elastogram (right). A freehand ROI polygon traced within the elastogram box was replicated onto the B-mode image, and, per ROI, the median SWV (m/s), Void (%), and Saturated (%) are returned in the results panel (right). 35

Figure 10. Bland–Altman plots representing the inter-rater agreement for the median shear wave velocity (m/s) in (A) the deep zone of the perineal complex imaged in the sagittal plane with the participant in a deep squat (n = 22) (bias −0.060 m/s; 95% limits of agreement −1.376 to +1.255 m/s) and (B) the perineal complex imaged in the transverse plane with the participant in standing (n = 26) (bias +0.020 m/s; 95% limits of agreement −0.195 to +0.235 m/s). Both panels share the same vertical scale. Solid line = bias; dashed lines = 95% limits of agreement. 43

Figure S 1. Bland–Altman plots representing the inter-rater agreement for the median shear wave velocity (m/s) of the perineal complex imaged in the sagittal plane at the superficial region of interest, with the participant in (A) supine (n = 27; bias +0.104 m/s; 95% limits of agreement −0.206 to +0.414 m/s), (B) standing (n = 27; bias +0.073 m/s; 95% limits of agreement −0.222 to +0.368 m/s) and (C) a deep squat (n = 27; bias +0.086 m/s; 95% limits of agreement −0.191 to +0.363 m/s). Solid line = bias; dashed lines = 95% limits of agreement. All three panels share a common vertical and horizontal scale. 88

Figure S 2. Bland–Altman plots representing the inter-rater agreement for the median shear wave velocity (m/s) of the perineal complex imaged in the sagittal plane at

the deep region of interest, with the participant in (A) supine (n = 17; bias +0.107 m/s; 95% limits of agreement −1.167 to +1.381 m/s), (B) standing (n = 12; bias −0.253 m/s; 95% limits of agreement −1.453 to +0.947 m/s) and (C) a deep squat (n = 22; bias −0.060 m/s; 95% limits of agreement −1.376 to +1.255 m/s). Solid line = bias; dashed lines = 95% limits of agreement. All three panels share a common vertical and horizontal scale. The estimate obtained in standing is based on a low effective sample size (n = 12). 89

Figure S 3. Bland–Altman plots representing the inter-rater agreement for the median shear wave velocity (m/s) of the perineal complex imaged in the transverse plane, with the participant in (A) supine (n = 27; bias +0.048 m/s; 95% limits of agreement −0.134 to +0.231 m/s), (B) standing (n = 26; bias +0.020 m/s; 95% limits of agreement −0.195 to +0.235 m/s) and (C) a deep squat (n = 26; bias +0.031 m/s; 95% limits of agreement −0.187 to +0.249 m/s). Solid line = bias; dashed lines = 95% limits of agreement. All three panels share a common vertical and horizontal scale. 89

LIST OF TABLES

Table 1. Participant Characteristics (nulliparous females, n = 27)..... 39

Table 2 Perineal Complex Shear Wave Velocity and Region-Of-Interest Geometry Presented by Posture, Image Plane, and Zone..... 40

Table 3. Intra-rater and Inter- rater Reliability of Shear Wave Velocity (m/s) recorded from the perineal complex in different imaging planes, zones and participant positions..... 42

Table 4. Intra- and inter-rater reliability of region-of-interest (ROI) geometry across postures and plane–zones. 44

Table 5. Friedman Omnibus Contrasts: Exploratory Postural Comparison of Shear Wave Velocity. 45

Table 6. Bonferroni-corrected Wilcoxon Pairwise contrasts comparing Shear Wave Velocity among postures..... 46

Table 7. Deep-zone ROI traceability by posture 46

Table S1. Full trial attrition by rater × condition (all conditions). 85

Table S2. Agreement Regarding the Region of Interest Traceability in the Deep Zone of the Perineal Complex (Cohen's κ; 229 paired trials). 86

Table S3. Per-Posture Concordance for the Region of Interest Traceability of the Deep Zone of the Perineal Complex..... 86

Table S4. Intra-Rater Reliability of Ensemble-Average Colour Map of Shear Wave Velocity (m/s). 87

Table S5. Inter-Rater Reliability of the Ensemble-Averaged Colour Map of Shear Wave Velocity (m/s) 87

Table S6. Parametric Versus Non-Parametric 95% Limits of Agreement for Median Shear Wave Velocity (m/s). 88

LIST OF ABBREVIATIONS

2D - Two-dimensional

3D – Three-dimensional

BMI – Body Mass Index

EAS – External Anal Sphincter

EVUS – Endovaginal Ultrasound

IAS – Internal Anal Sphincter

ICC – Intraclass Correlation Coefficient

IVS – Intravaginal Spacer

MDD – Minimal Detectable Difference

MHz – Megahertz

MRI – Magnetic Resonance Imaging

PC – Perineal Complex

PFD – Pelvic Floor Disorder

ROI – Region of Interest

SEM – Standard Error of Measurement

STP – Superficial Transverse Perineal Muscle

SWE – Shear Wave Elastography

SWV – Shear Wave Velocity

TPUS –Transperineal Ultrasound

TUI – Tomographic Ultrasound Imaging

US – Ultrasonography

1. Chapter 1 – General Introduction

Pelvic organ support depends on the structural and functional integration of multiple interdependent components, encompassing both the fascial connective tissue network and the muscular architecture of the pelvic floor (DeLancey, Mastrovito, et al., 2024; Muro & Akita, 2023). Among these, the perineal complex (PC) represents a key anatomical region that serves as a convergence zone bridging the urogenital and anorectal compartments (Corton, 2009; Woodman & Graney, 2002; Wu et al., 2015). Functionally, the pelvic floor contributes to pelvic organ support, maintenance of urinary and fecal continence, and sexual function (Frazão et al., 2025). Emerging evidence suggests that morphological or functional alterations within the PC may contribute to both structural and functional pelvic floor impairment (Cheng et al., 2023; Rusavy et al., 2022; Yeung et al., 2022).

From an anatomical standpoint, three-dimensional ultrasound and magnetic resonance imaging (MRI) studies describe the PC as a pyramidal (3D) or triangular (2D) structure composed of dense connective tissue interlaced with smooth and skeletal muscle fibres (Larson et al., 2010; Wu et al., 2015). It occupies the space bounded anteriorly by the posterior vaginal wall, posteriorly by the external anal sphincter (EAS), superiorly by the rectovaginal fascia and the puboperineal muscle, and laterally by the superficial transverse perineal and bulbospongiosus muscles (Gong et al., 2024; Santoro et al., 2016). Recent advances in imaging and histological mapping have revealed that this region is far more complex than previously recognized (Asfour et al., 2020; Gong et al., 2024; Santoro et al., 2016). In particular, the PC is not a single, discrete structure (attachment point), but is a heterogeneous, multilayered region where multiple muscular and connective tissue components converge (DeLancey, Mastrovito, et al., 2024; Muro & Akita, 2023).

Functionally, the PC contributes to both static and dynamic support of the pelvic organs. Within DeLancey's three-level model of pelvic organ support, the PC is the essential component of Level III, acting as a fibromuscular anchor that maintains the integrity of the urogenital hiatus and contributes to the closure mechanism of the pelvic outlet (DeLancey, 1999; DeLancey, Mastrovito, et al., 2024). Due to its position, the PC transmits forces between the vagina, rectum, and perineal membrane, influencing both structural stability and functional performance during pelvic floor loading and contraction (Asfour et al., 2020; Santoro et al., 2016). It thereby contributes to urinary and fecal continence and vaginal closure (Asfour et al., 2020; Woodman & Graney, 2002). Neural

mapping studies have revealed that nerve pathways traverse the connective tissue matrix of the PC, suggesting that its integrity is crucial for coordinating motor control and sensory feedback within the pelvic floor complex (He et al., 2022; Muro et al., 2020).

Given its role in pelvic floor continuity and in linking the anterior, urogenital, and posterior anorectal compartments, disruptions in PC morphology may trigger cascading biomechanical consequences across the pelvic support system, representing an underexplored contributor to urogenital and anorectal pelvic floor disorders (PFDs)(DeLancey et al., 2025; Muro & Akita, 2023). Studies suggest that insufficient PC stiffness may impair load transfer between compartments, reducing the effectiveness of muscle contraction and coordination within the pelvic floor (DeLancey et al., 2025; Muro & Akita, 2023). Although postpartum changes in the PC do not appear to affect pelvic organ support within the first 6 months, they may lead to a loss of support over time (Pipitone et al., 2025) or to compensatory adaptations, such as increased activity and hypertrophy of the levator ani muscles, helping to maintain hiatal closure (DeLancey et al., 2025). Understanding how to assess and characterize the PC can elucidate these associations and improve our understanding of the multifactorial nature of PFDs.

Despite the emerging theoretical understanding of its structural importance and its biomechanical function, the PC remains inconsistently characterized across imaging studies. Ultrasound imaging studies have marked heterogeneity in probe type, frequency characteristics, and beam orientation, which influence the visualization and echogenicity of the fibromuscular components of the PC, limiting comparability across studies and underscoring the need for standardized imaging protocols and measurement criteria (Vukasović et al., 2026). This difficulty may be attributed to its small size and heterogeneity, resulting from the layered structure of the PC described above (Gong et al., 2024; Santoro et al., 2016).

Each available imaging modality, such as magnetic resonance imaging (MRI) and conventional ultrasound (US), has limitations when applied to this region. Importantly, these modalities primarily provide structural architectural information rather than functional information. In contrast, ultrasound shear wave elastography (SWE) quantifies tissue stiffness. This functional property complements conventional morphological assessments and may inform us about the biomechanical behaviour of the PC and its relationship with PFDs. These modalities and their reliability are examined in Chapter 2. Across the approaches used, most studies on the PC are descriptive. Few studies have applied SWE specifically to the PC, and among those that have, there is a lack of

standardized acquisition protocol, and the reliability of SWE outcomes has not formally been assessed (Lallemant et al., 2025b; Li et al., 2024; Zhou et al., 2023). Establishing the reproducibility of standardized ultrasound-based measures of PC morphology and stiffness is a necessary first step toward using them to clarify the biomechanical role of the PC in pelvic organ support and dysfunction.

Through this study, I aimed to establish the image-analysis stage of intra- and inter-rater reliability for ultrasound-based SWE measures of PC stiffness. The outcomes of this study provide a methodological foundation for future investigations into the biomechanical role of the PC and facilitate the development of standardized imaging protocols for assessing PC morphology and function using SWE.

1.1. Purpose of the study

1.1.1. Research Question

Among images captured by a single operator, what is the intra- and inter-rater reliability of ultrasound-derived SWE measures of the stiffness of the PC in nulliparous females?

1.1.2. Overall Aim

To evaluate the analysis stage of intra- and inter-rater reliability of ultrasound-based measures of PC tissue stiffness in nulliparous females, obtained using high-frequency two-dimensional transperineal ultrasound (2D-TPUS) and shear wave elastography (SWE).

1.1.2.1. Specific objectives

I. To determine the intra- and inter-rater reliability of SWV at the PC measured using imaging in the mid-sagittal and transverse planes across three postures (supine, standing and deep squat) derived through 2D-TPUS SWE.

II. To determine the intra- and inter-rater reliability of user-selected region-of-interest (ROI) geometry (Area, Centre Depth) based on B-mode and elastogram images captured in the midsagittal and transverse planes.

III. To explore differences in PC stiffness across three postures: supine, standing, and deep squat.

2. Chapter 2 – Literature Review

2.1. Anatomy of the Perineal Complex

2.1.1. Definition, Morphology, and Tissue Composition

The PC is a multilayered anatomical region located at the caudal aspect of the pelvis. It is bounded by the posterior vaginal wall anteriorly, the anterior rectal wall posteriorly, the rectovaginal fascia and puboperineal muscle superiorly, and the superficial transverse perineal and bulbospongiosus muscles laterally, with lateral insertions into the ischial rami (Figure 1A–B) (Gong et al., 2024; Muro & Akita, 2023; Santoro et al., 2016; Woodman & Graney, 2002). In its traditional anatomical characterization, the PC is considered a pyramidal fibromuscular structure with heterogeneous echogenicity on ultrasound. Its sonographic shape depends on the imaging plane, appearing triangular in the midsagittal and coronal planes and ovoid in the axial plane (Larson et al., 2010; Santoro et al., 2016). Three dimensions of the PC are conventionally measured: its depth (anteroposterior) and height (cranio-caudal) in the midsagittal plane, and its width (laterolateral), taken at its widest point in the coronal plane (Santoro et al., 2016). In nulliparous individuals, using ultrasound imaging, Santoro et al. reported a mean depth of 14.49 ± 1.48 mm, a height of 7.57 ± 0.45 mm, and a width of 13.26 ± 1.19 mm, with excellent interobserver reproducibility for all three dimensions (ICC 0.927–0.969) (Santoro et al., 2016).

Definitions of the PC vary across the literature. Some authors describe it as a fibromuscular structure to which muscles attach (Asfour et al., 2020; Woodman & Graney, 2002), whereas others propose a more integrated anatomical system in which multiple muscular and fascial elements converge and interact across the region (DeLancey et al., 2026). Emerging histological evidence indicates that the PC contains skeletal muscle, dense connective tissue, and smooth muscle elements (Muro & Akita, 2023). The smooth muscle spreads through the surrounding connective tissue and fills the spaces between the pelvic organs and skeletal muscle, merging with the striated muscle across the pelvic outlet. Within this continuous network, some regions contain more smooth muscle than others (Muro & Akita, 2023). These multiple muscular and fascial components converge upon or traverse this region without clearly defined borders (Larson et al., 2010; Muro & Akita, 2023), forming a structural bridge between the urogenital and anorectal compartments (Corton, 2009; Woodman & Graney, 2002; Wu et al., 2015).

Although the literature commonly refers to this region as the *perineal body* (Woodman & Graney, 2002; Zhou et al., 2023), the term does not fully capture its structural and functional complexity. Accumulating anatomical and biomechanical evidence indicates that the PC is more appropriately conceptualized as a functional region than as a single, discrete structure. This reframing parallels the use of terms such as "the shoulder" or "the knee" to describe complex anatomical regions, rather than a single constituent muscle or isolated structure such as the patella (DeLancey et al., 2026; DeLancey, Mastrovito, et al., 2024). Under this latter view, structures such as the external anal sphincter traverse the PC, and the continuity of the surrounding musculature reinforces the concept of a regional network rather than a discrete attachment node. Whether these relationships constitute insertion into the PC or passage through it remains debated (Muro & Akita, 2023; Wu et al., 2015).

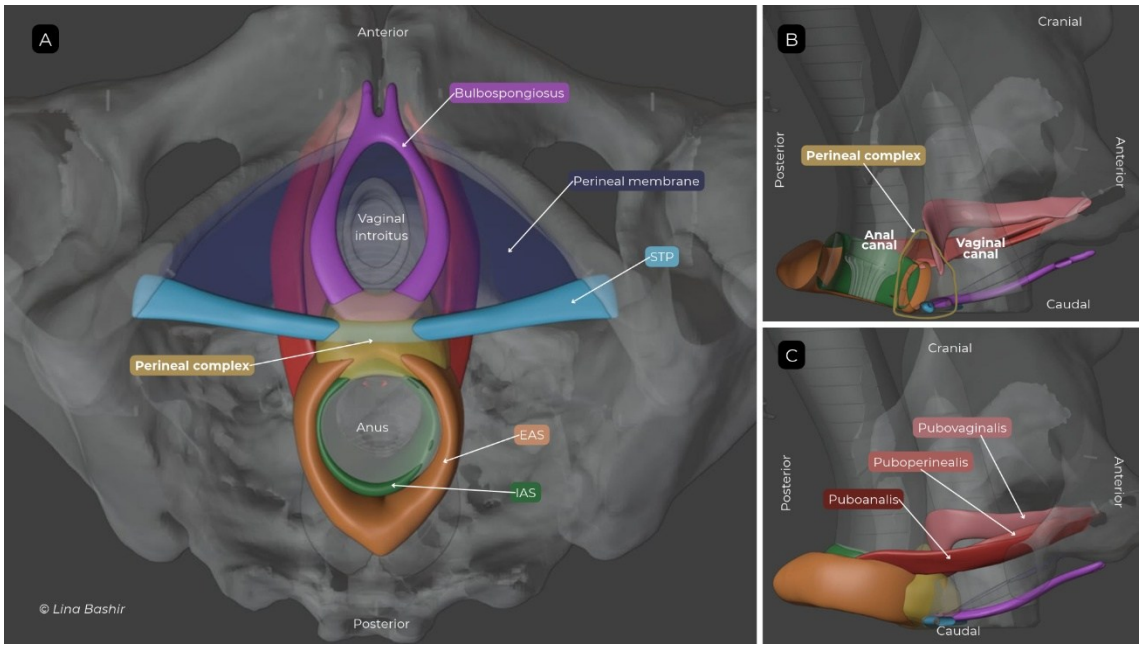


Figure 1. Three-dimensional model of the female Perineal Complex (PC). (A) Transverse (Caudal) view showing the PC in relation to the bulbospongiosus, superficial transverse perineal (STP) muscles, perineal membrane, and external (EAS) and internal (IAS) anal sphincters. (B) Mid-sagittal view showing the PC (outlined in yellow) between the vaginal canal and the anal canal. (C) Sagittal view showing the pubovisceral components of the levator ani: pubovaginalis, puboperinealis, and puboanalis. Schematic model based on the anatomical descriptions of Larson et al. (2010) and Santoro et al. (2016) (Section 2.1.2). Model created by Lina Bashir (MFM Lab, University of Ottawa); reproduced with permission.

2.1.2. Layered Architecture and Muscle Connectivity

The PC has a multilayered architecture in which muscular components converge across different depths. Using MRI reconstruction, Larson and colleagues resolved the

PC into three levels, superficial, mid, and deep, each defined by specific muscular relationships (Larson et al., 2010). At the superficial level, the bulbospongiosus inserts into the lateral margins of the PC, while the superficial transverse perineal muscle and external anal sphincter traverse the region and form part of its inferior boundary (Larson et al., 2010). In contrast, Santoro et al. describe STP fibres inserting into its lower portion (Santoro et al., 2016). Recent dissection studies have complicated this view; in females, the bulbospongiosus may run toward the lateral surface of the external anal sphincter instead of converging on the perineal midline, and the superficial transverse perineal muscle appears to form a continuous interhemispheric sling (Muro & Akita, 2023). Wu et al. reported the opposite, describing the bulbospongiosus and superficial transverse perineal fibres as meeting at the midline to form a bundle that attaches posteriorly to the PC (Wu et al., 2015). Together, these findings suggest that the PC's superficial connections may reflect lateral muscular continuity rather than direct midline insertion, an interpretation that remains debated (Muro & Akita, 2023; Vukasović et al., 2026).

In the mid-region, components of the pubovisceral part of the levator ani, specifically the puboperinealis and puboanalis, insert into the lateral margins of the PC (Figure 1C) (Larson et al., 2010; Santoro et al., 2016). On three-dimensional endovaginal ultrasound (3D-EVUS), the puboanalis appears as a triangular hypoechoic structure lateral to the puboperinealis and continuous with both the PC and the anal canal, forming part of a central integration zone (Santoro et al., 2016). On MRI, the distal internal anal sphincter is also visible in this zone (Larson et al., 2010). The levator ani contribution to the PC remains contested: DeLancey and colleagues identified puboperinealis fibres inserting into the mid-region, whereas earlier cadaveric work by Shafik found no direct levator ani–PC connection (Shafik et al., 2007; Vukasović et al., 2026).

In the deep region, MRI reconstruction has shown that the pubovaginalis fuses with the vaginal sidewall and sends fibres posteriorly to the PC (Figure 1C) (Larson et al., 2010). This finding is not universal. Using 3D-EVUS and cadaveric dissection, Santoro and colleagues could not confirm any contribution of the pubovaginalis to the PC, which is why they divided the region into two levels rather than three (Santoro et al., 2016). Beyond these striated components, histological and high-resolution imaging studies have identified smooth muscle in the deeper region, contributing to structural continuity between the PC and the adjacent visceral walls (Gong et al., 2024; Muro & Akita, 2023). The puborectalis, which forms a posterior sling around the anorectal junction, sends no fibres directly to the PC (Larson et al., 2010; Santoro et al., 2016), but

may exert an indirect suspensory influence through its attachment to the pubic bone (Larson et al., 2010). Across all three depths, the medial levator ani, the perineal membrane, and the PC are bound together by dense vaginal fascia (DeLancey, Pipitone, et al., 2024), an architecture whose mechanical consequences are examined in the following section.

2.2. Biomechanical Function of the Perineal Complex

2.2.1. Structural Support, Force Transmission, and Pelvic Floor Stability and Coordination

Building on the anatomy described above, the focus now turns to the biomechanical role of the PC as an integrated load-transmitting structure within the pelvic floor. Through its connections between the anterior and posterior and the superficial and deep components, the PC unites the perineal membranes and prevents lateral diastasis of the medial pubovisceral muscles (DeLancey, Pipitone, et al., 2024). It also contributes to Level III support, resisting the downward displacement of the pelvic organs at the inferior vaginal level (J. O. DeLancey, Mastrovito, et al., 2024). Due to its supportive role, the PC cannot be understood solely by changes in its dimensions or position. Its mechanical behaviour also depends on tissue properties, muscular connectivity, and the capacity to transmit load (Moura et al., 2025). Whenever the collagenous infrastructure fails, whether from levator ani injury, fascial compromise, or primary perineal damage, it may progressively destabilize the anorectal region and the pelvic floor as a whole (Asfour et al., 2020).

This interdependence extends across pelvic support levels. Woodman and Graney describe how downward force on the vagina draws the fibres of the perineal membrane taut, anchored laterally to the ischiopubic rami and posteriorly to the PC, so that they resist downward displacement, while the lateral vaginal attachments, including the levator ani and the tendinous arches of the pelvic fascia, are recruited at the same time (Woodman & Graney, 2002). Level III support, provided by the PC through the perineal membrane, therefore works together with the Level II suspension of the vagina through its connections to the tendinous arches and levator ani musculature (Woodman & Graney, 2002).

The PC may thus represent a region of active force transmission and muscular continuity between the anterior and posterior pelvic compartments, embedded within a

broader system of muscular and fascial coordination that extends beyond skeletal muscle activity alone. The structural continuity between the smooth muscle and the levator ani bundles, established above, appears to transmit the contractile forces of the skeletal muscles to the pelvic viscera (Muro & Akita, 2023). Within the perineal region, a complementary anteroposterior arrangement of smooth and skeletal muscle fibres maintains continuous muscular contact anterior to the anal canal. This zone, which Muro and Akita describe as the centre of the perineum, corresponds anatomically to the PC, and its muscular arrangement may contribute to local stabilization (Muro & Akita, 2023).

This arrangement has important functional implications. Because the two muscle types lie in close contact, contraction of the central smooth muscle would pull the surrounding skeletal muscle toward the centre of the pelvic outlet and alter its orientation and angle, while skeletal muscle contraction would displace the viscera anteriorly and reshape the smooth muscle network (Muro & Akita, 2023). The two muscle types, therefore, contract and relax while regulating each other's direction and force, producing what has been described as the functional dynamism of the pelvic floor (Muro & Akita, 2023). This bidirectional coupling supports the view that the PC is the dynamic epicentre of coordinated pelvic floor stability during functional loading.

The rectovaginal muscle, which arises from the longitudinal and circular fibres of the rectum and anal canal and merges with the smooth muscle of the lower posterior vaginal wall, has been proposed as a key stabilizing structure in this region, likely contributing to the mechanical support of the posterior vaginal wall and to posterior compartment stability (Muro & Akita, 2023). Together, these findings support a multi-structural view of pelvic floor support, achieved through the coordinated integration of smooth and skeletal muscle networks across the pelvic outlet (Muro & Akita, 2023).

2.2.2. Tissue Mechanical Properties

Physically, the PC is a viscoelastic, anisotropic tissue (Creze et al., 2018; Moura et al., 2025; Nitta et al., 2021). Its mechanical behaviour is primarily characterized by its stiffness, defined as its resistance to deformation under load, which integrates both passive and active properties (Creze et al., 2018). Passive properties become evident as collagen fibres are recruited during lengthening, whereas active properties are expressed when the interspersed muscle fibres contract (Creze et al., 2018; Moura et al., 2025). Tissue failure marks the upper limit of this mechanical response, defined by the ultimate stress, which is the length at which rupture occurs (Moura et al., 2025). Additionally,

viscoelasticity is the term used to describe the time-dependent behaviours of a tissue, including the decay in tension observed under a fixed stretch, a phenomenon termed stress relaxation (Moura et al., 2025; Nitta et al., 2021) as well as the increase in tissue strain under a fixed load over time, a phenomenon termed creep (Creze et al., 2018). Due to viscoelasticity, the ultimate stress of a tissue varies by the speed at which tissue deformation occurs.

Under increased intra-abdominal pressure (Valsalva maneuver), the PC exhibits stiffening behaviour observed across healthy controls and clinical populations (Li et al., 2024; Zhou et al., 2023). As the perineal membrane and the tendinous arches of the pelvic fascia tighten under downward pressure, they passively anchor the PC, limiting both its strain and displacement (Arenholt et al., 2017). Morphologically, the PC demonstrates modest elongation in its antero-posterior dimension alongside compression in its cranio-caudal height. Mechanically, however, measurements of its Young's modulus (E) reveal a notable stiffening response to caudally directed forces, increasing by over 60% in healthy controls (Li et al., 2024). Although baseline stiffness and stiffening capacity are significantly blunted among those with pelvic organ prolapse and stress urinary incontinence compared to healthy controls (Li et al., 2024; Zhou et al., 2023), the overall structural framework of the PC preserves its fundamental mechanical capacity to resist excessive passive deformation under transient increases in intra-abdominal pressure.

A recent study on human cadaveric perineal tissue detailed its viscoelastic properties (Moura et al., 2025). When held at a fixed 75% strain, the tissue exhibits pronounced stress relaxation, with mechanical tension falling by approximately 40% over 900 seconds. This gradual release of tension is hypothesized to allow perineal tissues to accommodate large deformations with reduced peak stress, a mechanism proposed to be particularly relevant during labour and vaginal delivery (Moura et al., 2025). Furthermore, under ultimate tensile testing, the tissue deformed to a stretch ratio of 1.97 at the ultimate Cauchy stress of 224.70 kPa, indicating that the perineal body sustains near-doubling of its unloaded length before failure (Moura et al., 2025). Histological analysis showed a dense anisotropic network of collagen fibres, aligned predominantly along the direction of stretch. This preferential fibre orientation means the tissue is stiffer along the fibre axis than in directions perpendicular to it. This anisotropic arrangement appears to underlie the PC’s load-bearing capacity and its viscoelastic behaviour (Moura et al., 2025).

These mechanical properties carry direct clinical implications. Obstetric trauma and cumulative mechanical loading are two primary mechanisms through which PC integrity may be compromised, placing its fibromuscular infrastructure under disproportionate strain and progressively destabilizing the pelvic floor (Asfour et al., 2020; Moura et al., 2025). Because altered tissue stiffness and altered relaxation dynamics directly affect how mechanical loads are distributed across the pelvic floor, objective, in vivo quantification of PC biomechanical properties remains essential for understanding tissue vulnerability and contributing to PFDs.

2.2.3. Contributions of the PC Beyond Pelvic Organ Support

The PC has also been described as part of the orgasmic platform. It provides a region of localized vasocongestion in the inferior third of the vagina and labia minora during the plateau phase of the sexual response cycle (Woodman & Graney, 2002). In addition, it may also support rapid sensorimotor integration through a mechanism intrinsic to its smooth muscle network. The pelvic floor is subject to sudden increases in abdominal pressure that require an immediate mechanical response. Smooth muscle distributed across the pelvic outlet exhibits the Bayliss effect, a property of smooth muscle that causes it to contract when suddenly stretched, independently of neural or humoral input (Muro & Akita, 2023). Since the pelvic floor experiences sudden loads, much as vessel walls experience blood pressure, this smooth muscle network may provide an instantaneous, neurally independent means of resisting intra-abdominal pressure surges (Muro & Akita, 2023). Operating alongside voluntary pelvic floor contraction, this capacity may represent a functionally significant aspect of PC physiology.

2.3. Perineal Complex Alterations and Pelvic Floor Disorders

Childbirth is the most common mechanical trauma to the PC. Delivery-related trauma to the PC has been reported to occur in 10% to 30% of women delivering vaginally, making childbirth the natural starting point for understanding how such trauma may lead to PFDs (Kearney et al., 2006; Komorowski et al., 2014; Mottet et al., 2017). Vaginal delivery imposes substantial mechanical stress on the pelvic floor, exposing both muscular and connective components to multidirectional forces. During the second stage of labour, descent of the fetal head stretches the pelvic floor muscles caudally, particularly the pubovisceral and puborectalis portions of the levator ani as the head passes through

the levator hiatus. At crowning, levator hiatal distension shifts from being midsagittally oriented to circumferentially oriented, producing extreme strain on the PC and adjacent fascial planes (Ashton-Miller & DeLancey, 2021; Cheng et al., 2023; DeLancey, Masteling, et al., 2024; Dietz & Lanzarone, 2005; Kearney et al., 2006; Lien et al., 2004). Perineal strain can exceed 300% of resting tissue length, approaching the physiological limits of muscle extensibility during this event (DeLancey, Mastrovito, et al., 2024; Lien et al., 2004).

This strain may tear or avulse the deep layers of the PC muscles and connective tissues, including the puboperinealis, pubovaginalis, and puboanalis muscles(DeLancey, Mastrovito, et al., 2024; Santoro et al., 2016; Wu et al., 2015). On second-degree perineal tears, disruption of the perineal muscles occurs without extending to the anal sphincter complex, affecting superficial components such as the bulbospongiosus and superficial transverse perineal muscles (Woodman & Graney, 2002), while on higher-grade tears the external anal sphincter and the rectovaginal fascia may be compromised, further destabilizing the posterior compartment (Cheng et al., 2023; Macedo et al., 2024; Miller et al., 2010; Rusavy et al., 2022). Parity compounds these alterations through cumulative loading and progressive remodelling of connective and muscular tissues, producing permanent elongation or altered fibre alignment within the PC (Cheng et al., 2023). Because of the heterogeneous nature of these factors across women, the resulting alterations in PC morphology and function follow a non-uniform pattern. In a cohort of 388 primiparous women, anatomical alterations in the muscles converging on the PC were present in 168 (43.3%) one year after delivery; however, 14% of those with a sonographically intact pelvic floor still reported clinically relevant symptoms, showing that perineal dysfunction can occur without any detectable gross change in pelvic floor complex morphology (Lilleberg et al., 2025).

Disruption of the PC, whether through separation of its two sides or failure of the collagenous infrastructure supporting the convergent musculature, translates structural alterations into measurable functional change (DeLancey, Pipitone, et al., 2024). Imaging studies show that postpartum females have larger PC diameters, and elastography shows a lower Young's modulus (stiffness) than nulliparous controls (Zhou et al., 2023). Whether this reduced stiffness stems mainly from muscle damage, collagen remodelling, or both remains uncertain, since the association is inferred rather than having been demonstrated directly. Whatever the cause, this loss of stiffness likely compromises the load-transmitting and force-coordinating role of the PC, disrupting the coordinated interplay

among the levator ani complex, perineal membrane, and anal sphincters (DeLancey, Masteling, et al., 2024)**.** Reductions in PC height, width, or stiffness produce a cascade of biomechanical consequences across the pelvic organ support system, including disconnection of the perineal membranes, their downward rotation around the pubic attachments, levator ani diastasis, and consequent enlargement of the urogenital hiatus (Cheng et al., 2023; DeLancey, Pipitone, et al., 2024).

Because the PC is not a single muscle or isolated structure, failure in one component may indirectly affect higher levels of support through its influence on the levator ani morphology and connective tissue load distribution (DeLancey, Mastrovito, et al., 2024). When PC stiffness or morphology is altered, the levator ani may compensate through increased activity or hypertrophy to maintain hiatal closure, as observed in women with complete PC loss but intact hiatus function (DeLancey et al., 2025). This compensation appears effective in the short term, since postpartum changes in the PC do not significantly affect pelvic organ support within the first six months (Pipitone et al., 2026). Over the medium to long term, however, the compensation may become unsustainable, contributing to overuse, muscle fatigue, and eventual levator avulsion or hiatal enlargement. Because compensatory capacity itself differs among women, comparable structural alterations of the PC may follow divergent trajectories, remaining clinically silent in some while progressing to overt dysfunction in others, which helps explain why PC injury does not map onto a single, predictable clinical outcome.

These structural and functional pathways translate into a range of clinical disorders. Reduced PC height and increased urogenital hiatus dimensions in women with clinically confirmed perineal lacerations are consistent with DeLancey's Level III model, in which the PC and perineal membrane stabilize the distal vagina and anal canal; once disrupted, they no longer adequately counteract intra-abdominal pressure, increasing the risk of posterior compartment defects and symptomatic PFDs (Asfour et al., 2020; Cheng et al., 2023; Woodman & Graney, 2002). A PC cross-sectional area below 2.4 cm^2 was strongly associated with posterior compartment prolapse and with Pelvic Organ Prolapse Quantification (POP-Q) genital hiatus measurements ($p < 0.001$), supporting the PC as a structural marker of distal pelvic organ support (Asfour et al., 2020). Midline disruption of the PC has likewise been linked to pelvic organ prolapse (Pipitone et al., 2026), and surgical repair of the PC is recognized as a strategy for symptom relief (Woodman & Graney, 2002).

PC integrity has also been linked to pelvic floor disorders beyond prolapse, including fecal incontinence and sexual dysfunction (Vukasović et al., 2026; Woodman & Graney, 2002). A PC thickness below 10 mm has been correlated with anal sphincter defects and fecal incontinence (Zetterström et al., 1998). Damage to the PC weakens the structural continuity between the levator ani and the external anal sphincter complex, diminishing the capacity of the pelvic floor to maintain vaginal and anal closure during increases in intra-abdominal pressure, a disruption associated with anal incontinence, and perineal descent (Woodman & Graney, 2002; Zhou et al., 2023). Moreover, its injury has also been linked to sexual dysfunction, since loss of its integrity can impair the orgasmic platform and affect sexual response and satisfaction (Woodman & Graney, 2002).

Given its role at the distal level of pelvic support and its involvement in the mechanical continuity of the pelvic floor, disruption of the PC represents an underexplored contributor to pelvic floor dysfunction. The variability in PC morphology and stiffness, arising from differences in injury severity, cumulative loading, and compensatory capacity, is precisely what current evidence cannot yet characterize with confidence. Resolving this requires reliable measurement of PC dimensions and stiffness, a prerequisite for clarifying the role of the PC in pelvic floor disorders and informing prevention, diagnosis, and management.

2.4. Clinical Assessment of the Perineal Complex

Digital palpation is a commonly used method for assessing the integrity of the PC in clinical practice, yet it remains poorly standardized. During the examination, the clinician places one finger in the vagina and one in the anal canal, assessing the intervening tissue through manual compression. Additionally, PC length is measured with a ruler, capturing the distance between the vaginal introitus and the anal sphincter (Shobeiri et al., 2002). Combined with this method, clinical assessment of the PC draws on the validated Pelvic Organ Prolapse Quantification system (POP-Q), through which *perineal body* length (POP-Q PB) is defined as the distance from the posterior margin of the hymen to the mid-anal opening (Madhu et al., 2018).

Ultrasound imaging has been proposed as a more objective alternative for assessing the PC, most commonly using an endoanal approach. With this technique, the assessor places a finger against the posterior vaginal wall without applying pressure, and PC thickness is estimated as the distance between the endoanal probe and the acoustic echo produced by the fingertip (Fornell et al., 2005; Shobeiri et al., 2002; Zetterström et

al., 1998). Using this approach, a small number of studies have associated low PC thickness, in the order of 10 mm, with pelvic floor disorders such as fecal incontinence (Zetterström et al., 1998).

A limited body of literature suggests that digital assessment correlates well with ultrasound measurements. This claim, however, rests on only a few studies and lacks validation, so the available evidence remains insufficient to establish the agreement between the two approaches (Fornell et al., 2005; Shobeiri et al., 2002; Zetterström et al., 1998). The POP-Q is similarly limited: it does not differ significantly between individuals with prolapse and healthy controls, nor does it correlate with ultrasound-based PC area, the parameter most strongly associated with posterior compartment prolapse (Asfour et al., 2020; Dunivan et al., 2016), suggesting that it likely reflects superficial tissue length rather than the structural or functional properties of the PC.

Taken together, these findings indicate that static and linear measurements alone may not adequately capture the functional behaviour of the PC. These observations support the need for assessment approaches that move beyond linear morphology toward biomechanical characterization.

2.5. Imaging Modalities for Assessing the Perineal Complex

Over the past two decades, MRI and ultrasound have substantially expanded our understanding of pelvic floor morphology. Few studies, however, have attempted to identify or characterize the PC as a distinct region, and consistent visualization and measurement remain difficult because of its small size and multilayered composition.

2.5.1. Magnetic Resonance Imaging (MRI)

MRI has been widely used to evaluate the posterior compartment pelvic floor structures (Zhou et al., 2023). Using multiplanar imaging and 3D modelling, Larson et al. reconstructed the various layers of the PC, as previously described (Larson et al., 2010). They noted, however, that the PC and its dimensions could not be precisely delineated on MRI at any level (Larson et al., 2010). Similarly, Gong et al. reported difficulty visualizing the superficial transverse perineal muscle at the PC level (Gong et al., 2024). Pipitone et al. developed an MRI-based approach to investigate childbirth-induced changes in the perineal membrane, identifying greater separation of the perineal membrane at the level of the PC among individuals who had delivered vaginally than in those who had not. (Pipitone et al., 2021).

These studies underscore the limitations of MRI for evaluating the PC morphology and function in clinical practice, particularly the difficulty resolving small, interwoven structures. This limited capacity to distinguish the individual layers of the PC has prompted researchers to seek alternative imaging modalities.

2.5.2. Ultrasound imaging

Compared with MRI, ultrasonography (US) offers a non-invasive, more accessible option for soft-tissue evaluation, particularly for the morphological and functional analysis of pelvic floor components. Although US is generally more feasible and cost-effective than MRI, visualization of the PC demands specialized expertise. In 2016, Santoro et al. characterized the PC in nulliparous cadavers using high-frequency 3D-EVUS. Interobserver repeatability for PC height, depth, and width was excellent. A key advantage of 3D-EVUS was its capacity to distinguish two anatomical levels, superficial and deep, in the midsagittal plane (Santoro et al., 2016). Gong et al. also acquired PC images from 40 parous and 9 nulliparous participants, using 3D-EVUS and MRI, respectively. Unlike the cadaver study by Santoro et al., they found the PC and its surrounding musculature difficult to identify in the ultrasound images because of the interlocking nature of the muscles (Gong et al., 2024). This gap between excellent repeatability in cadavers and poor characterization in living females is methodologically informative, since it suggests that the reliability reported by Santoro et al. may reflect the controlled conditions and the altered tissue properties when imaging cadavers. Although these specimens were fresh frozen rather than chemically fixed, the absence of perfusion and active muscle tone, combined with freeze-thaw effects, alters tissue acoustics in ways that may sharpen structural boundaries relative to living tissue. Consistent with this, Örnö et al. reported that 2D-EVUS was insufficient for visualizing the complete anatomy of the perineal muscles, which arise from the pelvic sidewalls and converge at the PC from varying angles (Örnö et al., 2008).

Wide-angle ultrasound acquisitions lack consensus among authors and have limited resolution for directly measuring the PC, given its small size and multilayered composition. Even so, this modality appears to be valuable for identifying qualitative indicators that may improve understanding of injury mechanisms affecting the PC. For example, two studies by Pipitone et al. used a rotating 360-degree endovaginal probe and described a "band of tissue/transverse band", an identifiable continuous echogenic connection between the two sides of the PC, bridging the vagina and rectum, and a

"pinched waist/hourglass sign", a symmetrical indentation of the tissues on either side of the perineum (Pipitone et al., 2024, 2025). These signs reflect the continuity of the muscles inserting into the PC rather than the dimensions of the PC itself. In addition to these qualitative features, the anovaginal distance (AVD) was introduced as a quantitative sonographic measure representing the thickness of the perineal tissue between the posterior vaginal wall and the internal anal sphincter (Pihl et al., 2018). None of these signs have yet been formally validated against anatomical or functional outcomes, nor evaluated for reliability.

Beyond visualization, the reliability of PC morphometry depends on the specific parameter being quantified. Chantarasorn et al. used two-dimensional transperineal ultrasound (2D-TPUS) (8–4 MHz transducer; 85° acquisition angle) to assess PC mobility and morphology before and after childbirth in 20 primiparous women, defining PC mobility as caudal positional displacement reflecting reduced pelvic organ support after vaginal delivery. PC mobility showed acceptable inter-observer repeatability (ICC ≈ 0.74), whereas dimensional parameters such as PC area and height showed moderate to poor repeatability (ICC 0.15–0.56) (Chantarasorn et al., 2012). Asfour et al. attributed this poor dimensional repeatability to a methodological limitation, since the PC measurements had been derived from images acquired to capture the entire pelvic floor rather than optimized for the region of the PC (Asfour et al., 2020). Using a curved 2D transperineal probe (7 MHz), maximal magnification and gain tuning to isolate the PC from the surrounding pelvic floor, they found that PC length, height, perimeter, and area could be measured consistently (Asfour et al., 2020).

A high-frequency linear transducer may be preferable to a curvilinear probe when imaging the PC, as it is tuned to visualize the superficial tissues with high spatial resolution. Indeed, Zhou et al. employed a high-frequency linear probe (10 MHz), using 2D-TPUS with SWE for the simultaneous assessment of PC morphology and elastic modulus (Zhou et al., 2023).

2.5.3. SWE Physical Principles

SWE has recently emerged as a promising method for evaluating viscoelastic properties of tissues, yet its interpretation requires an understanding of the physical principles that underlie this approach. The technique estimates tissue stiffness by tracking the extent to which a mechanically induced wave displaces the target tissue. The ultrasound probe delivers a focused acoustic radiation force impulse (ARFI) that

displaces the tissue locally, which generates shear waves that propagate transversely to the primary ultrasound beam (Taljanovic et al., 2017). The speed at which these waves travel reflects the mechanical properties of the medium: shear waves move faster through stiffer tissue and more slowly through softer tissue (Creze et al., 2018; Lee et al., 2020).

SWE outcomes are grounded in Hooke's law and the proportional relationship between applied stress and the resulting strain (Creze et al., 2018). SWE does not measure elasticity directly. What it measures is the shear wave velocity (SWV), which is converted into the shear modulus (G), according to the equation $G = \rho c^2$, where ρ represents the density of the tissue (assumed to be approximately 1000 kg/m³ for soft tissue) and c represents the SWV (m/s). G is then converted to Young's modulus (E) according to the equation $E = 3G$ (Creze et al., 2018; Sigrist et al., 2017). Each step rests on an assumption: first that the tissues are isotropic and linearly elastic (Nitta et al., 2021) and second that they are incompressible with a Poisson's ratio of 0.5 (Sigrist et al., 2017). For this reason, the literature recommends reporting stiffness in viscoelastic, heterogeneous, and anisotropic tissues as SWV (m/s) rather than as Young's modulus (kPa), since these assumptions are violated (Davis et al., 2019). The squared relationship between Young's modulus (E) and SWV reinforces this recommendation: it causes the mean and standard deviation computed over a heterogeneous region of interest (ROI) to differ depending on whether the SWV data are averaged and then converted to Young's modulus, or converted to Young's modulus (kPa) first, and then averaged, which compromises comparability across studies (Săftoiu et al., 2019).

Shear wave propagation, however, is not governed by stiffness alone. In a region characterized by interconnections and overlapping of structures such as the PC, the organization of the fibres introduces anisotropy, meaning that shear waves travel faster when their propagation direction is aligned with the fibre orientation than when it is perpendicular to it (Creze et al., 2018). Anisotropy is one of the physical properties, together with viscoelasticity and nonlinearity, that violate the assumption that the medium under SWE investigation is isotropic and purely elastic (Nitta et al., 2021). The measured velocity, therefore, depends on the orientation of the probe relative to the fibres, and a meaningful correspondence between the shear modulus and the Young's modulus is obtained only when the probe is aligned parallel to the fibre direction of the tissue of interest (Creze et al., 2018; Sigrist et al., 2017). For this reason, SWV is the preferred outcome from ultrasound SWE imaging of anisotropic tissues such as the PC.

A further confounding factor is the boundary conditions. As a shear wave propagates through tissue, its velocity changes wherever the medium changes, such as at tissue boundaries. Within the PC, tissues of different intrinsic stiffness properties meet, and the tissues are anisotropic due to variable fibre orientation. These features create internal boundaries between regions with different inherent SWV. Wherever a wave crosses a boundary, part of it is refracted, and part is reflected, in the same way that light refracts and reflects when it passes from water into air (Nitta et al., 2021). Where the incident and reflected waves overlap, they interfere, and this interference can corrupt the velocity estimate at the individual pixel level, producing isolated values markedly higher or lower than their surroundings that do not represent a true difference in tissue stiffness (Davis et al., 2019; Nitta et al., 2021). In a compositionally mixed, multi-directional structure such as the PC, these boundaries are numerous, so the elastogram is expected to contain scattered artefactual pixels alongside genuine, orientation-dependent variation. For this reason, shear velocity data obtained from the PC must be processed to eliminate these artifacts prior to interpretation.

2.5.4. Why SWE is promising

SWE offers some attributes that make it suitable for the biomechanical assessment of the PC, a region that has historically lacked mechanical characterization. The first is that it is objective and quantitative. In SWE, the ARFI that generates the shear wave is produced by the transducer rather than by manual compression, so the mechanical perturbation does not depend on the examiner. This differs from strain elastography, in which the deforming force is delivered through operator-applied compression, and which yields only qualitative or semiquantitative output (Sigrist et al., 2017; Taljanovic et al., 2017). Because the SWE impulse is operator-independent, tissue stiffness can be measured numerically, allowing objective quantification rather than the visual and subjective interpretation described in section 2.4. (Li et al., 2024; Zhou et al., 2023). This objectivity, however, describes the ARFI and not the examination as a whole. Probe placement, the extent of tissue compression, and the angle between the imaging plane and the underlying fibre architecture remain under examiner control and influence the measurement, which is why the reliability and validity of SWE outcomes cannot be assumed based on the objectivity of the method.

SWE provides information on functional and mechanical behaviour. SWE renders a real-time spatial map of SWV or estimated Young's modulus that is co-registered with

the anatomical image, such that stiffness can be measured at a defined location (Creze et al., 2018; Taljanovic et al., 2017). A clinically relevant property is that this stiffness is not static: SWV and the corresponding shear modulus rise as tensile load on the tissue increases, reflecting the nonlinear force-deformation behaviour of soft biological tissue (Nitta et al., 2021). The load and state dependence have been demonstrated directly in pelvic floor structures. Puborectalis shear modulus increases progressively from rest to maximal voluntary contraction, and this SWE-derived increase shows near-linear agreement with electromyographic amplitude across graded contraction, indicating that the signal tracks muscle activation rather than reflecting acquisition artifact (Morin et al., 2022). Tracking stiffness across functional states enables SWE to interrogate the PC as a load-bearing support region rather than a static landmark.

2.5.5. SWE at the Perineal Complex

A recent and growing body of work has applied SWE to quantify PC stiffness, with existing studies designed mainly to detect group-level differences or associations with clinical outcomes. Zhou et al. imaged the PC in 45 nulliparous women, 66 women with pelvic organ prolapse, and 70 postpartum women using high-frequency 2D ultrasound and SWE, measuring depth, height, and Young's modulus at rest, on maximal contraction, and on the Valsalva maneuver. The Young's modulus of the PC differed significantly across groups: nulliparous women showed the smallest dimensions and the highest modulus, while those with pelvic organ prolapse showed the lowest modulus. The modulus increased with contraction within each group (Zhou et al., 2023). Li et al. compared women with stress urinary incontinence (SUI) to continent controls. PC stiffness rose from rest to Valsalva in all participants yet was significantly lower in women with SUI during Valsalva. A maximum Young's modulus below 55.76 kPa predicted SUI with 100% specificity, which the authors proposed as a non-invasive marker of poor pelvic organ support (Li et al., 2024). Both studies reported Young’s modulus (in kPa) from images acquired in the mid-sagittal plane, and measured only the superficial zone of the PC, averaging over an ROI drawn along its border. Neither addressed the orientation dependence of shear wave propagation in fibromuscular tissue, nor reported any filtering of the elastographic map to exclude artefactual pixels or the frame selection method before averaging. Li et al. applied quality criteria at acquisition, whereas Zhou et al. reported none.

Two small feasibility studies from the same cohort confirmed that ultrasound SWE of the PC is technically achievable across pregnancy and labour. Lallemant et al. combined 2D transperineal ultrasound with SWE in 16 women at 36 to 40 weeks of gestation to measure the PC and anal sphincter biometry and stiffness at rest and during Valsalva, and to examine their associations with subsequent perineal tears. Ten women (62.5 %) sustained a perineal tear, all first degree, compared with six who did not. Group differences were significant, with tearing associated with a larger PC area and a thicker EAS, as well as a thinner and smaller IAS, but not with SWE-derived stiffness. In a companion study, the same group quantified PC and anal sphincter stiffness intrapartum in 10 women who delivered vaginally, measuring at the onset of labour and again before expulsive efforts. Young's modulus values increased from the onset of labour to before the expulsive stage; however, they again did not show a significant association with the occurrence of tearing (Lallemant et al., 2025b, 2025a). However, whether Young's modulus of the PC is reliable remains unknown: neither study reported image quality criteria, ROI dispersion, or any index of agreement, and although measurements were acquired five times and averaged, the variability across those repetitions was not given. This limits what the null stiffness findings might mean. With group sizes of four to ten and standard deviations often approaching the group means, neither study had adequate power to detect a difference in stiffness between those who tore and those who did not.

Together, these studies establish that SWE can be acquired from the PC and that the resulting stiffness values behave coherently with parity, functional state, and continence status. Their findings should nonetheless be interpreted with caution, less because of the limitations of any individual study than because of what the literature has yet to examine. No normative reference values have been established against which measurements can be compared. Across these reports, the PC was assessed almost exclusively in a supine position, with probe types, acquisition and analysis protocols that varied from one study to the next. Furthermore, reported intraclass correlation coefficients, such as those above 0.75 for Young's modulus reported by Li et al., have been limited to the superficial zone imaged in the mid-sagittal plane, leaving the reliability of measures taken in the deep zone and transverse plane unknown (Li et al., 2024). Crucially, existing repeatability metrics describe the consistency of image acquisition combined with analysis reproducibility; they do not establish whether the placement and size of the ROI over the elastogram independently alter the resulting SWV (Li et al., 2024; Morin et al., 2022; Starzec-Proserpio et al., 2023). Because the PC is

small, superficial, and anisotropic, the imaging technique and ROI delineation represent meaningful, uncharacterized sources of variability that must be evaluated before developing a standardized methodological framework.

2.6. Gaps in Current Assessment Methods and the Need for the Current Study

Three constraints emerge from the literature. The first is that MRI cannot reliably delineate the PC and is constrained by cost and acquisition time, while conventional ultrasound, although dynamic and accessible, does not capture the biomechanical properties of the PC (Gong et al., 2024; Vukasović et al., 2026; Zhou et al., 2023). The second is that morphology alone is unlikely to sufficiently characterize the PC, since the structural integrity of the PC is not determined by its geometry. Some postpartum women report symptoms of PFDs even when an ultrasound shows no morphometric deviation (Lilleberg et al., 2025). The third is that the small size, superficial location, and interconnecting musculature within the PC hinder consistent boundary identification (Gong et al., 2024; Santoro et al., 2016) .

SWE could address these gaps, yet the evidence for its use in assessing PC biomechanical function is sparse and methodologically fragmented. When used in the mid-sagittal plane and supine position, tissue stiffness recorded using SWE showed differences between rest, contraction, and the Valsalva manoeuvre, suggesting that this approach may have utility in evaluating the function of the PC. However, existing studies share no common acquisition or measurement protocol and have been conducted almost exclusively using recommendations that pertain to musculoskeletal tissue. All studies to date have imaged the PC in the supine position, which limits the interpretability of SWE outcomes as important functional information may be missed when the tissues are not loaded by gravity. Further, imaging the PC during straining depends on the participant's willingness and ability to strain. No study has assessed the PC in the transverse plane, stratified superficial and deep zones, nor have any compared outcomes among functional postures such as standing or squatting (Li et al., 2024; Morin et al., 2022; Rostaminia et al., 2019; Starzec-Proserpio et al., 2026; Zhou et al., 2023).

Without a standardized and reliable methodological framework that accounts for acquisition and ROI delineation variability, it remains difficult to determine how structural or biomechanical alterations of the PC relate to the PFD's symptoms. Reliable SWE-based measurement is therefore a prerequisite for characterizing the viscoelastic

properties and load-bearing role of the PC, and the present thesis is designed to provide that foundational methodological evidence.

3. Chapter 3 – Methods

This study received approval from the University of Ottawa Research Ethics Board (REB File No. H-05-25-11515) prior to initiating recruitment.

3.1. Study Design and Participants

This was an observational, cross-sectional study. Eligible participants were biologically female, aged ≥18 years, nulliparous, with a body mass index (BMI) <35 kg/m², not pregnant at the time of participation, with no history of urogenital surgery, and without a latex allergy. Recruitment was conducted within the Ottawa community through posters placed in local facilities, targeted social media announcements, and word-of-mouth referrals via academic and healthcare networks. Direct outreach also occurred within the university setting, including seminars, classes, and related events. Interested individuals were invited to contact the research team directly via email or phone. Once initial contact was made, a team member conducted a brief pre-screening interview by phone or in person to describe the study and confirm eligibility before scheduling participation.

The target sample size was 30 nulliparous participants, based on methodological guidelines for reliability studies (Koo & Li, 2016; McGraw & Wong, 1996). Simulations and empirical evidence indicated that 25–30 subjects were generally sufficient to yield stable ICC estimates with acceptable confidence intervals (Bujang & Baharum, 2022; Koo & Li, 2016). For example, assuming an expected ICC of 0.85, an alpha of 0.05, and a desired confidence interval of ±0.10, a sample size of approximately 28 participants would be required (Walter et al., 1998).

3.2. Instruments/Materials

After providing written informed consent, participants completed a brief background questionnaire before undergoing an ultrasound imaging assessment. Demographic and clinical information, including age, height, weight, ethnicity, and gender. Participants completed the International Consultation on Incontinence Questionnaire–Urinary Incontinence Short Form (ICIQ-UI SF), a validated self-report instrument used to screen for the severity of urinary incontinence symptoms, if present (Avery et al., 2004) and subjectively reported other pelvic floor dysfunction symptoms

(constipation, vaginal heaviness, and sexual dysfunction). Together, these instruments were intended to characterize the study sample.

3.3. Image Acquisition

All imaging was performed by the principal investigator, who was trained by postdoctoral fellow S. Vesting and the thesis supervisor, then practiced while being mentored on eight volunteers to ensure familiarity and competence with the acquisition protocol.

Ultrasound SWE imaging was performed using the Aixplorer Multiwave system (SuperSonic Imagine S.A., Aix-en-Provence, France). A high-frequency linear probe (SL 15-4; bandwidth 4–15 MHz) was used for 2D B-mode imaging with an operating frequency between 8 and 12 MHz. The SWE mode generates a colour-coded elastography map (elastogram), ranging from blue, which reflects slow shear-wave propagation through softer tissue, to red, which indicates faster shear-wave propagation through stiffer tissue. The elastogram display range was set to 0–100 kPa (Young's modulus) to avoid saturation, in accordance with prior literature reporting mean values of 26.97 ± 5.03 kPa at rest and 44.33 ± 6.59 kPa during the Valsalva maneuver (Li et al., 2024).

Image quality was optimized by adjusting the overall gain to achieve appropriate brightness, selecting a depth that provided the desired field of view, and refining SWE parameters, such as elastography resolution, by adapting penetration settings in the scanned region. Image depth was adjusted to between 3 and 4 cm to optimize spatial resolution over the entire PC target. A single focal point was positioned at the mid-region of the PC to optimize visualization.

For all acquisitions, probe pressure was minimized to mitigate compression artifacts. This precaution was adopted because probe compression elevates measured stiffness non-linearly: at low pressures, in porcine muscle, incremental probe loading raised SWV mean from 5.29 to 7.21 m/s (Rominger et al., 2018), and a ~10% compression increase in pressure has been reported to double SWV in human superficial soft tissue (Barr & Zhang, 2012; Davis et al., 2019). Frames identified visually as being affected by insufficient SWE filling or artifacts, namely motion-related banding, reverberation, inadequate transducer coupling, and near-field compression, were addressed immediately by adjusting the amount of coupling gel, probe angle and pressure, gain, and penetration mode, and the clip was re-recorded until three acceptable clips had been obtained for each condition.

All participants were instructed to empty their bladder immediately before the ultrasound session. To optimize image quality during measures of the PC in rest in the sagittal plane, a small, single-use intravaginal spacer (IVS) was employed (Figure 1). The spacer was constructed using a latex finger cot filled with water, with a retrieval string attached. The spacer was placed in the distal portion of the vaginal canal to enhance image contrast and improve visualization of vaginal borders. The spacer was either self-inserted by the participant or inserted by the researcher, who is a pelvic health physiotherapist, according to the participant's preference. The device could be removed at any time upon request.

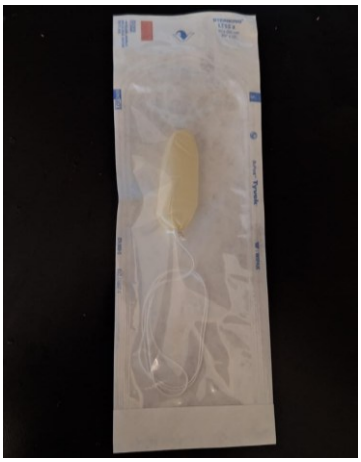


Figure 2. Intravaginal spacer

Given the multilayered organization of the PC and the functional distinctions attributed to its anatomical regions, the protocol included imaging in both the sagittal and transverse planes. In the sagittal plane, the region-of-interest (ROI) was divided into superficial and deep zones, following the conventions established in previous studies (Gong et al., 2024; Santoro et al., 2016). We did not target the deepest layer of the PC, as described by Larson, due to the loss of signal resolution and shear wave propagation in deeper regions based on the high frequency of the probe. Consequently, the zone we designated as “deep” is aligned with the mid-region layer of the PC identified in Larson et al. (Larson et al., 2010).

In the sagittal plane, the probe was placed perpendicular to the perineum to visualize the vaginal canal anteriorly and the anal canal posteriorly, centred over the PC (Figure 2). The PC was visualized as a mixed-echoic, pyramidal fibromuscular structure at a field depth of 3-4 cm. Once the anatomic structure bordering the PC, including the

vaginal and anal canals, was adequately visualized, the IVS was removed before SWE acquisition to avoid interference with shear wave propagation. The same procedure was repeated in the transverse plane by rotating the probe 90° to visualize the superficial transverse perineal muscle and the anterior border of the external anal sphincter, with the probe positioned at an approximate 45° angle (Figure 3). In the sagittal plane, the elastogram box (Field of view) was configured as a rectangle and sized within the borders of the PC. In the transverse plane, the rectangular field of view was placed between the probe surface and the anal sphincter complex (Figure 4). In the transverse plane, the flat probe surface placed against the concave perineum concentrates stress at the transducer edges, producing focal edge-loading artifacts independent of mean pressure (Figure 4); thus, the region of interest excluded these regions. Acquisition geometry was further controlled by centring the elastogram box over the PC, since lateral box placement has been shown to bias measured SWV, plausibly through increased refraction at oblique incidence angles (Lim et al., 2025).

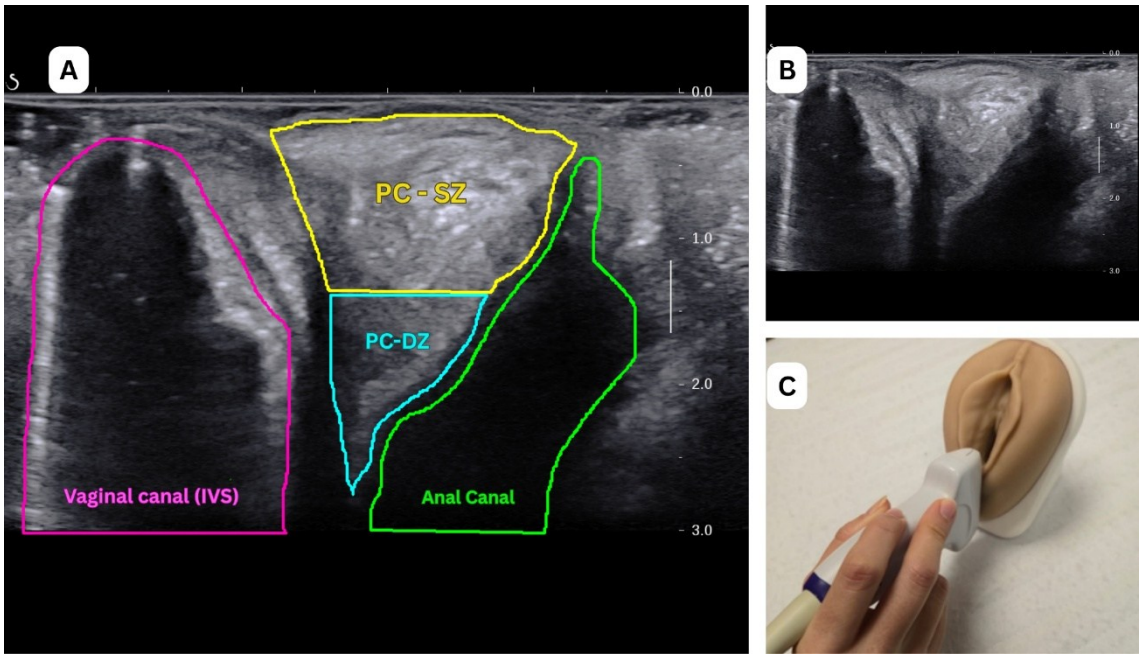


Figure 3. Perineal complex (PC) imaged in the sagittal plane. **(A)** B-mode image of the PC. The yellow outline delineates the PC superficial zone (PC-SZ), and the blue outline represents its deep zone (PC-DZ). The vaginal canal, containing the intravaginal spacer (IVS), is outlined in pink, and the anal canal is outlined in green. Depth is indicated by the scale on the right (cm). **(B)** The same unannotated B-mode image. **(C)** Probe positioning over the perineum with a linear transducer in the sagittal plane, demonstrated on a model.

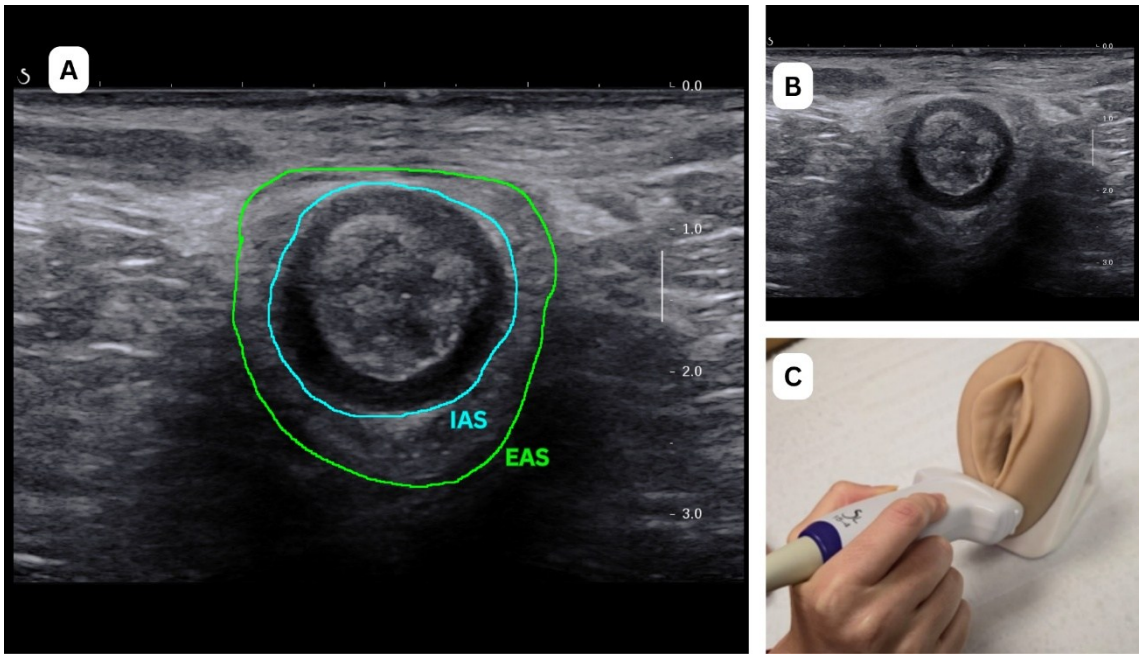


Figure 4. Perineal complex (PC) imaged in the transverse plane. **(A)** B-mode image showing the transverse view at the level of the anal sphincter complex. The extreme boundary of the external anal sphincter (EAS) is outlined in green, and the extreme boundary of the internal anal sphincter (IAS) is outlined in blue. The perineal complex (PC) lies superficial to the sphincter complex in this plane, largely corresponding to the superficial transverse perineal muscle. **(B)** The same unannotated B-mode image. **(C)** Probe positioning over the perineum with a linear transducer in the transverse plane, demonstrated on a model.

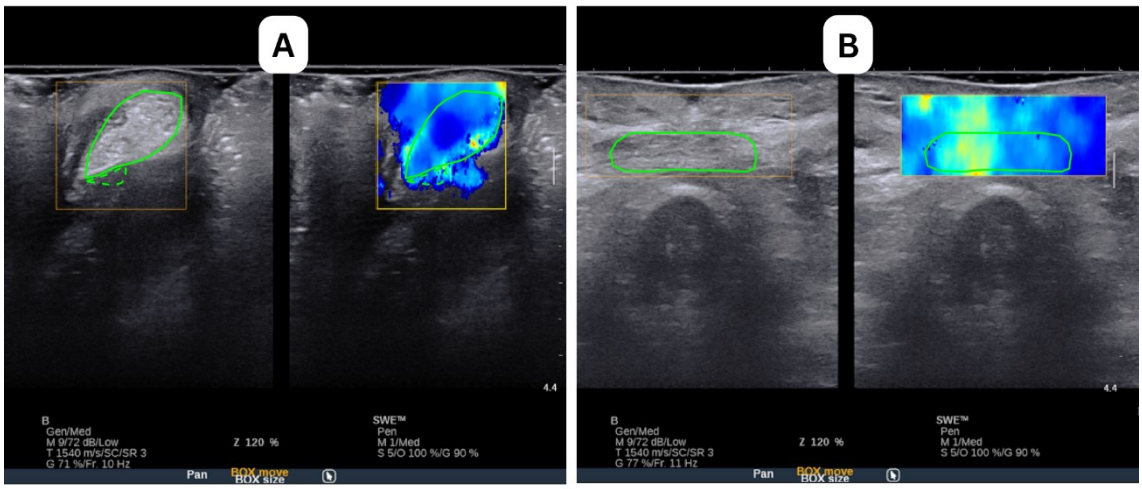


Figure 5. Shear wave elastography (SWE) of the perineal complex in the supine position with the rectangular elastogram field of view indicated. The regions of interest were drawn freehand as indicated in green. **(A)** The sagittal plane view, illustrating two ROIs within the superficial and deep zones of the elastogram field of view. **(B)** Transverse-plane view showing the ROI

SWE images of the PC were acquired in each imaging plane across three postures: supine at rest (unloaded), standing (under gravitational load), and deep squat (passive elongation). The probe was removed and replaced between repeated captures to avoid memory effects. For each posture, participants were instructed to remain as still as possible, refrain from speaking, and pause their breathing at the end of exhalation during image acquisition (Figure 5). Three ten-second video clips were recorded during SWE imaging in each posture and plane. Participants rested for 60–90 seconds between deep squat trials to minimize discomfort and fatigue.

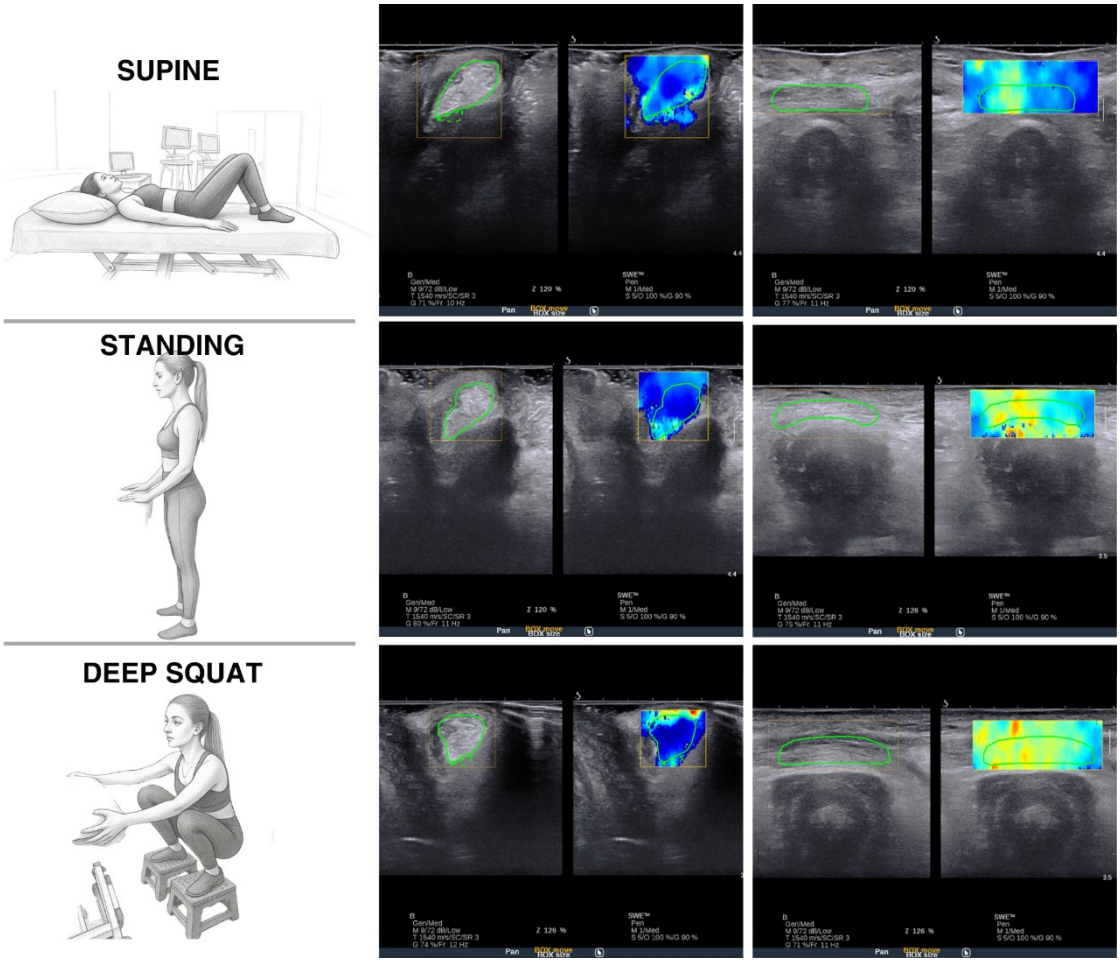


Figure 6. SWE of the PC in sagittal and transverse plane views under three postures.

3.4. Image Analysis

SWV was quantified using a standardized offline post-processing pipeline with four sequential stages (Figure 6): elastogram calibration (Stage 0), smoothing (Stage 1), ROI delineation and quality-control gating (Stage 2), and independent ROI re-delineation and SWV extraction (Stage 3). Stages 0 and 1 were performed once by Rater A (the principal investigator). In Stage 2, Rater A delineated the ROIs in a first session (A1), and

the gates were applied to these ROIs; excluded trials were removed from all subsequent sessions. In Stage 3, Rater A repeated the delineation one week later (A2), and Rater B performed it independently (B). Intra-rater reliability compared A1 with A2, and inter-rater reliability compared A1 with B. Operational details are provided in Appendix D.

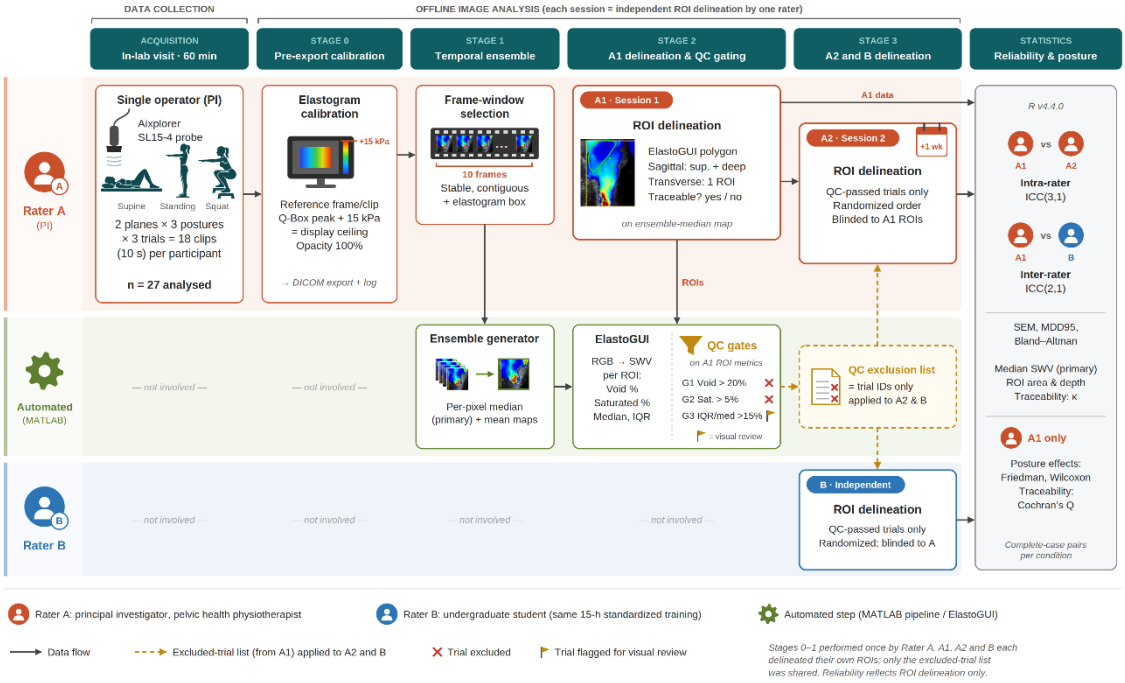


Figure 7. Data collection and image-analysis workflow by operator. Rater A acquired all clips and performed Stages 0–1 once. Quality-control gates were applied to Rater A's first-session ROIs (A1), and the resulting excluded-trial list was applied to Rater A's second session (A2; one week later) and to Rater B's session (B). Each session delineated its own ROIs, in randomized order and blinded to the other sessions. Intra-rater reliability: A1 vs. A2; inter-rater reliability: A1 vs. B. ICC, intraclass correlation coefficient; MDD95, minimal detectable difference (95%); QC, quality control; ROI, region of interest; SEM, standard error of measurement; SWV, shear wave velocity.

3.4.1. Analytical rationale.

Because the analytical methods depart from standard hepatic or muscle SWE, a rationale is provided for each aspect of the procedure. Three constraints distinguished this protocol from conventional SWE analysis and governed every downstream decision. First, the target tissue is morphologically complex, as described in Chapter 2. Because the PC is anisotropic, SWV is direction-dependent, and the elastogram is expected to be spatially non-uniform. Two distinct phenomena follow from this, and the pipeline treats them differently. Our quality-control strategy had to preserve expected tissue heterogeneity while remaining insensitive to localized artefactual pixels. The variation in the colour maps due to changes in fibre orientation across the ROI is an expected property

of the tissues within the PC and is preserved rather than removed, while spatial heterogeneity is flagged for review (Stage 2). Separately, the internal boundaries of this compositionally complex tissue produce reflection and refraction, which cause wave interference that can generate isolated, artefactual high- or low-SWV pixels (Davis et al., 2019; Nitta et al., 2021). Moreover, SWV is distributed unevenly not only spatially but also temporally, fluctuates rapidly during ultrafast acquisition, and is influenced by movement and compression artifacts, such that single images may not yield generalizable SWV measures (Haueise et al., 2025). These outliers are an artifact of estimation and motivate a summary statistic that is robust to them (the ensemble median, Stage 1).

Second, the Stability Index (the Aixplorer's real-time quality metric) is restricted to hepatic and abdominal probe–preset combinations and was not available for the high-frequency linear probe (SL15-4) used, a limitation shared by prior studies that substituted an offline colour-fill metric, the percentage of pixels carrying elasticity values within the ROI, as their quality indicator (Haueise et al., 2025). An offline, multi-stage quality-control strategy was therefore implemented as an alternative.

Third, the system does not export raw radiofrequency data, so post-processing was performed on the exported pseudocolor DICOM images, which encode SWV as a linear red-green-blue (RGB) gradient. Offline decoding of SWV from the RGB colour map is an emerging approach developed to address the limitations of manufacturer-provided analysis tools, which were designed to identify discrete regions of high stiffness in homogeneous tissue rather than to characterize stiffness distribution across anisotropic fibromuscular structures (Haueise et al., 2025). This approach has been validated against on-board system Q-Box measurement in musculoskeletal tissue using the same SL15-4 transducer, with agreement holding when values were decoded as SWV but not as Young's modulus (Haueise et al., 2025). Unlike on-board system Q-box measurements, in which estimates incorporate proprietary signal-quality assessments and spatial smoothing, offline RGB analysis treats every ROI pixel as valid. The pipeline, therefore, applies stricter image-quality criteria than real-time analysis requires (Davis et al., 2019; Haueise et al., 2025).

3.4.2. Stage 0 — Pre-export elastogram calibration.

Before export, a per-trial elastogram calibration was performed on the Aixplorer system. A reference frame was selected from each clip in which the elastogram fill was most complete, the colour distribution was homogeneous, and no motion-related banding

was visible. The peak Young's Modulus within the PC was recorded with the Q-box tool; the display range was set to 15 kPa above that peak, and elastogram opacity was set to 100%. This calibration served two purposes: it maximized the RGB dynamic range by matching the colour gradient to the actual SWV range within each trial, and it positioned the display ceiling a fixed 15 kPa above the observed peak, so that any later saturation within the ROI could be interpreted as an anomalous event rather than faster shear-wave propagation. This calibration strategy aligns with validated practice on the same system. Haueise et al. likewise set an individually chosen display range for each clip before DICOM export to maximize colour resolution, reporting that pilot testing showed higher colour resolution yielded the best agreement between offline and Q-Box results. Their Bland–Altman analysis further demonstrated a proportional bias indicating that decoding performs best when the colormap displays a wide range of colours (Haueise et al., 2025). Per-trial display-range values were adjusted and subsequently exported for each participant, session, posture, and plane for entry during Stages 2 and 3.

3.4.3. Stage 1 — Smoothing.

For each DICOM file, a contiguous window of ten temporally stable frames (including the reference frame from Stage 0) was selected by visual inspection, using temporal consistency of the colour pattern and the absence of banding, flicker, or motion as criteria (Figure 8A). The Aixplorer system acquired duplex B-mode and SWE frames at approximately 11 frames/second. A higher acquisition rate facilitates the selection of temporally stable colour-coded maps and reduces interframe variability. Whereas the representativeness of frame ensembles at high acquisition rates has been questioned specifically for protocols averaging as few as three frames, the ten-frame window used here was drawn from a single stable segment and falls outside that concern (Starzec-Proserpio et al., 2026).

In the absence of the Stability Index, this visual selection followed an established practice: acquiring until propagation contours were parallel and stable before measurement (Lim et al., 2025), and was supported by evidence that automated quality-based frame selection yields liver stiffness values equivalent to expert manual selection (Kang et al., 2026). Within the elastogram box, per-pixel statistics were computed across frames to produce an ensemble median image and an ensemble average frame (Figure 8B); the underlying three-channel (RGB) elastogram was decomposed and processed channel-wise (Lee et al., 2020), a general approach to quantitative elastogram analysis

that has since been extended to calibrated stiffness decoding on the Aixplorer platform (Haueise et al., 2025). The per-pixel median was designated the primary ensemble statistic because it is insensitive to transient high-SWV pixels that affect fewer than half of the frames at a given pixel. This temporal robustness is the first line of prevention against the reflection and refraction outliers described in Section 3.4.1, applied before any spatial extraction or gating. Analyzing the median with the IQR/median serves as a reliability criterion for repeated liver acquisitions, describing agreement across acquisitions of the same site (Ferraioli et al., 2024). That principle was adapted here for a different reason: the suppression of transient artefactual pixels within a single clip, in a tissue far more prone to such artifacts than the liver.

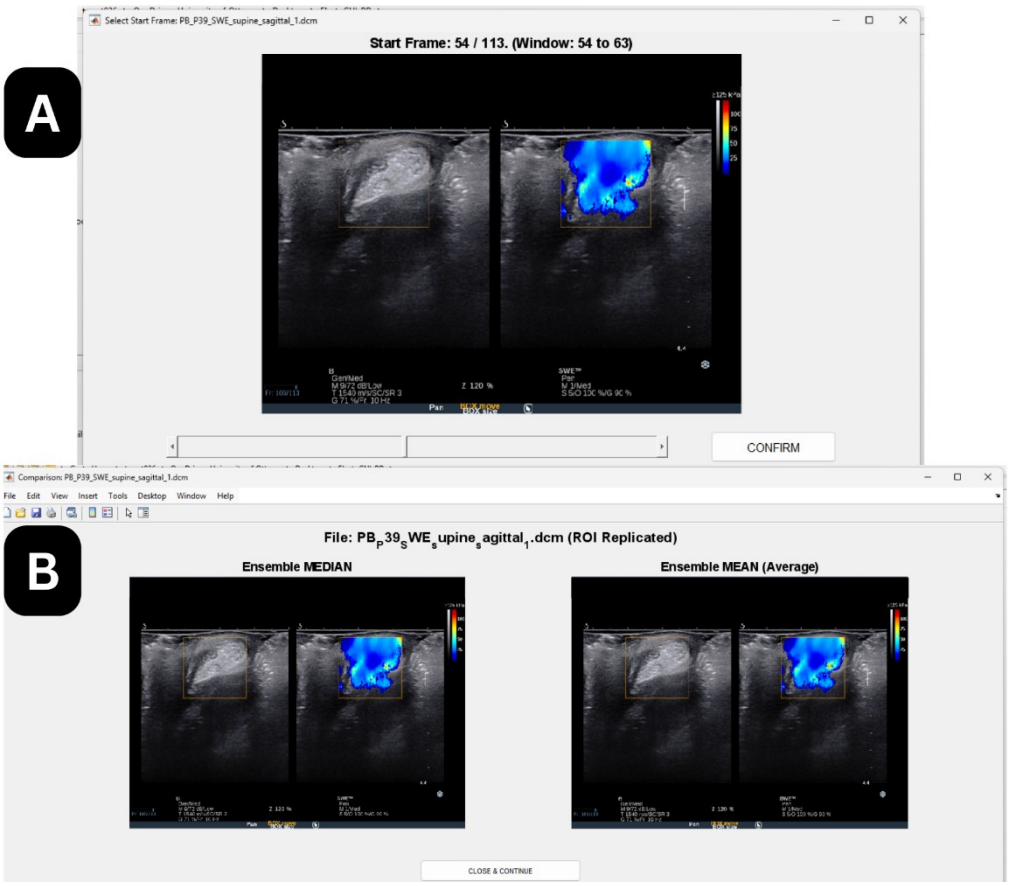


Figure 8. Smoothing. (A) Frame selection; (B) Ensemble median and ensemble averaged colour maps.

3.4.4. Stage 2 — ROI delineation and sequential quality-control gating.

Three pre-specified gates were applied uniformly to all ROI metrics from session A1 before any statistical analyses (Săftoiu et al., 2019). Gate 1 (Elastogram Fill) excluded

trials with Void (%) > 20% within the ROI. This 80% minimum fill criterion was a pragmatic threshold defined for the present study and is not drawn from published guidelines (see limitations). Gate 2 (Ceiling Artifact) excluded trials in which saturated pixels exceeded 5% of the ROI. The display ceiling was set 15 kPa above each trial's Q-Box peak; a saturated pixel was therefore defined as one whose true SWV exceeded the displayed range and was clipped to that upper limit, so its real value would be unknown. Because the transient reflection- and refraction-related outliers described in Section 3.4.1 are already suppressed by the ensemble median colour map (Stage 1), a saturated pixel that survives to this gate recurs consistently across the ten frames rather than a momentary spike. A small, saturated fraction was therefore tolerated as expected tissue anisotropy. When saturation is greater (>5%), however, it may indicate systematic ceiling truncation of the signal: true SWV values exceeding the display range are clipped, biasing the median downward and compromising its validity as a trial summary. Two lines of published evidence support this reasoning. Skerl et al. documented that when values exceeding the colour-map ceiling were clipped to that ceiling, SD estimates from DICOM files were systematically smaller than those obtained from the manufacturer's numeric export in stiffer breast lesions, confirming that ceiling truncation compresses measured dispersion (Skerl et al., 2017). Independently, agreement between offline and on-system measurement is poorest when pixels fall outside the mid-scale colour range (Haueise et al., 2025), which is precisely the condition of a saturated pixel. Under the protocol, where minimal pressure was applied through the ultrasound probe, such widespread saturation is not physiologically expected. No published threshold exists for this tissue; therefore, a 5% limit was set *a priori* for the present study (see limitations).

Gate 3 (Spatial Heterogeneity) did not exclude automatically but flagged trials with IQR/Median > 30% (kPa) or > 15% (m/s) for secondary visual inspection, thresholds adapted from hepatic recommendations (Ferraioli et al., 2018; Săftoiu et al., 2019). Flagging was preferred over automatic exclusion as explained above; the anisotropy of the PC produces higher heterogeneity than liver parenchyma, so applying the same threshold risked over-excluding valid trials (Davis et al., 2019; Moura et al., 2025).

3.4.5. Stage 3 — ROI-based SWV extraction.

Ensemble medians and ensemble averaged colour maps were analyzed in ElastoGUI, a MATLAB interface that encodes the RGB pseudocolor gradient from the exported elastogram in Young's Modulus (kPa) (stage 0) and obtains the SWV (m/s) by

conversion (Doguet et al., 2019). The per-trial saturation value ([Peak + 15 kPa]) was entered first to calibrate the RGB-to-SWV mapping. The software reads the colour bar displayed in each image to build a reference scale, then assigns every pixel the value of the closest matching colour on that scale. The saturation value sets the upper end of the scale, so an incorrect entry would shift all derived values by a constant factor; therefore, each entry was verified. PC boundaries were then delineated using a propagating freehand polygon that applied the same geometry to the ensemble-median and ensemble-mean colour maps simultaneously, eliminating variability in boundary selection among trials. In the sagittal plane, two ROIs were drawn on the ensemble median: a superficial ROI at the base of the triangular PC and a deep ROI at its apex (Figures 4 and 8). In the transverse plane, a single ROI followed the hyperechoic band superior to the external anal sphincter, bounded laterally by the sphincter diameter (Figure 4). Void regions corresponding to the anal and vaginal canals, where shear waves could not propagate, were excluded from all polygons (Davis et al., 2019). An ROI was recorded as traceable only when the rater judged the ROI to show sufficient elastogram fill, together with a B-mode image of adequate quality to delineate the region (neither excessively blurred nor markedly hypoechoic); acquisitions not meeting this criterion yielded no valid trial for that participant, posture, and zone.

For each ROI, ElastoGUI returned the summary metrics: mean, median, IQR, and SD of Young's Modulus and SWV, together with Void (%) and Saturated (%). Void (%) within the freehand polygon; the software additionally reported void fraction across the full elastogram box, which was not used for gating. Median SWV (m/s) was the primary outcome. While Young’s modulus values were retained descriptively, statistical analyses were performed using SWV only.

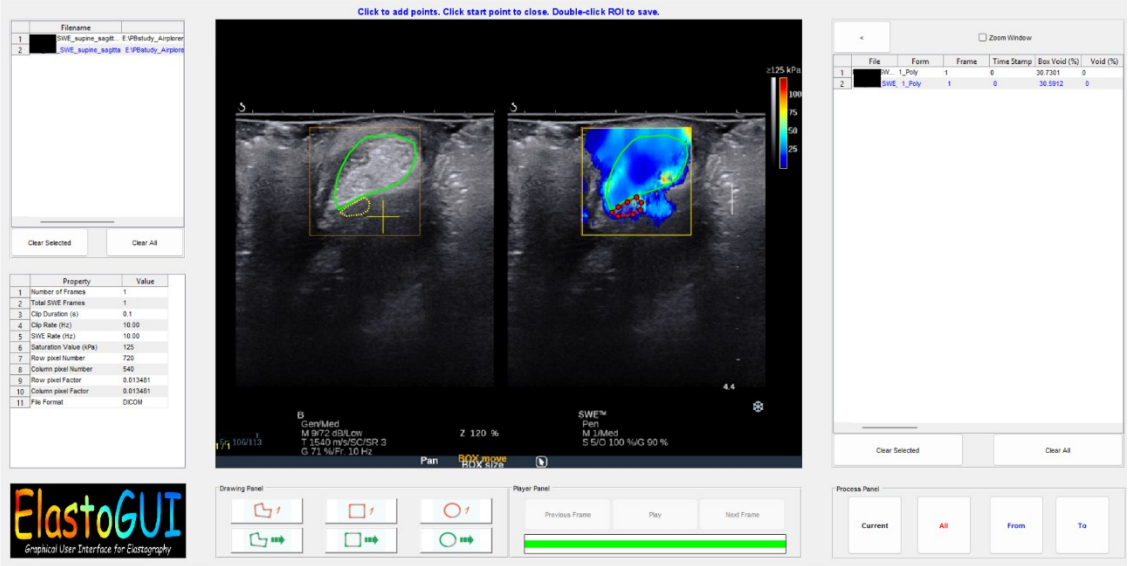


Figure 9. ElastoGUI (MATLAB) interface during region of interest (ROI) delineation of the perineal complex on a sagittal supine trial. Showing the co-registered B-mode image (left) and the elastogram (right). A freehand ROI polygon traced within the elastogram box was replicated onto the B-mode image, and, per ROI, the median SWV (m/s), Void (%), and Saturated (%) are returned in the results panel (right).

3.4.6. Assessor Training, Independent Assessment, and Bias Mitigation

Image analysis was conducted by two raters. Rater A was the principal investigator, who is a pelvic health physiotherapist with prior clinical experience in pelvic floor assessment, and Rater B was an undergraduate student in Human Kinetics working under the postdoctoral fellow's supervision. Both completed the same standardized training protocol (minimum of 15 hours) of one-on-one training in PC ultrasound imaging and SWE ElastoGUI-based analysis. Beyond this training, Rater A had additional exposure to the images through acquisition and Stages 0–1. Neither had prior experience with SWE of the PC, which had not previously been characterized using the methods described here.

3.4.7. Intra-rater reliability

Within-rater reliability was assessed by having the primary rater (assessor) repeat all outcome measurements twice on the same acquired images. The second rating session occurred one week after the first. The image sets were presented in a randomized order, and the rater was blinded to the order of acquisition and to their previous measurements, thereby reducing memory and expectation bias.

3.4.8. Inter-rater reliability

Between-rater reliability was evaluated by having Rater B independently delineate the ROIs on the same ensemble colour maps (Stage 3), in randomized order and blinded to Rater A's traceability decisions, ROIs, and values. Both raters followed the same standardized protocol as described in the image analysis section. Any uncertainties regarding protocol interpretation were adjudicated by the thesis supervisor, who did not participate in primary measurements to avoid bias.

3.5. Outcome measures

The primary outcome was the SWV (m/s) of the PC. Inter- and intra-rater reliability was assessed independently for each combination of imaging plane, depth zone, and posture. One secondary analysis involved the intra- and inter-rater reliability of user-selected ROI geometry, namely ROI area and centre depth, derived from the B-mode and elastogram images. Another secondary analysis explored whether SWV differed across the three postures.

3.6. Data Analysis

All statistical analyses were performed using R (v4.4.0). Incomplete elastogram filling or unstable shear-wave propagation that prevented extraction of a stiffness value was classified as missing for that posture or plane, and all reasons for missingness (e.g., insufficient elastogram box filling, artifacts, or inability to delineate the PC) were systematically documented. Excluded trials differed systematically across postures, with more trials excluded in the deep zone of the PC imaged in the sagittal plane. Reliability was therefore estimated on a complete-case basis within each condition: only participant–condition cells with a value from both raters (inter-rater) or sessions (intra-rater) entered the reliability analysis, and the number of paired data points is reported for every condition (superficial vs deep zone; supine, standing, and squat).

Descriptive statistics were computed to summarize all quantitative variables. The normality of data distributions was assessed using the Shapiro–Wilk test. Variables with normal distributions were reported as mean ± standard deviation, while non-normally distributed variables were reported as median and interquartile range. Reliability analyses were conducted following best-practice recommendations for studies of measurement reproducibility (Koo & Li, 2016; McGraw & Wong, 1996).

For continuous variables (SWV), intraclass correlation coefficients (ICCs) were calculated using two-way analysis of variance models based on absolute agreement. Inter-rater reliability was assessed using a two-way random-effects model [ICC(2,1)], while intra-rater reliability was evaluated using a two-way mixed-effects model [ICC(3,1)], following the guidelines by Koo and Li and McGraw and Wong (Koo & Li, 2016; McGraw & Wong, 1996). All ICC point estimates were reported with 95% confidence intervals, calculated using the F-distribution method, and interpreted according to the benchmarks proposed by Koo and Li: < 0.50 = poor, 0.50–0.75 = moderate, 0.75–0.90 = good, and > 0.90 = excellent (Koo & Li, 2016). ICC analyses assumed approximate normality of model residuals; if severe non-normality was detected via Q–Q plot inspection and the Shapiro–Wilk test, results were interpreted with caution and accompanied by a sensitivity note. The standard error of measurement (SEM) was calculated as SEM = √MS_error, where MS_error is the mean square error term extracted from the two-way ANOVA model. The minimal detectable difference at the 95% confidence level (MDD_{95}) was computed as $MDD_{95} = SEM \times 1.96 \times \sqrt{2}$. These indices quantified measurement precision and the smallest detectable difference beyond within- and between-rater measurement error. Bland–Altman plots were used to visualize bias and limits of agreement. Because Bland–Altman analysis assumes symmetric distribution of measurement differences, residuals were visually inspected (histograms and Q–Q plots) to confirm acceptable distributional patterns. If proportional bias was detected, regression-adjusted limits of agreement were reported.

To characterize within-subject variation in SWV across postures, an exploratory postural comparison was conducted independently for each imaging plane (sagittal superficial, sagittal deep, and transverse), using the median SWV (m/s) from the principal investigator's first session. Because ROI traceability was expected to vary by posture, particularly in the deep sagittal zone, where elastogram fill is most sensitive to acquisition conditions, missingness was not assumed to be uniform across postures. Postural comparisons were therefore restricted to participants with valid data in all three postures within a given zone (complete-case analysis); the contributing sample size is reported per zone, and the resulting potential for selection bias is acknowledged as a limitation.

Postural differences in SWV were evaluated using the Friedman test in each image plane and zone, with supine as the reference condition. Pairwise post hoc contrasts were assessed using the Wilcoxon signed-rank test, Bonferroni-corrected for three comparisons. A uniform non-parametric approach was adopted across all zones given the

small number of complete cases per zone (as few as eight participants in the sagittal deep zone) and the exploratory nature of the analysis. Normality of the within-subject differences was inspected per contrast (Shapiro–Wilk test and Q–Q plots) and used solely as a descriptive flag: effect sizes for contrasts whose differences departed from normality were marked as fragile, but the test applied was not changed. Each contrast was benchmarked against the larger of the two intra-rater MDD95 values for the involved postures; differences exceeding this threshold were considered to exceed measurement-error bounds.

To test whether ROI traceability, rather than SWV, depended on posture, a complementary analysis was performed in the deep zone imaged in the sagittal plane on the binary outcome of whether a traceable ROI (Stages 2 and 3) was obtained in at least one trial per participant and posture. Equality of traceability proportions across postures was tested using Cochran's Q test**,** with Bonferroni-corrected pairwise McNemar tests as post hoc contrasts. Given the small sample and potentially extreme proportions, exact (Clopper–Pearson) 95% confidence intervals were reported, and Cochran's Q was interpreted as supportive rather than confirmatory. This analysis addressed posture-dependent acquisition feasibility and quantified the posture-dependent missingness.

4. Chapter 4 – Results

A total of 30 participants were recruited; of these, data from three were excluded owing to corrupted or missing DICOM files during the exportation stage (P01, P02, P38), yielding a final analytic sample of n=27. Participant characteristics are summarised in Table 2. While some participants had mild symptoms of incontinence, no participant scored in the moderate- or high-severity categories on the ICIQ-UI SF (Klovning et al., 2009). Two participants (7.4%) reported symptoms of chronic constipation and three (11.1%) reported sexual dysfunction; no participant reported fecal incontinence or symptoms of pelvic organ prolapse.

Table 1. Participant Characteristics (nulliparous females, n = 27).

Characteristic	Value
Anthropometric and demographic	**mean ± SD**
Age, years	26.1 ± 5.9
Height, cm	165.0 ± 7.5
Weight, kg	64.0 ± 13.2
Body mass index, kg/m²	23.4 ± 4.3
Ethnicity	**n (%)**
White	9 (33.3)
Latin American	7 (25.9)
Middle Eastern	4 (14.8)
White / Latin American	2 (7.4)
Black / African	2 (7.4)
Mixed	2 (7.4)
South Asian	1 (3.7)
Menstrual status	
Menstruating	20 (74.1)
Not menstruating (incl. IUD/implant)	5 (18.5)
Irregular	2 (7.4)
Urinary continence (ICIQ-UI SF)	
No leakage (score 0)	20 (74.1)
Mild leakage (score 1–5)	7 (25.9)

SD, standard deviation; ICIQ-UI SF, International Consultation on Incontinence Questionnaire–Urinary Incontinence Short Form; IUD, intrauterine device.

The number of included trials differed across postures and image planes. In the superficial zone, images from all 27 participants were included for every posture. In the transverse plane, images from all 27 participants were included when performed in supine, and images from 26 participants were included when imaged in the standing and deep-squat postures. In the deep zone, the number of included images was lower and was posture-dependent (17 in supine, 12 in standing, and 23 in the deep squat). The number

of images included in the deep zone reflects exclusions based on the quality-control gates rather than incidental participant-level missingness (Section 3.4.3); full per-posture image counts across all planes are reported in Supplementary Material, Table S1. Because the effective sample size differed across conditions, the descriptive estimates in this section are reported per condition and are not contrasted across them**.**

The Shapiro–Wilk test identified non-normality in at least two conditions for each reported variable: median SWV (3 of 9 conditions), ROI area (3 of 9, all in the deep zone), ROI centre depth (2 of 9), and ROI void percentage (9 of 9). These data are therefore uniformly presented as median [interquartile range]; means and standard deviations are provided in Supplementary Material, Table S1.

Median SWV was lowest in the supine and highest in the deep squat posture across imaging planes, except in the deep zone, where the highest value occurred in standing. Within standing and deep squat postures, the deep zone yielded the highest velocity estimates but also the smallest ROI area and the largest ROI centre depth. ROI void percentage remained below one in all conditions.

Table 2 Perineal Complex Shear Wave Velocity and Region-Of-Interest Geometry Presented by Posture, Image Plane, and Zone.

Posture	Plane – zone	n	SWV (m/s)	ROI area (cm²)	ROI depth (cm)	ROI void (%)
Supine	Sagittal – superficial	27	2.45 [2.12, 2.93]	0.58 [0.47, 0.74]	0.83 [0.75, 0.95]	0.11 [0.04, 0.25]
	Sagittal – deep	17	2.31 [2.09, 3.91]	0.08 [0.06, 0.12]	1.30 [1.20, 1.46]	0.55 [0.00, 1.18]
	Transverse	27	2.50 [2.20, 2.74]	1.10 [0.98, 1.19]	0.93 [0.81, 1.06]	0.00 [0.00, 0.11]
Standing	Sagittal – superficial	27	2.69 [2.44, 3.10]	0.48 [0.43, 0.69]	0.88 [0.78, 1.04]	0.19 [0.11, 0.39]
	Sagittal – deep	12	4.53 [3.49, 5.43]	0.07 [0.05, 0.10]	1.31 [1.26, 1.42]	0.27 [0.00, 0.72]
	Transverse	26	2.75 [2.52, 3.28]	1.06 [0.93, 1.15]	0.85 [0.75, 1.05]	0.00 [0.00, 0.02]
Deep squat	Sagittal – superficial	27	3.49 [3.00, 3.82]	0.47 [0.38, 0.52]	0.69 [0.61, 0.78]	0.29 [0.13, 0.93]
	Sagittal – deep	23	4.03 [3.34, 5.24]	0.07 [0.06, 0.12]	1.19 [1.11, 1.27]	0.05 [0.00, 1.08]
	Transverse	26	3.80 [3.48, 4.56]	1.01 [0.89, 1.15]	0.69 [0.66, 0.84]	0.00 [0.00, 0.00]

Note. Rater A, first session; Values are medians [interquartile range (IQR)], n is the number of participants contributing a valid data point to each posture × plane × zone, computed and differs across conditions due to image exclusion based on the quality-control gates. Attrition is concentrated in the deep zone imaged in the sagittal plane. SWV, shear wave velocity; ROI, region of interest.

4.1. Reliability of Shear Wave Velocity

The intra- and inter-rater reliability of median SWV, derived from the ensemble median colour map, across conditions is presented in Table 3. Intra-rater reliability [ICC(3,1)] was excellent in all nine conditions, ranging from 0.968 to 0.995. Inter-rater reliability [ICC(2,1)] was excellent in six of the nine conditions (range 0.951–0.989) and good in the three deep zone conditions. The inter-rater reliability estimate of SWV in the deep zone acquired in the standing position is considered underpowered due to the low effective sample size (n=12). Inter-rater MDD_{95} of SWV observed in the deep zone of the PC in all positions (supine 1.27 m/s, standing 1.20 m/s, deep squat 1.32 m/s) was approximately four to seven times greater than that observed in the superficial zone and in the transverse plane (range 0.18–0.31 m/s). This divergence is illustrated in Figure 10, which contrasts the widest and narrowest between-rater limits of agreement. The Bland–Altman plots for the remaining conditions are provided in Supplementary Figures S1, S2 and S3, and the corresponding bias and limits of agreement for all 18 conditions are presented in Supplementary Table S6.

Systematic (rater) bias was observed in several conditions across both inter- and intra-rater reliability and in both imaging planes (Table 3, footnote). While the bias was non-normal in 11 of the 18 conditions, the limits of agreement are reported parametrically (bias ± 1.96 SD) for consistency and comparability across conditions, with non-parametric values provided in Supplementary Table S6.

A sensitivity analysis using the mean SWV, derived from the ensemble averaged colour map, as the outcome of interest yielded the same result, confirming that the reliability estimates were not driven by the choice of mean vs median as the measure of central tendency (Supplementary Table S4/S5).

Table 3. Intra-rater and Inter- rater Reliability of Shear Wave Velocity (m/s) recorded from the perineal complex in different imaging planes, zones and participant positions.

Posture	Plane-Zone	SWV (m/s) [IQR]	INTRA-RATER				INTER-RATER			
			n	ICC [95% CI]	SEM	MDD $_{95}$	n	ICC [95% CI]	SEM	MDD $_{95}$
Supine	Sagittal – superficial	2.45 [2.12, 2.93]	27	0.982 [0.960, 0.992]	0.080	0.221	27	0.951 [0.838, 0.981]	0.112[a]	0.310
	Sagittal – deep	2.31 [2.09, 3.91]	16	0.975 [0.930, 0.991]	0.221	0.611	17	0.882 [0.709, 0.955]	0.460	1.274
	Transverse	2.50 [2.20, 2.74]	27	0.968 [0.931, 0.985]	0.076[a]	0.211	27	0.970 [0.919, 0.987]	0.066[a]	0.183
Standing	Sagittal – superficial	2.69 [2.44, 3.10]	27	0.987 [0.971, 0.994]	0.063	0.174	27	0.957 [0.893, 0.981]	0.106[a]	0.295
	Sagittal – deep	4.53 [3.49, 5.43]	12	0.995 [0.981, 0.998]	0.100	0.276	12	0.872 [0.627, 0.961]	0.433	1.200
	Transverse	2.75 [2.52, 3.28]	26	0.979 [0.954, 0.991]	0.085[a]	0.237	26	0.983 [0.962, 0.992]	0.078	0.215
Deep squat	Sagittal – superficial	3.49 [3.00, 3.82]	27	0.987 [0.971, 0.994]	0.108[a]	0.298	27	0.986 [0.955, 0.995]	0.100[a]	0.277
	Sagittal – deep	4.03 [3.34, 5.24]	23	0.977 [0.946, 0.990]	0.206	0.571	22	0.864 [0.702, 0.941]	0.475	1.315
	Transverse	3.80 [3.48, 4.56]	26	0.988 [0.973, 0.995]	0.084	0.232	26	0.989 [0.976, 0.995]	0.079	0.218

Shear wave velocity (SWV) [Interquartile range (IQR)] is the reference distribution derived from rater A at the first session. Intraclass correlation coefficients (ICCs) with 95% confidence intervals are presented for SWV determined using the median of the ensemble-median colour maps. n = participants with paired ratings (complete-case) and differs between columns where the number of extractable trials differed. [a] indicates a systematic difference between raters ($p < 0.05$): SEM reflects random error. *Abbreviations:* CI, confidence interval; MDD_{95}, minimal detectable difference at 95% confidence.

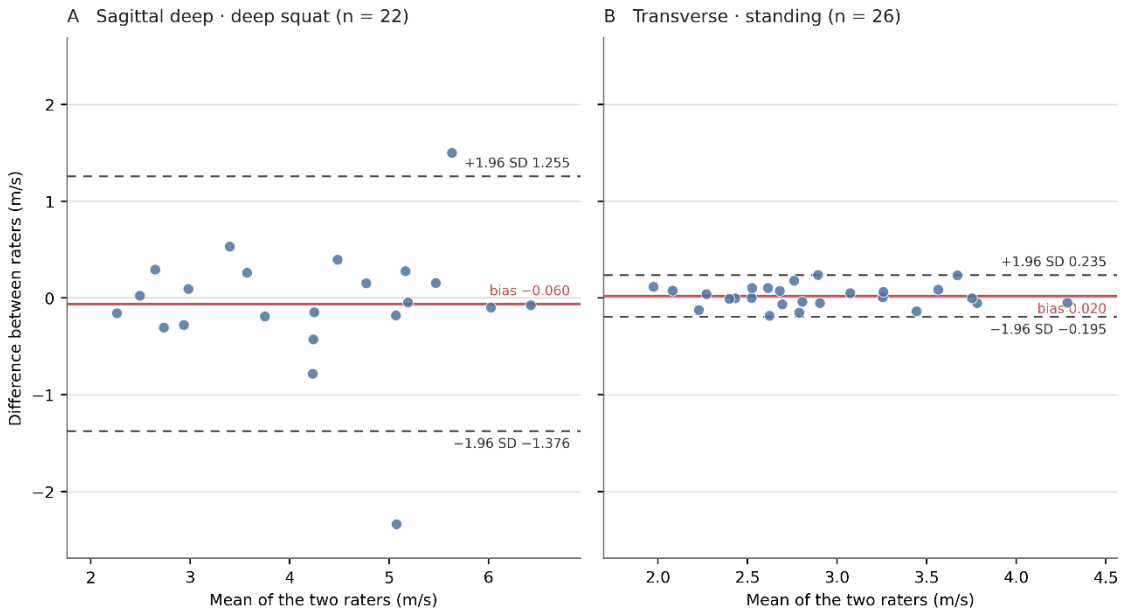


Figure 10. Bland–Altman plots representing the inter-rater agreement for the median shear wave velocity (m/s) in (A) the deep zone of the perineal complex imaged in the sagittal plane with the participant in a deep squat (n = 22) (bias −0.060 m/s; 95% limits of agreement −1.376 to +1.255 m/s) and (B) the perineal complex imaged in the transverse plane with the participant in standing (n = 26) (bias +0.020 m/s; 95% limits of agreement −0.195 to +0.235 m/s). Both panels share the same vertical scale. Solid line = bias; dashed lines = 95% limits of agreement.

4.2. Reliability of Region-of-Interest Geometry

The reliability of the ROI centre depth and area is reported in Table 4. The reliability of the ROI centre depth was good to excellent throughout, whereas the reliability of the ROI area was lower; several conditions reached only poor or moderate agreement.

Table 4. Intra- and inter-rater reliability of region-of-interest (ROI) geometry across postures and plane–zones.

Posture	Plane-Zone	Intra-Rater ICC [95% CI]			Inter-Rater ICC [95% CI]		
		n	ROI depth	ROI area ICC	n	ROI depth	ROI area ICC
Supine	Sagittal – superficial	27	0.972 [0.941, 0.987]	0.838 [0.675, 0.923]	27	0.917 [0.829, 0.961]	0.627 [−0.003, 0.860]
	Sagittal – deep	16	0.946 [0.852, 0.981]	0.138 [a] [−0.368, 0.582]	17	0.932 [0.826, 0.975]	0.225 [a] [−0.243, 0.620]
	Transverse	27	0.863 [0.722, 0.935]	0.698 [0.438, 0.850]	27	0.869 [0.732, 0.938]	0.319 [a] [−0.044, 0.613]
Standing	Sagittal – superficial	27	0.989 [0.977, 0.995]	0.938 [0.869, 0.971]	27	0.957 [0.898, 0.981]	0.731 [0.130, 0.903]
	Sagittal – deep	12	0.969 [0.897, 0.991]	0.793 [0.428, 0.936]	12	0.970 [0.900, 0.991]	0.627 [0.149, 0.874]
	Transverse	26	0.948 [0.887, 0.976]	0.641 [0.345, 0.822]	26	0.926 [0.844, 0.966]	0.377 [a] [0.018, 0.657]
Deep squat	Sagittal – superficial	27	0.987 [0.971, 0.994]	0.908 [0.808, 0.957]	27	0.980 [0.956, 0.991]	0.608 [−0.075, 0.863]
	Sagittal – deep	23	0.935 [0.854, 0.972]	0.818 [0.619, 0.919]	22	0.954 [0.891, 0.980]	0.949 [0.867, 0.980]
	Transverse	26	0.941 [0.873, 0.973]	0.744 [0.507, 0.876]	26	0.942 [0.859, 0.975]	0.371 [a] [0.004, 0.654]

Intraclass correlation coefficients (ICCs) with 95% confidence intervals are presented for the depth of the region-of-interest (ROI) centre (cm) and the ROI area (cm²), the two geometric descriptors of the polygon traced for SWV extraction. n = participants with paired ratings (complete-case) and differs between columns where the number of extractable trials differed. [a] indicates poor agreement (ICC < 0.50).
CI, confidence interval; ICC, intraclass correlation coefficient; ROI, region of interest.

4.3. Trial attrition and deep-zone ROI traceability

Trial attrition per rater × condition is reported in Supplementary Table S1. In the superficial zone imaged in the sagittal plane and in the transverse plane, the proportion of valid trials was high across postures (87.7–100%). In the deep zone imaged in the sagittal plane, the proportion of valid trials was lower and was posture-dependent, driven predominantly by untraceable ROIs (Stage 3) rather than by quality-control exclusions (Stage 2); For Rater A (first session), the proportion of invalid trials was 43.2% in supine (35 of 81: 34 not traced, 1 quality-control excluded), 63.0% in standing (51 of 81: 47 not traced, 4 excluded), and 33.3% in the deep squat (27 of 81: 18 not traced, 9 excluded).

Inter- and intra-rater agreement on ROI traceability (Stage 3; traced vs. not traced, paired trials; Supplementary Tables S2 and S3) was substantial within raters ($\kappa = 0.755$;

88.2% agreement; 229 paired trials) and fair between raters ($\kappa = 0.337$; 69.4% agreement; 229 paired trials). In most cases, rater B traced more ROIs than rater A (60 trials).

4.4. Comparison of Shear Wave Velocity Among Postures

The complete-case sample size differed markedly across planes and zones (sagittal-superficial n = 27, transverse n = 25, sagittal-deep n = 8), and the three zones were therefore not compared with one another. The Friedman omnibus test indicated a posture effect in the superficial zone and in the transverse plane. Pairwise contrasts (Wilcoxon signed-rank, Bonferroni-corrected; Cohen's dz) are reported in Table 6. In the deep zone, the omnibus test was non-significant, therefore, no pairwise contrasts were pursued for this zone (Table 5). In the superficial zone, SWV was higher in deep squat than in both standing and supine, and both differences exceeded the MDD_{95}, whereas SWV in standing and supine did not differ and lay within measurement error. In the transverse plane, SWV was highest in deep squat and lowest in supine, and all three pairwise differences exceeded the MDD_{95}.

Table 5. Friedman Omnibus Contrasts: Exploratory Postural Comparison of Shear Wave Velocity.

Plane-Zone	Complete-case N	χ^2	df	p
Sagittal – superficial	27	13.41	2	0.0012*
Sagittal – deep	8	1.00	2	0.6065
Transverse	25	32.00	2	<0.0001*

Postural differences in SWV were tested by the Friedman test in each posture (supine as reference); complete-case analysis, with the contributing sample reported per plane-zone. The deep zone (n = 8) is likely underpowered and thus its non-significant result cannot be interpreted as evidence of no postural effect. * $p < 0.05$. df, degrees of freedom.

Table 6. Bonferroni-corrected Wilcoxon Pairwise contrasts comparing Shear Wave Velocity among postures.

Plane-Zone	Contrast	n	Mean diff (m/s)	p	Cohen's dz	vs MDD_{95}
Sagittal – superficial	standing − supine	27	0.154	0.2995	0.319	within
	deepsquat − supine	27	0.775	0.0014	0.817	beyond
	deepsquat − standing	27	0.621	0.0020	0.739	beyond [a]
Transverse	standing − supine	25	0.441	0.0045	0.859	beyond
	deepsquat − supine	25	1.585	<0.0001	2.009	beyond [a]
	deepsquat − standing	25	1.144	0.0002	1.303	beyond

Pairwise contrasts testing differences in SWV at the superficial zone in the sagittal plane (sagittal-superficial) and the transverse plane. The MDD_{95} benchmark is the larger of the two values for each posture in the contrast; "beyond" and "within" denote differences exceeding or falling within this benchmark. The deep zone contrasts are not reported because the omnibus was non-significant. [a] Within-subject differences were non-normal (Shapiro–Wilk, $p < 0.05$); this flags the effect-size estimate only and did not alter the test applied. dz, Cohen's dz; MDD_{95}, minimal detectable difference at 95% confidence.

A complementary analysis tested whether deep-zone ROI traceability depended on posture (Table 7; N = 27). Traceability denotes whether an ROI could be delimited at all (extractability), and a colour map was deemed traceable if at least one valid trial was traceable for a given participant. It is, therefore, a construct distinct from value agreement (ICC) and tracing agreement (κ). Traceability was highest in the deep squat, lowest in standing, and intermediate in supine. Cochran's Q indicated a difference across postures. Among participants whose traceability differed between two postures, the ROI was traceable in the deep squat but not in standing in every case. The confidence intervals were wide and overlapping, reflecting the small sample; thus, this analysis is considered supportive rather than confirmatory.

Table 7. Deep-zone ROI traceability by posture

Posture	Traceable (n / 27)	Proportion	95% CI
Supine	17	0.630	0.424, 0.806
Standing	12	0.444	0.255, 0.647
Deep squat	23	0.852	0.663, 0.958

Proportion of participants in whom the deep-zone ROI was traceable; traceability as defined in Section 3.4. 95% CIs are Clopper–Pearson exact intervals. Cochran's Q = 10.71, df = 2, p = 0.0047; in pairwise exact McNemar tests (Bonferroni-corrected for three contrasts), only deep squat versus standing was significant (p = 0.0029*).* CI, confidence interval; df, degrees of freedom; ROI, region of interest.

5. Chapter 5 – General Discussion

5.1. Summary of findings

Overall, among nulliparous females who were predominantly continent, with a minority presenting mild symptoms of urinary incontinence, stiffness of the PC**,** inferred from SWV, could be analyzed reproducibly. Drawn from a diverse Canadian female cohort, these findings may serve as a normative baseline for non-disrupted PC mechanical properties, providing a reference for comparison with clinical populations such as postpartum or those with PFDs. In the supine position, baseline median SWV values were 2.45 m/s in the superficial zone and 2.50 m/s in the transverse plane.

The superficial zone of the PC imaged in the sagittal plane broadly corresponds to the ROI evaluated in previous PC elastography literature. Direct comparison across studies is constrained by differences in reporting metrics, as earlier reports quantified stiffness using Young's modulus. When converted to a mean-based equivalent, the superficial-zone stiffness found in this study (24.3 kPa) aligns closely with resting values reported for nulliparous controls by Zhou et al. (23.8 kPa) and Li et al. (26.9 kPa) (Li et al., 2024; Zhou et al., 2023).

Reliability was excellent within the same rater across all conditions, and between raters across all postures when measured in the transverse plane and in the superficial zone imaged in the sagittal plane. Imaging in the transverse plane, which focuses on the superficial transverse perineal muscle above the external anal sphincter, an approach not previously reported in the literature, yielded excellent reliability of SWV within and between raters and in all three postures. In contrast, visualization and signal fidelity within the deep zone of the PC presented challenges, resulting in a high proportion of trials being excluded from the analysis, particularly when images were acquired in the standing position. Among the smaller number of images that met the quality criteria within this zone, the reliability of SWV was good.

The reliability metrics for the SWV estimates were strong despite poor-to-moderate reliability of the ROI area identified across raters, indicating that the SWV computed using the analysis pipeline presented in this thesis is robust to variation in the size of the ROI determined by the rater. Finally, the exploratory analysis suggests that the SWV of the PC is responsive to changes in tissue loading and passive elongation, with

the deep squat position significantly elevating stiffness while optimizing signal recovery and ROI traceability in the deep zone (85.2%) and appears to provide an adequate load to evaluate the biomechanical function of the PC.

5.2. Reliability of Shear Wave Velocity Determined in the Perineal Complex

The median SWV of different regions within the PC extracted from the ROI delineated from the generated ensemble-median colour map was reproducible in all conditions. In the superficial zone imaged in the sagittal plane and in the transverse plane, intra- and inter-rater reliability were both excellent. The sensitivity analysis that compared the findings using the ensemble average instead of the ensemble median colour map confirmed that the image analysis protocol was robust. The reliability metrics for SWV were slightly lower in the deep zone of the PC. The most likely reason was signal attenuation. Where the elastogram was fully infilled, two raters had little room to diverge; where it was sparse, the raters' choice of traceable pixels drove higher variance.

Consistent with the reliability metrics, the minimum detectable difference (MDD_{95}) was smaller in the superficial regions across both planes than in the deep zone. Error variance was lowest in the transverse plane, where the MDD_{95} ranged from 0.18 to 0.22 m/s across postures, equivalent to 6 to 8% of the median SWV. It remained low in the superficial zone imaged in the sagittal plane (0.28 to 0.31 m/s, or 8 to 13%). In the deep zone, the MDD_{95} was four to seven times wider (1.20 to 1.32 m/s, or 26 to 55%), reaching its highest fraction in supine, where resting SWV is lowest, indicating that only large differences would be detectable. Where there was significant bias between- or within-raters, it was minimal, ranging from 0.05 to 0.10 m/s and thus well below the MDD_{95}.

To date, available SWE reliability data for the PC are limited to protocols that evaluated superficial layers and combined acquisition and analysis variance into a single coefficient. The closest methodological comparator to the current study is a conference abstract by Starzec-Proserpio et al., who also performed offline analysis of SWV on the PC using MATLAB. They reported good-to-excellent intra-rater reliability (ICC 0.69 to 0.89) and fair-to-good inter-rater reliability (ICC 0.48 to 0.69). For the transverse perineal muscle, the closest correspondent to the PC imaged in the transverse plane in this study, reproducibility was good to excellent within and between raters (ICC 0.79-0.95 and ICC 0.72-0.89, respectively). While their methods resemble ours, the abstract format limits

access to key details for direct comparison. Further, in the study by Starzec-Proserpio et al., values acquired at rest and during contraction of the pelvic floor muscles were merged rather than providing state-specific ICCs (Starzec-Proserpio et al., 2023).

Li et al. also reported on the reliability of Young's modulus computed using SWE of the PC, but their protocol was confined to images taken in the mid-sagittal plane, and their image analysis was performed using system-on-board image processing tools. At rest, PC stiffness (E_{mean}) showed good inter-rater (ICC = 0.78) and excellent intra-rater reliability (ICC = 0.94). Under maximal Valsalva, reliability remained good, with ICCs of 0.83 (inter-rater) and 0.80 (intra-rater) (Li et al., 2024)**.** Because neither of the studies noted above separated the analysis stage from image acquisition, it is not surprising that the reliability metrics found in the current study were higher. By using a single acquisition, we removed the error associated with probe repositioning.

Beyond the PC, the reliability of tissue stiffness outcomes has been reported for the levator ani group of muscles within the female pelvic floor. Gachon et al. reported excellent intra-operator reproducibility for levator ani shear modulus at rest (ICC 0.90) and during Valsalva (ICC 0.94), and Tang et al. reported excellent intra-observer reliability for Young's modulus at rest (ICC 0.91) and good reliability during Valsalva (ICC 0.83). Both studies quantified reliability using variance across separate acquisitions, yet they nonetheless provide a regional benchmark for reliability of pelvic floor imaging outcomes using SWE (Gachon et al., 2021; Tang et al., 2020).

5.3. Signal Availability and the Reliability of the Shear Wave Velocity Estimate

Agreement on the extracted SWV did not require agreement on the ROI within the elastogram that raters delineated. The clearest example of this dissociation is in the transverse plane, where inter-rater agreement on ROI area was poor in all three postures while agreement on the extracted SWV was excellent. Because the transverse plane elastogram was large and locally homogeneous, two raters could enclose different amounts of traceable territory and still recover a similar central velocity.

The deep zone of the PC was the most difficult region from which to recover a stable SWV estimate. Correspondingly, this region yielded the lowest number of traceable trials (17 of 27 participants in supine, 12 in standing, and 23 in deep squat), and all inter-rater reliability conditions failed to reach excellent agreement for SWV, where MDD_{95} values were four to seven times higher than those in the superficial layers. Indeed,

the elastograms in the deep zone were often sparse or absent, and B-mode visualization of the underlying tissue was limited, leaving raters to approximate the size and position of the ROI from unclear images. Notably, ROI area agreement improved from poor in supine to excellent in the deep squat, paralleling an overall improvement in image quality in that position. Interestingly, inter-rater reliability for ROI centre depth remained excellent across all postures, demonstrating that the primary obstacle was not uncertainty regarding anatomical localization, but was in obtaining sufficient signal quality within the ROI to derive a stable SWV estimate.

Poor visualization of the deep zone of the PC has been reported with other ultrasound modalities as well (Gong et al., 2024; Örnö et al., 2008). While greater depth of the tissue is known to attenuate the shear wave (Wang et al., 2020), depth alone does not fully explain the signal dropout observed. The depth of the ROI centre in this zone was between 1.19 cm and 1.31 cm across postures, well within the range of depths (<4 cm) where SWE of skeletal muscle (vastus lateralis and biceps femoris) maintains high reliability (Alfuraih et al., 2018). Instead, this pattern points to the acoustic path above the deep zone. In SWE, both the acoustic push that generates the shear wave and the tracking pulses that detect it must first cross the superficial zone. Within this layer, the ultrasound energy may be heavily scattered or attenuated by the mixed tissue composition and complex fibre arrangement of the PC before reaching its deep zone (Nitta et al., 2021).The deep zone findings are thus best understood as acquisition limitations rather than evidence that stiffness in this region cannot be measured reliably, reinforcing that image quality was the primary constraint.

5.4. Postural Modulation of Perineal Complex Stiffness

A posture effect was present in the superficial zone and the transverse plane but not in the deep zone of the PC, where the small effective sample size (n = 8) impacted study power. Among the three postures, the deep squat produced the highest SWV (Table 6). These contrasts were large, survived correction for multiple comparisons, and exceeded the minimal detectable difference. Moving from supine to standing produced a small increase in SWV (0.15 m/s), which was within the measurement error, so the standing posture alone did not measurably alter the SWV in the superficial zone of the PC. The deep squat position did significantly increase the SWV. In the transverse plane, SWV increased progressively from supine to standing to deep squat, with all three pairwise differences exceeding the MDD_{95}.

The capture of valid SWV in the deep zone was itself posture-dependent, with standing proving least favourable for deep-zone signal recovery (only 44.4% of participants had a traceable ROI within the PC) and the deep squat most favourable (85.2% of participants with traceable ROI). This pattern may be explained by the interaction between the participant's posture and the constraints of SWE. In conventional transperineal ultrasound imaging of deep pelvic floor structures, examiners often apply firm transducer pressure to compress superficial tissue and shorten the distance to the target enough to acquire a clear image. In SWE, such pressure cannot be applied as it artificially increases the measured stiffness (Rominger et al., 2018; Wang et al., 2020). When imaging the PC, posture governs the quality of contact between probe and tissue.

A standing position brings the hips into extension and adduction, which narrows the perineal space and makes uniform contact with a probe difficult; coupling is compromised, and, because shear wave attenuation increases with acquisition depth and with the thickness of overlying tissue (Creze et al., 2018; Starzec-Proserpio et al., 2026) the signal decays before reaching the deep zone. Conversely, the deep squat position brings the hips into flexion, abduction, and lateral rotation, which opens the perineal region and increases the effective contact area between the probe and the skin. It also shortens the effective distance between the probe and the deep zone of the PC, as evidenced by the data on the depth of the ROI, which was smaller in the deep squat (1.19 cm) compared to standing (1.31 cm; Table 2). While this reduction in absolute depth is modest, posture may also decrease the thickness of the overlying superficial layer, which, as hypothesized in Section 5.3, may act as a primary attenuating barrier.

Deep squatting is expected to place the convergent components of the PC in a lengthened position, which is itself known to raise measured SWV in skeletal muscle (Creze et al., 2018). Beyond simply elevating stiffness, this posture-induced tension may reorganize and align the complex myofascial architecture of the PC. Such realignment could reduce acoustic scattering and refraction in the superficial zone, thereby improving both the generation and the detection of shear waves in its deep zone and contributing to the higher signal recovery observed in this position (85.2%). While these findings indicate that the deep squat may have value for evaluating PC mechanical properties, a critical caveat qualifies this conclusion. The PC is an anisotropic fibromuscular network whose fibres align with the direction of physiological stretch (Moura et al., 2025), meaning that posture changes alter pelvic geometry and the angle between fibre orientation and the

acoustic beam. Whether the elevated SWV in the deep squat reflects genuine viscoelastic stiffening under increased myofascial tension or is partly driven by a shift in fibre-to-beam geometry warrants controlled biomechanical investigation. Understanding the nature of the increase in SWV observed in the deep squat is important for clinical translation, as the interpretation of SWE used in the deep zone of the PC is governed by the interplay of patient posture, acoustic coupling, and tissue compression, rather than by transducer frequency alone.

5.5. Strengths and Limitations

Several features of the study design support the reliability estimates reported here. From an image-processing perspective, the analysis stage was designed to operate within the documented constraints of the acquisition platform, as the manufacturer restricts the SWE Stability Index to a specific transducer and presets on the machine, and provided no multi-frame aggregation. To compensate, each elastogram was calibrated per trial to optimize image resolution from the colourmap before analysis began. The offline post-processing pipeline applied pre-specified quality-control gates for void proportion, saturation, and elastogram coherence consistently across all trials. This made it possible to compute explicit signal quality metrics that are not available when data are analyzed on the ultrasound system itself. The offline workflow is not a substitute for the internal stability index, yet it offers a plausible alternative grounded in explicit, auditable descriptors and is well suited to research settings that require a reproducible offline protocol. Moreover, stiffness was expressed in SWV in line with recommendations for musculoskeletal tissue (Săftoiu et al., 2019; Starzec-Proserpio et al., 2026), and the analysis was stratified by three postures and ROIs under two image planes.

The analysis protocol was also a strength. Repeat analyses by the same rater were separated by a one-week washout and presented in randomized order with the rater blinded to their prior analysis, reducing the likelihood that agreement was inflated by recall. Because both analyses drew on stored images rather than repeat acquisitions, however, the washout addressed recall of the earlier analysis rather than independence of image capture, and residual familiarity with individual images cannot be fully excluded. In the between-rater analysis, the raters followed a strict processing protocol and did so independently and blinded to each other's analyses. However, the intra-rater and inter-rater ICC values reported here are reading-stage estimates; the findings do not reflect the

reliability metrics that would arise when different raters acquire and process their own images or the same rater reacquires images after some washout period.

Rater characteristics and training may also have influenced the findings. Rater A was an experienced pelvic health physiotherapist, whereas Rater B was an undergraduate student without such experience, and this difference may underlie the directional pattern in which the less experienced rater traced the ROI more frequently in deep-zone trials. The experienced rater tended to evaluate image quality more judiciously, discarding more trials based on insufficient image quality. This difference in judgement is likely overcome through training and experience.

Sample size imposed a further constraint. While the cohort of 30 nulliparous females met our *a priori* sample size calculation, the effective sample size fell to as few as 12 when SWV was measured from the deep zone in sagittal-plane images. Because image plane, zone, and posture combinations were restricted to trials in which both raters identified an extractable shear-wave signal, the deep-zone SWV estimates are subject to selection bias toward the subset in which images were of the highest quality.

Operator-controllable acquisition parameters can bias measured SWV cumulatively (Lim et al., 2025), which reinforces the need for the standardized acquisition and processing protocol applied throughout this study. However, there were limitations in the signal analysis pipeline. Some thresholds were defined pragmatically or adapted from practices used when evaluating the liver. These include the 80% valid-fill criterion, the Saturated (%) < 5% rule, and the IQR/Median flagging thresholds, none of which have been independently validated for the PC. The distribution of SWVs was also frequently non-normal, so the parametric limits of agreement should be interpreted with caution. Averaging the per-condition trials before computing the ICC also tends to inflate the ICC relative to a single-trial design; the averaged trials nonetheless spanned probe repositioning between captures, and reliability under that more demanding condition remained excellent.

5.6. Implications and Future Directions

The findings of this study support the use of SWV as a reliable outcome when evaluating PC tissue stiffness. SWV had excellent reliability at the analysis stage and was robust to variation in ROI placement and area across raters. Further, a single trained rater is sufficient at the analysis stage of the protocol. The MDD_{95} provides a concrete

benchmark for separating true differences from measurement noise and can serve as provisional thresholds for studies that adopt this offline post-processing protocol across the image and posture conditions tested here. For images acquired in the sagittal plane, the deep squat may optimize signal quality in the deep zone of the PC.

The results of the postural analysis motivate a dedicated study of how changes in the geometric relationship between fibre orientation and shear wave propagation might confound velocity estimates when the PC is imaged under passive elongation or load, as in the deep squat. Because these recommendations are constrained to the analysis stage, the principal direction for future work follows directly from that boundary: test-retest reliability must be established with raters who acquire as well as analyze their own images.

Current SWE recommendations are derived from tissues whose fibre organization and composition differ from those of the PC, and their transferability has not been tested. In the present work, elastogram field of view filling varied markedly across planes. Within the transverse plane elastogram field of view, the median proportion of signal dropout ranged from 1.4% to 3.4% across postures, compared with 23.7% to 36.8% in the superficial zone of the sagittal plane elastograms. The two planes also differed in uniformity. Within the ROI, the spread of velocity values (IQR) was about half as wide in the transverse plane as in the superficial zone. The transverse elastogram was therefore both more complete and more internally consistent. Since the transverse plane corresponds largely to the superficial transverse perineal muscle, its more homogeneous fibre orientation offers the most defensible account of this difference. These observations do not identify an optimal plane; rather, they emphasize the need for feasibility work defining which planes, probe orientations, and signal criteria yield interpretable elastograms, so that acquisition standards are derived from data acquired from the PC itself rather than inherited from pelvic floor muscles or other tissues with distinct architecture and composition.

Building on this, because signal dropout in the deep zone appears to be driven by the attenuating acoustic path above it, future studies should evaluate whether different transducers can mitigate the deep-zone dropout observed in this study with a linear transducer: a curvilinear probe would offer greater penetration at the cost of spatial

resolution, whereas an endocavitary probe placed within the anal canal would provide higher resolution from a shorter acquisition distance.

A related standardization issue concerns the spatial summary metric applied within the ROI. As noted, our sensitivity analysis demonstrated that using spatial means or medians yielded near-identical reliability across all conditions tested, confirming the robustness of the pipeline. We retained the spatial median because it inherently provides greater stability against localized artifacts in anisotropic tissue. While recent technical guidance recommends using the spatial mean, those recommendations were developed for different processing workflows and did not evaluate median statistics applied to multi-frame ensemble maps (Starzec-Proserpio et al., 2026). Nevertheless, because spatial means and medians are not directly interchangeable, future protocols should explicitly declare their chosen metric.

Taken together, these findings establish analysis-stage reliability for SWV of the PC under a defined offline reading protocol. Extending these measurements to populations affected by obstetric trauma, in whom perineal stiffness may be clinically consequential, would be a necessary step toward using SWE as a clinical measurement tool.

6. Conclusion

This work establishes a reproducible offline analysis protocol for the evaluation of tissue stiffness within the perineal complex and extends SWE assessment to a transverse imaging plane and in vertical postures not previously reported for this region. Among nulliparous females, SWE of the perineal complex demonstrates good to excellent within- and between-rater reliability in the analysis stage. Agreement on ROI geometry was lower than agreement on SWV in the transverse plane, yet the SWV outcomes were robust to differences in the area of the ROI selected by the rater. The deep-zone results translate better into acquisition feasibility than into measurement reliability, since raters agreed on where to measure, but the elastogram at that depth was often too sparse to generate an estimate. SWV within the PC increased with passive elongation and loading induced by changes in posture. These findings show promise as a measure of the perineal complex tissue function in females.

7. References

Alfuraih, A. M., O'Connor, P., Hensor, E., Tan, A. L., Emery, P., & Wakefield, R. J. (2018). The effect of unit, depth, and probe load on the reliability of muscle shear wave elastography: Variables affecting reliability of SWE. *Journal of Clinical Ultrasound*, *46*(2), 108–115. https://doi.org/10.1002/jcu.22534

Arenholt, L. T. S., Pedersen, B. G., Glavind, K., Glavind-Kristensen, M., & DeLancey, J. O. L. (2017). Paravaginal defect: Anatomy, clinical findings, and imaging. *International Urogynecology Journal*, *28*(5), 661–673. https://doi.org/10.1007/s00192-016-3096-3

Asfour, V., Digesu, G. A., Fernando, R., & Khullar, V. (2020). Ultrasound imaging of the perineal body: A useful clinical tool. *International Urogynecology Journal*, *31*(6), 1197–1202. https://doi.org/10.1007/s00192-019-04166-7

Ashton-Miller, J. A., & DeLancey, J. O. L. (2021). Mechanisms of Pelvic Floor Trauma During Vaginal Delivery. In G. A. Santoro, A. P. Wieczorek, & A. H. Sultan (Eds.), *Pelvic Floor Disorders* (pp. 189–209). Springer International Publishing. https://doi.org/10.1007/978-3-030-40862-6_12

Avery, K., Donovan, J., Peters, T. J., Shaw, C., Gotoh, M., & Abrams, P. (2004). ICIQ: A brief and robust measure for evaluating the symptoms and impact of urinary incontinence. *Neurourology and Urodynamics*, *23*(4), 322–330. https://doi.org/10.1002/nau.20041

Barr, R. G., & Zhang, Z. (2012). Effects of Precompression on Elasticity Imaging of the Breast: Development of a Clinically Useful Semiquantitative Method of Precompression Assessment. *Journal of Ultrasound in Medicine*, *31*(6), 895–902. https://doi.org/10.7863/jum.2012.31.6.895

Bujang, M. A., & Baharum, N. (2022). Guidelines of the minimum sample size requirements for Kappa agreement test. *Epidemiology, Biostatistics, and Public Health*, *14*(2). https://doi.org/10.2427/12267

Chantarasorn, V., Shek, K. L., & Dietz, H. P. (2012). Mobility of the perineal body and anorectal junction before and after childbirth. *International Urogynecology Journal*, *23*(6), 729–733. https://doi.org/10.1007/s00192-012-1672-8

Cheng, W., English, E., Horner, W., Swenson, C. W., Chen, L., Pipitone, F., Ashton-Miller, J. A., & DeLancey, J. O. L. (2023). Hiatal failure: Effects of pregnancy, delivery, and pelvic floor disorders on level III factors. *International Urogynecology Journal*, *34*(2), 327–343. https://doi.org/10.1007/s00192-022-05354-8

Corton, M. M. (2009). Anatomy of Pelvic Floor Dysfunction. *Obstetrics and Gynecology Clinics of North America*, *36*(3), 401–419. https://doi.org/10.1016/j.ogc.2009.09.002

Creze, M., Nordez, A., Soubeyrand, M., Rocher, L., Maître, X., & Bellin, M.-F. (2018). Shear wave sonoelastography of skeletal muscle: Basic principles, biomechanical concepts, clinical applications, and future perspectives. *Skeletal Radiology*, *47*(4), 457–471. https://doi.org/10.1007/s00256-017-2843-y

Davis, L. C., Baumer, T. G., Bey, M. J., & Holsbeeck, M. V. (2019). Clinical utilization of shear wave elastography in the musculoskeletal system. *Ultrasonography*, *38*(1), 2–12. https://doi.org/10.14366/usg.18039

DeLancey, J. O. L. (1999). Structural anatomy of the posterior pelvic compartment as it relates to rectocele. *American Journal of Obstetrics and Gynecology*, *180*(4), 815–823. https://doi.org/10.1016/s0002-9378(99)70652-6

DeLancey, J. O. L., Ashton-Miller, J. A., LaCross, J., Pipitone, F., Schmidt, P., & Chen, L. (2025). Urogenital Hiatus Closure: Facts, Fallacies, and Why a Unified Theory of Hiatal Failure is Needed. *International Urogynecology Journal*. https://doi.org/10.1007/s00192-025-06153-7

DeLancey, J. O. L., Ashton-Miller, J. A., LaCross, J., Schmidt, P., Masteling, M., Pipitone, F., Hong, C. X., & Chen, L. (2026). Urogenital Hiatus Closure System: A Framework for Understanding how Muscle, Motor Control, and Fascial Connections Interact in Normal and Failed Closure. *International Urogynecology Journal*. https://doi.org/10.1007/s00192-026-06641-4

DeLancey, J. O. L., Masteling, M., Pipitone, F., LaCross, J., Mastrovito, S., & Ashton-Miller, J. A. (2024). Pelvic floor injury during vaginal birth is life-altering and preventable: What can we do about it? *American Journal of Obstetrics and Gynecology*, *230*(3), 279-294.e2. https://doi.org/10.1016/j.ajog.2023.11.1253

DeLancey, J. O. L., Mastrovito, S., Masteling, M., Horner, W., Ashton-Miller, J. A., & Chen, L. (2024). A unified pelvic floor conceptual model for studying morphological changes with prolapse, age, and parity. *American Journal of Obstetrics and Gynecology*, *230*(5), 476-484.e2. https://doi.org/10.1016/j.ajog.2023.11.1247

DeLancey, J. O. L., Pipitone, F., Masteling, M., Xie, B., Ashton-Miller, J. A., & Chen, L. (2024). Functional Anatomy of Urogenital Hiatus Closure: The Perineal Complex Triad Hypothesis. *International Urogynecology Journal*, *35*(2), 441–449. https://doi.org/10.1007/s00192-023-05708-w

Dietz, H. P., & Lanzarone, V. (2005). Levator Trauma After Vaginal Delivery: *Obstetrics & Gynecology*, *106*(4), 707–712. https://doi.org/10.1097/01.AOG.0000178779.62181.01

Doguet, V., Hug, F., Nordez, A., & Savery, D. (2019). *ElastoGUI: Software for the acquisition and analysis of elastography data from Aixplorer® ultrasound scanners* [Manual]. MATLAB Central File Exchange. https://www.mathworks.com/matlabcentral/fileexchange/74037-elastogui/

Dunivan, G. C., Lyons, K. E., Jeppson, P. C., Ninivaggio, C. S., Komesu, Y. M., Alba, F. M., & Rogers, R. G. (2016). Pelvic Organ Prolapse Stage and the Relationship to Genital Hiatus and Perineal Body Measurements. *Female Pelvic Medicine & Reconstructive Surgery*, *22*(6), 497–500. https://doi.org/10.1097/SPV.0000000000000323

Ferraioli, G., Barr, R. G., Berzigotti, A., Sporea, I., Wong, V. W., Reiberger, T., Karlas, T., Thiele, M., Cardoso, A. C., Ayonrinde, O. T., Castera, L., Dietrich, C. F., Iijima, H., Lee, D. H., Kemp, W., Oliveira, C. P., & Sarin, S. K. (2024). WFUMB Guideline/Guidance on Liver Multiparametric Ultrasound: Part 1. Update to 2018 Guidelines on Liver Ultrasound Elastography. *Ultrasound in Medicine & Biology*, *50*(8), 1071–1087. https://doi.org/10.1016/j.ultrasmedbio.2024.03.013

Ferraioli, G., Wong, V. W.-S., Castera, L., Berzigotti, A., Sporea, I., Dietrich, C. F., Choi, B. I., Wilson, S. R., Kudo, M., & Barr, R. G. (2018). Liver Ultrasound Elastography: An Update to the World Federation for Ultrasound in Medicine and Biology Guidelines and Recommendations. *Ultrasound in Medicine & Biology*, *44*(12), 2419–2440. https://doi.org/10.1016/j.ultrasmedbio.2018.07.008

Fornell, E. U., Matthiesen, L., Sjödahl, R., & Berg, G. (2005). Obstetric anal sphincter injury ten years after: Subjective and objective long term effects. *BJOG: An International Journal of Obstetrics & Gynaecology*, *112*(3), 312–316. https://doi.org/10.1111/j.1471-0528.2004.00400.x

Frazão, L., Couto, L., Peres, A. C., Marques, A., & Pássaro, A. (2025). Assessment of Female Pelvic Floor Muscles: An Integrative Review. *International Journal of Women's Health*, *Volume 17*, 2377–2393. https://doi.org/10.2147/IJWH.S532149

Gachon, B., Fritel, X., Pierre, F., & Nordez, A. (2021). Transperineal ultrasound shear-wave elastography is a reliable tool for assessment of the elastic properties of the levator ani muscle in women. *Scientific Reports*, *11*(1), 15532. https://doi.org/10.1038/s41598-021-95012-8

Gong, Q., Wang, Y., Duan, L., Lei, L., Liu, J., Yao, J., Qi, J., Xu, Z., Nian, Y., & Wu, Y. (2024). Comparative study of female pelvic floor among undeformed high-resolution thin-sectional anatomical (visible human) images and MRI and ultrasound images. *Journal of Clinical Ultrasound*, *52*(2), 208–218. https://doi.org/10.1002/jcu.23616

Haueise, A., Carvalho, G. F., Azan, M., Gehring, D., Skerl, K., & Dieterich, A. V. (2025). Development and validation of a semi-automated algorithm to analyze shear wave elastography clips in muscle tissue. *Scientific Reports*, *15*(1), 20147. https://doi.org/10.1038/s41598-025-05154-2

He, M., Muro, S., & Akita, K. (2022). Positional relationship between the lateral border of Denonvilliers' fascia and pelvic plexus. *Anatomical Science International*, *97*(1), 101–109. https://doi.org/10.1007/s12565-021-00629-4

Kang, H.-J., Yoon, J. H., & Lee, J. M. (2026). Fully automated frame selection and region-of-interest placement in 2D shear wave elastography: Reduced examination time with comparable reproducibility in diffuse liver disease. *Ultrasonography*, *45*(1), 69–79. https://doi.org/10.14366/usg.25161

Kearney, R., Miller, J. M., Ashton-Miller, J. A., & DeLancey, J. O. L. (2006). Obstetric Factors Associated With Levator Ani Muscle Injury After Vaginal Birth:

Obstetrics & Gynecology, *107*(1), 144–149. https://doi.org/10.1097/01.AOG.0000194063.63206.1c

Klovning, A., Avery, K., Sandvik, H., & Hunskaar, S. (2009). Comparison of two questionnaires for assessing the severity of urinary incontinence: The ICIQ-UI SF versus the incontinence severity index. *Neurourology and Urodynamics*, *28*(5), 411–415. https://doi.org/10.1002/nau.20674

Komorowski, L. K., Leeman, L. M., Fullilove, A. M., Bedrick, E. J., Migliaccio, L. D., & Rogers, R. G. (2014). Does a Large Infant Head or a Short Perineal Body Increase the Risk of Obstetrical Perineal Trauma? *Birth*, *41*(2), 147–152. https://doi.org/10.1111/birt.12101

Koo, T. K., & Li, M. Y. (2016). A Guideline of Selecting and Reporting Intraclass Correlation Coefficients for Reliability Research. *Journal of Chiropractic Medicine*, *15*(2), 155–163. https://doi.org/10.1016/j.jcm.2016.02.012

Lallemant, M., Kadiaké, T., Lejeune, A., Cosson, M., Chambert, J., Jacquet, E., & Mottet, N. (2025a). Exploring the influence of perineal biometrics and stiffness measured by elastography during pregnancy on perineal tears: A pilot study. *Journal of Gynecology Obstetrics and Human Reproduction*, *54*(3), 102904. https://doi.org/10.1016/j.jogoh.2025.102904

Lallemant, M., Kadiaké, T., Lejeune, A., Cosson, M., Chambert, J., Jacquet, E., & Mottet, N. (2025b). Perineal body and anal sphincter biometrics and stiffness using elastography during labor: A feasibility study. *European Journal of Obstetrics & Gynecology and Reproductive Biology*, *309*, 48–54. https://doi.org/10.1016/j.ejogrb.2025.03.034

Larson, K. A., Yousuf, A., Lewicky-Gaupp, C., Fenner, D. E., & DeLancey, J. O. L. (2010). Perineal body anatomy in living women: 3-dimensional analysis using

thin-slice magnetic resonance imaging. *American Journal of Obstetrics and Gynecology*, *203*(5), 494.e15-494.e21. https://doi.org/10.1016/j.ajog.2010.06.008

Lee, H., Kim, K., & Lee, Y. (2020). Development of Stiffness Measurement Program Using Color Mapping in Shear Wave Elastography. *Diagnostics*, *10*(6), 362. https://doi.org/10.3390/diagnostics10060362

Li, X., Zhang, L., Li, Y., Jiang, Y., Zhao, C., Fang, S., Yang, Z., & Sun, L. (2024). Assessment of perineal body properties in women with stress urinary incontinence using Transperineal shear wave elastography. *Scientific Reports*, *14*(1), 21647. https://doi.org/10.1038/s41598-024-72429-5

Lien, K.-C., Mooney, B., DeLancey, J. O. L., & Ashton-Miller, J. A. (2004). Levator Ani Muscle Stretch Induced by Simulated Vaginal Birth: *Obstetrics & Gynecology*, *103*(1), 31–40. https://doi.org/10.1097/01.AOG.0000109207.22354.65

Lilleberg, H. S., Siafarikas, F., Starck, M., Bø, K., Rotstein, E., & Ellström Engh, M. (2025). Association Between Sonographic Deviations in the Perineum and Symptoms of a Deficient Perineum in Primiparous Women One Year After Birth: A Prospective Cohort Study. *BJOG: An International Journal of Obstetrics & Gynaecology*, *132*(8), 1114–1121. https://doi.org/10.1111/1471-0528.18135

Lim, N. E., Abbott, S., Zelesco, M., & Welman, C. J. (2025). Shear Wave Elastography Acquisition Parameters May Bias Shear Wave Velocity Measurements. *Australasian Journal of Ultrasound in Medicine*, *28*(3), e70018. https://doi.org/10.1002/ajum.70018

Macedo, M. D., Risløkken, J., Halle, T., Ellström Engh, M., & Siafarikas, F. (2024). Occurrence and risk factors for second-degree perineal tears: A prospective cohort study using a detailed classification system. *Birth*, *51*(3), 602–611. https://doi.org/10.1111/birt.12817

Madhu, C., Swift, S., Moloney-Geany, S., & Drake, M. J. (2018). How to use the Pelvic Organ Prolapse Quantification (POP-Q) system? *Neurourology and Urodynamics*, *37*(S6). https://doi.org/10.1002/nau.23740

McGraw, K. O., & Wong, S. P. (1996). Forming inferences about some intraclass correlation coefficients. *Psychological Methods*, *1*(1), 30–46. https://doi.org/10.1037/1082-989X.1.1.30

Miller, J. M., Brandon, C., Jacobson, J. A., Low, L. K., Zielinski, R., Ashton-Miller, J., & DeLancey, J. O. L. (2010). MRI Findings in Patients Considered High Risk for Pelvic Floor Injury Studied Serially After Vaginal Childbirth. *American Journal of Roentgenology*, *195*(3), 786–791. https://doi.org/10.2214/AJR.09.3508

Morin, M., Salomoni, S. E., Stafford, R. E., Hall, L. M., & Hodges, P. W. (2022). Validation of shear wave elastography as a noninvasive measure of pelvic floor muscle stiffness. *Neurourology and Urodynamics*, *41*(7), 1620–1628. https://doi.org/10.1002/nau.25010

Mottet, N., Bonneaud, M., Eckman-Lacroix, A., Ramanah, R., & Riethmuller, D. (2017). Active delivery of the anterior arm and incidence of second-degree perineal tears: A clinical practice evaluation. *BMC Pregnancy and Childbirth*, *17*(1), 141. https://doi.org/10.1186/s12884-017-1322-8

Moura, R., A. Oliveira, D., R. Carvalho, M., Pirker, T. M., Hammer, N., P.L. Parente, M., & Vom Scheidt, A. (2025). Experimental characterization of the non-linear viscoelastic properties of human female perineal tissue. *Scientific Reports*, *15*(1), 42483. https://doi.org/10.1038/s41598-025-26576-y

Muro, S., & Akita, K. (2023). Pelvic floor and perineal muscles: A dynamic coordination between skeletal and smooth muscles on pelvic floor stabilization. *Anatomical*

Science International, *98*(3), 407–425. https://doi.org/10.1007/s12565-023-00717-7

Muro, S., Kagawa, R., Habu, M., Ka, H., Harada, M., & Akita, K. (2020). Coexistence of Dense and Sparse Areas in the Longitudinal Smooth Muscle of the Anal Canal: Anatomical and Histological Analyses Inspired by Magnetic Resonance Images. *Clinical Anatomy*, *33*(4), 619–626. https://doi.org/10.1002/ca.23467

Nitta, N., Yamakawa, M., Hachiya, H., & Shiina, T. (2021). A review of physical and engineering factors potentially affecting shear wave elastography. *Journal of Medical Ultrasonics*, *48*(4), 403–414. https://doi.org/10.1007/s10396-021-01127-w

Örnö, A. -K., Maršál, K., & Herbst, A. (2008). Ultrasonographic anatomy of perineal structures during pregnancy and immediately following obstetric injury. *Ultrasound in Obstetrics & Gynecology*, *32*(4), 527–534. https://doi.org/10.1002/uog.6122

Pihl, S., Uustal, E., Hjertberg, L., & Blomberg, M. (2018). Interobserver agreement in perineal ultrasound measurement of the anovaginal distance: A methodological study. *International Urogynecology Journal*, *29*(5), 697–701. https://doi.org/10.1007/s00192-017-3392-6

Pipitone, F., Haddad, J. M., Chen, L., Masteling, M., Schmidt, P. C., Fairchild, P. S., Ashton-Miller, J. A., & DeLancey, J. O. L. (2025). Perineal structural changes on 3D endovaginal ultrasound six months after vaginal birth: The Hourglass-Band pattern and how it relates to levator ani avulsion and hiatus size. *American Journal of Obstetrics and Gynecology*, S0002937825008300. https://doi.org/10.1016/j.ajog.2025.11.007

Pipitone, F., Masteling, M., Chen, L., Ashton-Miller, J. A., Schmidt, P., Haddad, J. M., & DeLancey, J. O. L. (2024, October 25). *Postpartum Perineal Complex Disruption in 3D Endovaginal Ultrasound*. PFD Week 2024 – Concurrent Session 12: Imaging and Office Practice. https://pfdweek24.eventscribe.net/fsPopup.asp?efp=SEJFVkpKU1kxOTE3MQ&PresentationID=1450857&mode=presInfo

Pipitone, F., Swenson, C. W., DeLancey, J. O. L., Ashton-Miller, J. A., & Chen, L. (2026). Perineal Membrane Structural Changes: An Unstudied Aspect of Prolapse. *International Urogynecology Journal*. https://doi.org/10.1007/s00192-026-06614-7

Pipitone, F., Swenson, C. W., DeLancey, J. O. L., & Chen, L. (2021). Novel 3D MRI technique to measure perineal membrane structural changes with pregnancy and childbirth: Technique development and measurement feasibility. *International Urogynecology Journal*, *32*(9), 2413–2420. https://doi.org/10.1007/s00192-021-04795-x

Rominger, M., Kälin, P., Mastalerz, M., Martini, K., Klingmüller, V., Sanabria, S., & Frauenfelder, T. (2018). Influencing Factors of 2D Shear Wave Elastography of the Muscle – An Ex Vivo Animal Study. *Ultrasound International Open*, *04*(02), E54–E60. https://doi.org/10.1055/a-0619-6058

Rostaminia, G., Awad, C., Chang, C., Sikdar, S., Wei, Q., & Shobeiri, S. A. (2019). Shear Wave Elastography to Assess Perineal Body Stiffness During Labor. *Female Pelvic Medicine & Reconstructive Surgery*, *25*(6), 443–447. https://doi.org/10.1097/SPV.0000000000000585

Rusavy, Z., Paymova, L., Kozerovsky, M., Veverkova, A., Kalis, V., Kamel, R., & Ismail, K. (2022). Levator ani avulsion: A Systematic evidence review (LASER). *BJOG:*

An International Journal of Obstetrics & Gynaecology, *129*(4), 517–528. https://doi.org/10.1111/1471-0528.16837

Săftoiu, A., Gilja, O. H., Sidhu, P. S., Dietrich, C. F., Cantisani, V., Amy, D., Bachmann-Nielsen, M., Bob, F., Bojunga, J., Brock, M., Calliada, F., Clevert, D. A., Correas, J.-M., D'Onofrio, M., Ewertsen, C., Farrokh, A., Fodor, D., Fusaroli, P., Havre, R. F., … Vilmann, P. (2019). The EFSUMB Guidelines and Recommendations for the Clinical Practice of Elastography in Non-Hepatic Applications: Update 2018. *Ultraschall in der Medizin - European Journal of Ultrasound*, *40*(04), 425–453. https://doi.org/10.1055/a-0838-9937

Santoro, G. A., Shobeiri, S. A., Petros, P. P., Zapater, P., & Wieczorek, A. P. (2016). Perineal body anatomy seen by three-dimensional endovaginal ultrasound of asymptomatic nulliparae. *Colorectal Disease*, *18*(4), 400–409. https://doi.org/10.1111/codi.13119

Shafik, A., Sibai, O. E., Shafik, A. A., & Shafik, I. A. (2007). A Novel Concept for the Surgical Anatomy of the Perineal Body. *Diseases of the Colon & Rectum*, *50*(12), 2120–2125. https://doi.org/10.1007/s10350-007-9064-8

Shobeiri, S. A., Nolan, T. E., Yordan-Jovet, R., Echols, K. T., & Chesson, R. R. (2002). Digital examination compared to trans-perineal ultrasound for the evaluation of anal sphincter repair. *International Journal of Gynecology & Obstetrics*, *78*(1), 31–36. https://doi.org/10.1016/S0020-7292(02)00068-1

Sigrist, R. M. S., Liau, J., Kaffas, A. E., Chammas, M. C., & Willmann, J. K. (2017). Ultrasound Elastography: Review of Techniques and Clinical Applications. *Theranostics*, *7*(5), 1303–1329. https://doi.org/10.7150/thno.18650

Skerl, K., Cochran, S., & Evans, A. (2017). First step to facilitate long-term and multi-centre studies of shear wave elastography in solid breast lesions using a computer-

assisted algorithm. *International Journal of Computer Assisted Radiology and Surgery*, *12*(9), 1533–1542. https://doi.org/10.1007/s11548-017-1596-3

Starzec-Proserpio, M., Cloutier, G., Gaudreault, N., Bureau, N., & Morin, M. (2026). Ultrasound shear wave elastography for the assessment of pelvic floor muscle stiffness: Technical and analytical challenges in practice. *Ultrasonography*, *45*(4), 402–418. https://doi.org/10.14366/usg.26031

Starzec-Proserpio, M., Gaudreault, N., Roch, M., Daigle, F., Bureau, N., & Morin, M. (2023). ASSESSMENT OF PELVIC FLOOR MUSCLE STIFFNESS IN WOMEN USING SHEAR WAVE ELASTOGRAPHY: AN INTRA- AND INTER-RATER RELIABILITY STUDY. *Continence*, *7*, 100994. https://doi.org/10.1016/j.cont.2023.100994

Taljanovic, M. S., Gimber, L. H., Becker, G. W., Latt, L. D., Klauser, A. S., Melville, D. M., Gao, L., & Witte, R. S. (2017). Shear-Wave Elastography: Basic Physics and Musculoskeletal Applications. *RadioGraphics*, *37*(3), 855–870. https://doi.org/10.1148/rg.2017160116

Tang, J., Zhong, C., Wen, W., Wu, R., Liu, Y., & Du, L. (2020). Quantifying Levator Ani Muscle Elasticity Under Normal and Prolapse Conditions by Shear Wave Elastography: A Preliminary Study. *Journal of Ultrasound in Medicine*, *39*(7), 1379–1388. https://doi.org/10.1002/jum.15232

Vukasović, I., Kalafatić, D., Banović, M., & Banović, V. (2026). Ultrasound assessment of the perineal body: A scoping review. *European Journal of Obstetrics & Gynecology and Reproductive Biology*, *318*, 114904. https://doi.org/10.1016/j.ejogrb.2025.114904

Walter, S. D., Eliasziw, M., & Donner, A. (1998). Sample size and optimal designs for reliability studies. *Statistics in Medicine*, *17*(1), 101–110.

https://doi.org/10.1002/(sici)1097-0258(19980115)17:1%3C101::aid-sim727%3E3.0.co;2-e

Wang, X., Hu, Y., Zhu, J., Gao, J., Chen, S., Liu, F., Li, W., Liu, Y., & Ariun, B. (2020). Effect of acquisition depth and precompression from probe and couplant on shear wave elastography in soft tissue: An in vitro and in vivo study. *Quantitative Imaging in Medicine and Surgery*, *10*(3), 754–765. https://doi.org/10.21037/qims.2020.01.15

Woodman, P. J., & Graney, D. O. (2002). Anatomy and physiology of the female perineal body with relevance to obstetrical injury and repair. *Clinical Anatomy*, *15*(5), 321–334. https://doi.org/10.1002/ca.10034

Wu, Y., Dabhoiwala, N. F., Hagoort, J., Shan, J.-L., Tan, L.-W., Fang, B.-J., Zhang, S.-X., & Lamers, W. H. (2015). 3D Topography of the Young Adult Anal Sphincter Complex Reconstructed from Undeformed Serial Anatomical Sections. *PLOS ONE*, *10*(8), e0132226. https://doi.org/10.1371/journal.pone.0132226

Yeung, E., Malacova, E., & Maher, C. (2022). Is levator ani avulsion a risk factor for prolapse recurrence? A systematic review and meta-analysis. *International Urogynecology Journal*, *33*(7), 1813–1826. https://doi.org/10.1007/s00192-022-05217-2

Zetterström, J. P., Mellgren, A., Madoff, R. D., Kim, D. G., & Wong, D. W. (1998). Perineal body measurement improves evaluation of anterior sphincter lesions during endoanal ultrasonography. *Diseases of the Colon & Rectum*, *41*(6), 705–713. https://doi.org/10.1007/BF02236256

Zhou, M., Shui, W., Bai, W., Wu, X., & Ying, T. (2023). Ultrasonographic study of female perineal body and its supportive function on pelvic floor. *Frontiers in Medicine*, *10*, 1176360. https://doi.org/10.3389/fmed.2023.1176360

8. Appendix

8.1. Appendix A — REB Approval Letter

05/06/2026

Université d'Ottawa
Bureau d'éthique et d'intégrité de la recherche

University of Ottawa
Office of Research Ethics and Integrity

CERTIFICAT D'APPROBATION ÉTHIQUE | CERTIFICATE OF ETHICS APPROVAL

Numéro du dossier / Ethics File Number	H-05-25-11515
Titre du projet / Project Title	The assessment of perineal body morphology in females: An inter-rater reliability and correlation study
Type de projet / Project Type	Recherche postdoctorale / Postdoctoral research project
Statut du projet / Project Status	Renouvelé / Renewed
Date d'approbation (jj/mm/aaaa) / Approval Date (dd/mm/yyyy)	09/06/2025
Date d'expiration (jj/mm/aaaa) / Expiry Date (dd/mm/yyyy)	08/06/2027

Équipe de recherche / Research Team

Chercheur / Researcher	Affiliation	Role
Sabine VESTING	École des sciences de la réadaptation / School of Rehabilitation Sciences	Chercheur Principal / Principal Investigator
Linda MCLEAN	École des sciences de la réadaptation / School of Rehabilitation Sciences	Superviseur / Supervisor
Talita MARTINS	École des sciences de l'activité physique / School of Human Kinetics	Étudiant-chercheur / Student-researcher
Anne-Marie LAKE	École des sciences de la réadaptation / School of Rehabilitation Sciences	Coordonnateur de recherche / Research Coordinator

Conditions spéciales ou commentaires / Special conditions or comments

550, rue Cumberland, pièce 154 Ottawa (Ontario) K1N 6N5 Canada
550 Cumberland Street, Room 154 Ottawa, Ontario K1N 6N5 Canada

613-562-5387 • 613-562-5338 • ethique@uOttawa.ca / ethics@uOttawa.ca
www.recherche.uottawa.ca/deontologie | www.recherche.uottawa.ca/ethics

Université d'Ottawa
Bureau d'éthique et d'intégrité de la recherche

University of Ottawa
Office of Research Ethics and Integrity

Le Comité d'éthique de la recherche (CÉR) de l'Université d'Ottawa, opérant conformément à l'*Énoncé de politique des Trois conseils* (2014) et toutes autres lois et tous règlements applicables, a examiné et approuvé la demande d'éthique du projet de recherche ci-nommé.

L'approbation est valide pour la durée indiquée plus haut et est sujette aux conditions énumérées dans la section intitulée "Conditions Spéciales ou Commentaires". Le formulaire « Renouvellement ou Fermeture de Projet » doit être complété quatre semaines avant la date d'échéance indiquée ci-haut afin de demander un renouvellement de cette approbation éthique ou afin de fermer le dossier.

Toutes modifications apportées au projet doivent être approuvées par le CÉR avant leur mise en place, sauf si le participant doit être retiré en raison d'un danger immédiat ou s'il s'agit d'un changement ayant trait à des éléments administratifs ou logistiques du projet. Les chercheurs doivent aviser le CÉR dans les plus brefs délais de tout changement pouvant augmenter le niveau de risque aux participants ou pouvant affecter considérablement le déroulement du projet, rapporter tout évènement imprévu ou indésirable et soumettre toute nouvelle information pouvant nuire à la conduite du projet ou à la sécurité des participants.

The University of Ottawa Research Ethics Board, which operates in accordance with the *Tri-Council Policy Statement* (2014) and other applicable laws and regulations, has examined and approved the ethics application for the above-named research project.

Ethics approval is valid for the period indicated above and is subject to the conditions listed in the section entitled "Special Conditions or Comments". The "Renewal/Project Closure" form must be completedfour weeks before the above-referenced expiry date to request a renewal of this ethics approval or closure of the file.

Any changes made to the project must be approved by the REB before being implemented, except when necessary to remove participants from immediate endangerment or when the modification(s) only pertain to administrative or logistical components of the project. Investigators must also promptly alert the REB of any changes that increase the risk to participant(s), any changes that considerably affect the conduct of the project, all unanticipated and harmful events that occur, and new information that may negatively affect the conduct of the project or the safety of the participant(s).

Coordonateur / COORDINATOR
Coordonnateur de l'éthique / Ethics Coordinator
Pour/For **Daniel LAGAREC** Président(e) du/ Chair of the **Comité d'éthique de la recherche en sciences de la santé et sciences / Health Sciences and Sciences Research Ethics Board**

550, rue Cumberland, pièce 154
Ottawa (Ontario) K1N 6N5 Canada

550 Cumberland Street, Room 154
Ottawa, Ontario K1N 6N5 Canada

613-562-5387 • 613-562-5338 • ethique@uOttawa.ca / ethics@uOttawa.ca
www.recherche.uottawa.ca/deontologie | www.recherche.uottawa.ca/ethics

8.2. Appendix B — Participant Consent Form



uOttawa

Faculté des sciences de la santé
Faculty of Health Sciences

Letter of Information and Consent Form

Title of the study: The assessment of perineal body morphology in females: An inter-rater reliability and correlation study

Principal investigator: Linda McLean, PhD, Full Professor, School of Rehabilitation Sciences, University of Ottawa. 613-562-5800 ext 2544.

Postdoctoral fellow: Sabine Vesting, PhD, PT, School of Rehabilitation Sciences, University of Ottawa, 613-562-5800 ext 4102.

Individuals with female anatomy are at high risk of developing pelvic floor disorders over their lifetime, and 1 in 5 will require pelvic floor surgery. Pregnancy and childbirth are well-known risk factors. While vaginal delivery is an established risk factor, the underlying mechanisms leading to these symptoms remain inadequately understood.

Tears in the perineal body can range from grade 2, affecting only the muscles of the perineal body, to grades 3 and 4, which involve the anal sphincter. However, even less severe trauma, such as intense stretching or loss of muscle mass, can impact the perineal body. Increasing evidence highlights the importance of the perineal body in overall pelvic floor function. Currently, clinically accessible methods to assess these changes are not yet validated. The purpose of this project is to enhance our understanding of perineal body morphology in individuals with female anatomy by developing and validating reliable ultrasound-based imaging techniques.

The aims of the project are:

1. To assess the inter-rater reliability of perineal body morphology measurements, including perineal body area, qualitative signs indicative of a defect (e.g., absence of a "band of tissue" or the "pinched waist sign"), and the dimensions of the urogenital hiatus relative to the perineal body.

2. To explore the correlation between these imaging assessments and clinical parameters, including pelvic floor symptom severity, parity status, and the degree of perineal body tearing.

Inclusion criteria: Individuals with female anatomy, over 18 years, no history of urogenital surgery, BMI < 30 kg/m², not currently pregnant or within 6 months postpartum and ability to communicate in English.

Exclusion Criteria: Presence of any diagnosed cardiac, pulmonary, metabolic, or neurological condition, pain during gynecological assessments or tampon insertion, which may interfere with study procedures.

A member of the research team will read this information document with you and you will be provided with a copy to read on your own. Please ask questions and/or voice any concerns that you have, and please ensure that we have answered to your satisfaction before agreeing to participate in this study. If you choose to participate in the study, you will be required to sign the consent form that follows, indicating your consent to undergo the assessment procedures described here. You are, however, permitted to withdraw from the study at any time, and you are not required to provide us with any reason if you do not wish to.

Data collection procedures

At this stage of the study, you already filled in the questionnaires of the study. The laboratory-based assessments will take place at the Motor Function Measurement Lab (Dr. McLean's Laboratory) at the University of Ottawa at 200 Lees Ave. in room 226C. The session will last approximately 30 minutes and will be scheduled at your convenience within the first two weeks after your menstrual period (if you have one). If you choose to drive to your assessment visit, parking will be provided at no charge through a reserved parking space.

A member of the research team will greet you when you arrive at the laboratory. She will read through this form with you and ensure that your questions are answered to your satisfaction before you consent to participate in this study. In the laboratory, Dr. Sabine Vesting who is a pelvic floor physiotherapist from Sweden, will perform the assessment. Dr. Vesting holds a doctorate degree and has 9 years of experience in assessing and treating pelvic floor dysfunction. She has been trained by local experts on the evaluation procedures. Dr. Vesting will be assisted by a female research assistant who

will help to prepare instrumentation and operate the computers used to collect the data but will not perform any clinical assessment techniques. On site, Dr. Vesting, will measure your height, weight, waist circumference and hip circumference. We will ask you to visit the bathroom to empty your bladder. You will then be left in a private area to undress from your waist down and will be given a gown to cover yourself. When you are ready, Dr. Vesting and her assistant will be invited back into the assessment room. You will lie on your back with a pillow behind your head. Ultrasound imaging of your pelvic floor will be performed while you are in a supine position. Dr. Vesting will provide clear instructions and guide you through each task before the ultrasound images are taken.

The ultrasound assessment involves three different probes:

1. **The first probe (curvilinear)** will be covered with a condom and gel and placed over your genital area (perineum). This probe is not inserted into your vagina—it simply rests against your skin.
2. **The second part of the assessment** involves a small intravaginal device, similar to a tampon, which will be inserted approximately 2–3 cm into the vagina. Then, the **second probe (endovaginal)** will be placed just behind the device, about 0.5 cm into the vaginal opening.
3. ***The final probe (linear)*** *will again rest against the perineum to assess the dimensions and stiffness of the perineal body.*

Potential harms

There are no known risks associated with any of the testing procedures used in this study, including ultrasound imaging. The post-doctoral fellow will wear gloves at all times and all probes will be covered with a condom. All of our equipment is disinfected after each use according to manufacturer specifications. All sheets, gowns and pillowcases are laundered after each use.

Discomfort

It is possible that you might experience some discomfort with the insertion or removal of the intravaginal device. Please inform the research team if this is the case as we can adjust the amount of lubricant used.

Inconveniences

The laboratory protocol takes around 30 minutes to complete, which might be inconvenient. You will be able to schedule your assessment outside of regular work hours, during the evening or on weekends if you prefer.

Those who suffer from urinary incontinence or other pelvic floor symptoms commonly report embarrassment associated with sharing their symptoms or having us measure how much leakage you experience in the incontinence pad. Our team includes pelvic health physiotherapists who are experts in female pelvic health. We have studied urine leakage and pelvic floor disorders in females for over 18 years. We will always respect your privacy and will strive to make you as comfortable as possible during the study – indeed, through you sharing your symptoms with us, we hope to improve the management of pelvic floor symptoms so that females do not have to feel embarrassed.

In the event of any research-related injury you will be referred to your regular health care provider to receive appropriate medical treatment/care through your provincial health plan. If urgent care is required while you are in the Motor Function Measurement Lab, we will contact University of Ottawa Campus security, and you will be escorted by the research staff to the Emergency Department of a local hospital to receive care. You are not waiving your legal rights by agreeing to participate in this study.

Benefits

Participation in this study will allow you to learn about the pelvic floor muscles. Moreover, you help us to understand more about pelvic floor morphology, how to assess it and how it is related to symptoms, further improving female pelvic floor research.

Relevant experience working with this population or topic

Our laboratory personnel have tremendous expertise and experience evaluating pelvic floor muscle structure and function in women and are well trained in the use and safety of all methods described above. Dr. Linda McLean, the principal investigator of this research, has been working for over 20 years to promote and to improve women's health particularly as it relates to urinary incontinence. She supervises a multidisciplinary team of students, staff, and collaborators from varied backgrounds, who work together in women's pelvic health research. Dr. Vesting, the postdoctoral fellow, is a physiotherapist with 9 years of clinical and research experience working with females who experience pelvic floor dysfunction. She has trained to perform all assessments described above.

Compensation

Your participation is voluntary, and you will not be paid for it.

Withdrawal from the Study

You have the right to withdraw your participation from this study at any time and without providing any reason. If you choose to withdraw from the study, any data provided to that point will be destroyed unless you explicitly provide the research team permission to use the data collected up to the point of your withdrawal.

Confidentiality

You will not be identifiable in any publications or presentations resulting from this study. No identifying information will leave the University of Ottawa. There will be one password protected electronic file, stored on the encrypted University of Ottawa drive (Sharepoint), that links your name to your participant number. This file will only be accessible by Dr. McLean and her staff and students at The University of Ottawa who have all been instructed on proper procedures for protecting privacy and confidentiality and who have provided signed confidentiality agreements. All electronic records will be stored in a secure database at the University of Ottawa and will be protected by a user password, only accessible by Dr. McLean and her students and staff. These records will not include your name or other identifying information. All paper records will be stored in a filing cabinet within the Motor Function Measurement Lab, which is a restricted access area. All files will be kept for a period of 10 years after the study has been completed. At the end of the retention period, all paper records will be shredded, and all electronic records will be permanently deleted from the data server.

Participant Rights

Your participation in this study is voluntary. You may withdraw from this study at any time and without consequences. If you were referred to the study by a health care provider, the provider will not know whether you ultimately decided to participate or not, and this decision will in no way affect the care you receive. You are free to refuse to undergo any aspect of the testing, without giving any reason. The researchers may withdraw you from the study for scientific reasons at any time. In this case, they would give you a clear and valid reason. You have the right to obtain copies of any study forms that contain your personal information. As a participant in this study, you have the right

to an environment that you feel comfortable in. For your safety and for the safety of our team, we will have a third person (female research assistant) present in the evaluation room during all assessment procedures. You may also bring a friend or family member with you to be present in the room if this makes you feel more comfortable.

If at any time, you have further questions or problems, you can contact the study investigators:

Linda McLean, PhD at 613-562-5800 ex 2544 or linda.mclean@uottawa.ca or Sabine Vesting, PT, Postdoctoral fellow at 613-562-5800 ex 7978 or svesting@uottawa.ca.

If you have any questions about this study or if you feel that you have experienced a research-related injury, please contact Dr. Linda McLean at your earliest convenience.

The University of Ottawa Sciences and Health Sciences Research Ethics Board has reviewed this protocol and has found it to comply with standards for ethical aspects of research studies involving human participants at The University of Ottawa. If you have any questions about your rights as a research participant, you may contact the Protocol Officer for Ethics in Research at the University of Ottawa at 613-562-5800 ext. 5387 or ethics@uottawa.ca

Consent to Participate in Research Title of Study: The assessment of perineal body morphology in females: An inter-rater reliability and correlation study

I understand that I am being asked to participate in a research study and that my participation is voluntary. This study protocol has been explained to me by a member of the research team listed on the first page of this document.

I have read this 5 -page Participant Information Sheet and Consent Form or have had this document read to me. All my questions have been answered to my satisfaction. If I decide at a later stage in the study that I would like to withdraw my consent, I may do so at any time.

I voluntarily agree to participate, in the assessment part, in this study.

A copy of the Participant Information Sheet and the signed Consent Form will be provided to me for my records.

Signatures

_____

Participant's Name (Please Print)

_____ _____

Participant's Signature Date

Investigator Statement (or Person Explaining the Consent)

I have carefully explained to the research participant the nature of the above research study. To the best of my knowledge, the research participant signing this consent form understands the nature, demands, risks and benefits involved in participating in this study. I acknowledge my responsibility for the care and well-being of the above research participant, to respect the rights and wishes of the research participant, and to conduct the study according to applicable Good Clinical Practice guidelines and regulations.

_____

Name of Investigator/Delegate (Please Print)

_____ _____

Investigator's Signature Date

8.3. Appendix C — Participant Questionnaire

Participant Demographic & Obstetric History Form

☐ I have read the letter of information, had the opportunity to ask questions, and I consent to participating

Participant ID: _____

Date: ___ / ___ / _____

1. Basic Demographic Information

- **Age:** _____ years
- **Height:** _____ cm
- **Weight:** _____ kg
- **Ethnicity (please select one or more):**
    - White / Caucasian
    - Black / African / Caribbean
    - East Asian (e.g., Chinese, Japanese, Korean)
    - South Asian (e.g., Indian, Pakistani, Bangladeshi)
    - Southeast Asian (e.g., Filipino, Vietnamese, Thai)
    - Indigenous / First Nations / Métis / Inuit
    - Middle Eastern / North African
    - Latin American / Hispanic
    - Mixed ethnicity
    - Other: _____
    - Prefer not to answer

2. Reproductive and Menstrual History

- **Are you menstruating?**
    - Yes
    - No
    - Irregular
    - Not applicable (e.g., postmenopausal)
- **Menopausal status:**
    - Premenopausal
    - Perimenopausal
    - Postmenopausal
    - Unsure

3. Obstetric History

- **Number of births (parity):** _____
- **Multiple pregnancies (e.g., twins):**
    - Yes
    - No

Most recent delivery:

- **Date:** ___ / ___ / _____
- **Mode of deliveries:**
    - Spontaneous vaginal delivery (number: _____)
    - Assisted vaginal delivery (forceps/vacuum) (number: _____)
    - Planned caesarean section (number: _____)
    - Emergency caesarean section (number: _____)
- **Birthweight of most recent infant:** _____ g
- **Perineal tearing during vaginal deliveries:**
    - None
    - 1st degree
    - 2nd degree
    - 3rd degree
    - 4th degree
    - Episiotomy
    - Unknown
- **Time since last delivery:** _____ weeks / months

4. Additional Health Information

- **Pelvic floor symptoms (check all that apply):**
    - Urinary incontinence
    - Fecal incontinence
    - Pelvic organ prolapse symptoms (e.g., bulging, vaginal heaviness)
    - Constipation
    - None
    - Other: _____
- **Relevant medical conditions (if any):** _____

8.4. Appendix D — Detailed Offline SWE Post-Processing Workflow

This appendix provides the operational implementation of the four-stage SWE post-processing pipeline, summarized conceptually in the Image Analysis section. It is intended to support computational reproducibility; the methodological rationale for each step is given in the main text and is not repeated here. The pipeline was executed through a single MATLAB launcher (SWE_ElastoGUI_Launcher, version March 2025; MathWorks, Natick, MA, USA), which ran the ensemble generator and then passed its outputs automatically into ElastoGUI.

Stage 0 — Acquisition Conditions and Pre-Export Calibration

SWE clips were acquired over the perineum with the SL15-4 linear probe (General preset) under a generous gel layer. For each clip, a reference frame was selected (temporally central frame when quality was uniform; otherwise, the frame with the most complete fill, most homogeneous colour distribution, and no motion banding). The peak Young's Modulus within the PC was read from the Q-box tool; the Aixplorer display range was set to that peak + 15 kPa; and elastogram opacity was set to 100%. Each per-trial display-range value was recorded in the data log against participant ID, session, posture, and imaging plane, for later entry as the ElastoGUI saturation value (Stages 2 and 3). Clips were then exported in DICOM format, each as a multi-frame array co-registering the B-mode image and the superimposed colour elastogram.

Stage 1 — Temporal Ensemble Generation (SWE_Ensemble_Folder_Generator)

File handling. DICOM files were selected through a file dialogue (multi-select supported), and an output directory was chosen. For each input file, a subfolder named after the source file was created to hold its outputs.

Stack reading. The DICOM array and its metadata header were read (dicominfo, dicomread) and squeezed to a four-dimensional matrix of the form rows × columns × 3 (RGB) × frames.

Frame-window selection. For multi-frame stacks, an interactive figure displayed the stack with a slider (ui_select_frame). The assessor scrolled to the desired start frame n; the on-screen label reported the active window as frames n to n + 9. The processing window was fixed at frames n through min(n + 9, numFrames), so that the window never

exceeded the recording length. Single-frame files defaulted to one frame. Selection criteria (temporal colour-pattern consistency; absence of banding, flicker, or motion) are given in Section 3.4.3.

Elastogram bounding box. On the reference frame, the assessor positioned a rectangular bounding box (ui_get_right_box) over the elastogram panel, excluding the B-mode region and the colour-scale bar. The box was initialized at the right side of the image (≈60% width, ≈20% height, 200 × 200 px), adjusted manually, and confirmed with ENTER. Its coordinates (x, y, width, height) defined the pixel ranges xRange = x : min(x + w, width) and yRange = y : min(y + h, height).

Ensemble computation. Within the bounding box, the selected frames were stacked into a double-precision array of dimensions (rows × columns × 3 RGB channels × frames). The three-channel (RGB) elastogram was processed channel-wise: per-pixel statistics were computed across frames along the temporal (fourth) dimension, independently for each RGB channel, and obtained in double precision before being quantized back to 8-bit unsigned integers (median(roiStack, 4) and mean(roiStack, 4), each cast to uint8). Each ensemble was written back into a copy of the reference frame at the bounding-box location, yielding a full-size ensemble median colour map and a full-size ensemble averaged colour map.

Output. For each input file, four outputs were saved to its subfolder: [file]_Median.tif, [file]_Mean.tif, [file]_Median.dcm, and [file]_Mean.dcm. Each DICOM output (save_as_dicom) copied the original header with NumberOfFrames reset to 1, InstanceNumber incremented by 1000, and ImageComments set to “Generated [Median/Mean] SWE Heatmap (10-frame)”, preserving an auditable link to the source recording. A dual preview (show_dual_preview) displayed the ensemble median colour map and ensemble averaged colour map side by side for inspection before the assessor clicked CLOSE & CONTINUE. All ensemble DICOM paths were collected and passed automatically to ElastoGUI.

Stage 2 — Sequential Quality-Control Gates

The three gates below were applied uniformly to 100% of the ROI metrics from session A1, in order, before any statistical analysis. Rationale and threshold provenance are given in Section 3.4

Gate 1 — Elastogram Fill: exclude if Void (%) > 20% within the ROI.

Gate 2 — Ceiling Artifact: exclude if Saturated (%) > 5% within the ROI.

Gate 3 — Spatial Heterogeneity: flag for secondary visual review if IQR/Median > 30% (kPa) or > 15% (m/s); not an automatic exclusion.

A trial-attrition table was generated reporting the number and proportion of trials excluded at each gate, stratified by posture (supine, standing, deep squat) and imaging plane (sagittal superficial, sagittal deep, transverse).

Stage 3 — ROI-Based Stiffness Extraction (ElastoGUI)

Import. ElastoGUI launched with the Stage 1 ensemble files already imported.

Saturation value. In the File Properties table (bottom-left), the per-trial saturation value — the maximum probe scale value used at export, i.e. [Peak + 15 kPa] — was entered for each file. This value calibrates the linear RGB-to-stiffness mapping (blue anchor = 0 kPa; red anchor = entered saturation value) and was verified against the data log before analysis.

ROI tool. The propagating (green) polygon tool was selected so that one ROI geometry applied identically to all loaded files (ensemble median colour map and ensemble averaged colour map simultaneously), eliminating inter-file delineation variability; the current-file-only (red) tool was reserved for exceptions.

ROI delineation. The polygon was drawn inside the elastogram (Q-box) heatmap; a mirrored cursor on the co-registered B-mode image aided anatomical placement. The polygon was snapped closed, adjusted as needed, and saved by double-clicking the boundary (right-click opened a vertex-editing menu). In the sagittal plane, two ROIs were drawn on the ensemble median colour map — a superficial ROI at the base of the triangular PC and a deep ROI at its apex. In the transverse plane, a single ROI followed the hyperechoic band superior to the external anal sphincter, bounded laterally by the sphincter diameter. Void regions corresponding to the anal and vaginal canals were excluded from all polygons.

Calculation and output. Analysis was run on the current file, a range (From/To), or all files. For each ROI, ElastoGUI returned, in the results panel: Void (%) (proportion of ROI pixels with no valid signal), Saturated (%) (proportion reaching the scale

maximum), and the Max, Mean, Median, IQR, and SD of Young's Modulus (kPa) and shear wave velocity (m/s). All variables were exported to an Excel file for Stage 3 gating.

8.5. Appendix E — Supplementary Material

Table S1. Full trial attrition by rater × condition (all conditions).

Rater	Posture	Plane – zone	Total	Valid (n)	Valid %	Not traced %	Excluded %
A 1st	Deep squat	Sagittal – deep	81	54	66.7	22.2	11.1
		Sagittal – superficial	81	74	91.4	0	8.6
		Transverse – central	81	71	87.7	3.7	8.6
A 1st	Standing	Sagittal – deep	81	30	37.0	58.0	4.9
		Sagittal – superficial	81	81	100	0	0
		Transverse – central	81	75	92.6	0	7.4
A 1st	Supine	Sagittal – deep	81	46	56.8	42.0	1.2
		Sagittal – superficial	81	81	100	0	0
		Transverse – central	81	78	96.3	0	3.7
A 2nd	Deep squat	Sagittal – deep	81	57	70.4	18.5	11.1
		Sagittal – superficial	81	74	91.4	0	8.6
		Transverse – central	81	71	87.7	3.7	8.6
A 2nd	Standing	Sagittal – deep	81	35	43.2	51.9	4.9
		Sagittal – superficial	81	81	100	0	0
		Transverse – central	81	75	92.6	0	7.4
A 2nd	Supine	Sagittal – deep	81	55	67.9	30.9	1.2
		Sagittal – superficial	81	81	100	0	0
		Transverse – central	81	78	96.3	0	3.7
B 1st	Deep squat	Sagittal – deep	81	58	71.6	17.3	11.1
		Sagittal – superficial	81	74	91.4	0	8.6
		Transverse – central	81	71	87.7	3.7	8.6
B 1st	Standing	Sagittal – deep	81	58	71.6	23.5	4.9
		Sagittal – superficial	81	81	100	0	0
		Transverse – central	81	75	92.6	0	7.4
B 1st	Supine	Sagittal – deep	81	64	79.0	19.8	1.2
		Sagittal – superficial	81	81	100	0	0

	Transverse – central	81	78	96.3	0	3.7

Total = 27 participants × 3 trials = 81 expected trials per cell. Not traced = ROI not delineable (NA). Excluded = failed quality-control gate (void%/saturation).

Table S2. Agreement Regarding the Region of Interest Traceability in the Deep Zone of the Perineal Complex (Cohen's κ; 229 paired trials).

Comparison	Agreement (%)	Cohen's κ	Interpretation
Intra (A1 vs A2)	88.2	0.755	Substantial
Inter (A1 vs B1)	69.4	0.337	Fair

Each deep-zone trial was scored as traceable (1) versus not traceable/NA (0), paired by participant × posture × trial. NA, not available; κ, Cohen's kappa.

Table S3. Per-Posture Concordance for the Region of Interest Traceability of the Deep Zone of the Perineal Complex

Comparison	Posture	n	Concordant	Agreement %
Intra (A1 vs A2)	Supine	80	65	81.2
	Standing	77	72	93.5
	Deep squat	72	65	90.3
Inter (A1 vs B1)	Supine	80	52	65.0
	Standing	77	49	63.6
	Deep squat	72	58	80.6

Each deep-zone trial was scored as traceable versus not traceable, with not-traced/NA/excluded trials retained (a trial absent from one rater's or session's file was treated as not traceable). Trials were paired by participant × trial within each posture. n = paired trials contributing to each comparison; concordant = trials scored identically across raters (inter) or sessions (intra); agreement (%) = concordant / n. NA, not available.

Table S4. Intra-Rater Reliability of Ensemble-Average Colour Map of Shear Wave Velocity (m/s).

Posture	Plane – zone	n	ICC [95% CI]	Interp.	SEM	MDD_{95}
Supine	Sagittal – superficial	27	0.977 [0.951, 0.990]	Excellent	0.084	0.233
	Sagittal – deep	16	0.971 [0.920, 0.990]	Excellent	0.236	0.654
	Transverse – central	27	0.978 [0.952, 0.990]	Excellent	0.062	0.171
Standing	Sagittal – superficial	27	0.992 [0.983, 0.996]	Excellent	0.048	0.133
	Sagittal – deep	12	0.991 [0.969, 0.997]	Excellent	0.120	0.333
	Transverse – central	26	0.970 [0.935, 0.986]	Excellent	0.099	0.275
Deep squat	Sagittal – superficial	27	0.983 [0.963, 0.992]	Excellent	0.107	0.296
	Sagittal – deep	23	0.984 [0.963, 0.993]	Excellent	0.175	0.484
	Transverse – central	26	0.993 [0.983, 0.997]	Excellent	0.063	0.173

Values are derived from the ensemble average colour map of the mean shear wave velocity (m/s). Complete-case analysis per posture and zone; n denotes the number of participants with paired valid measurements. Reliability labels follow Koo & Li (2016): Poor (< 0.50), Moderate (0.50–0.75), Good (0.75–0.90), Excellent (≥ 0.90). ICC, intraclass correlation coefficient; CI, confidence interval; SEM, standard error of measurement; MDD_{95}, minimal detectable difference at 95% confidence.

Table S5. Inter-Rater Reliability of the Ensemble-Averaged Colour Map of Shear Wave Velocity (m/s)

Posture	Plane – zone	n	ICC [95% CI]	Interp.	SEM	MDD_{95}
Supine	Sagittal – superficial	27	0.960 [0.850, 0.985]	Excellent	0.095	0.263
	Sagittal – deep	17	0.861 [0.657, 0.947]	Good	0.492	1.364
	Transverse – central	27	0.977 [0.937, 0.991]	Excellent	0.056	0.154
Standing	Sagittal – superficial	27	0.957 [0.866, 0.983]	Excellent	0.102	0.284
	Sagittal – deep	12	0.859 [0.585, 0.957]	Good	0.427	1.185
	Transverse – central	26	0.978 [0.952, 0.990]	Excellent	0.084	0.233
Deep squat	Sagittal – superficial	27	0.967 [0.919, 0.986]	Excellent	0.148	0.411
	Sagittal – deep	22	0.867 [0.707, 0.943]	Good	0.479	1.329
	Transverse – central	26	0.993 [0.984, 0.997]	Excellent	0.063	0.175

Values are derived from the ensemble average colour map of the mean shear wave velocity (m/s). Complete-case analysis per posture and zone; n denotes the number of participants with paired valid measurements. Reliability labels follow Koo & Li (2016): Poor (< 0.50), Moderate (0.50–0.75), Good (0.75–0.90), Excellent (≥ 0.90). ICC, intraclass correlation coefficient; CI, confidence interval; SEM, standard error of measurement; MDD_{95}, minimal detectable difference at 95% confidence.

Table S6. Parametric Versus Non-Parametric 95% Limits of Agreement for Median Shear Wave Velocity (m/s).

Posture	Zone	Intra-rater				Inter-rater			
		n	Bias (m/s)	Parametric 95% LoA (bias ± 1.96 SD)	Non-parametric 95% LoA (2.5th–97.5th pct)	n	Bias (m/s)	Parametric 95% LoA (bias ± 1.96 SD)	Non-parametric 95% LoA (2.5th–97.5th pct)
Supine	Sagittal superficial	27	-0.02	-0.25, 0.20 [a]	-0.30, 0.12	27	0.1	-0.21, 0.41 [a]	-0.08, 0.46
	Sagittal deep	16	0.11	-0.50, 0.72 [a]	-0.39, 0.72	17	0.11	-1.17, 1.38 [a]	-0.79, 1.63
	Transverse	27	-0.05	-0.26, 0.16	-0.26, 0.14	27	0.05	-0.13, 0.23	-0.17, 0.20
Standing	Sagittal superficial	27	0.01	-0.17, 0.18	-0.17, 0.13	27	0.07	-0.22, 0.37	-0.21, 0.35
	Sagittal deep	12	0.07	-0.20, 0.35	-0.10, 0.35	12	-0.25	-1.45, 0.95 [a]	-1.65, 0.26
	Transverse	26	-0.09	-0.33, 0.14 [a]	-0.37, 0.06	26	0.02	-0.19, 0.23	-0.16, 0.24
Deep squat	Sagittal superficial	27	0.08	-0.22, 0.38 [a]	-0.05, 0.47	27	0.09	-0.19, 0.36	-0.18, 0.32
	Sagittal deep	23	0.02	-0.55, 0.59 [a]	-0.66, 0.40	22	-0.06	-1.38, 1.26 [a]	-1.52, 0.99
	Transverse	26	0.02	-0.21, 0.25 [a]	-0.17, 0.26	26	0.03	-0.19, 0.25 [a]	-0.12, 0.30

LoA are presented for median shear wave velocity. Bias is the mean paired within-rater (intra) or between-rater (inter) difference. Parametric LoA are bias ± 1.96 SD of the differences; non-parametric LoA are the empirical 2.5th and 97.5th percentiles of the same differences. n = participants with paired ratings (complete-case) and differs between columns where the number of extractable trials differed. [a] indicates non-normal differences (Shapiro–Wilk $p < 0.05$).
LoA, limits of agreement; SD, standard deviation.

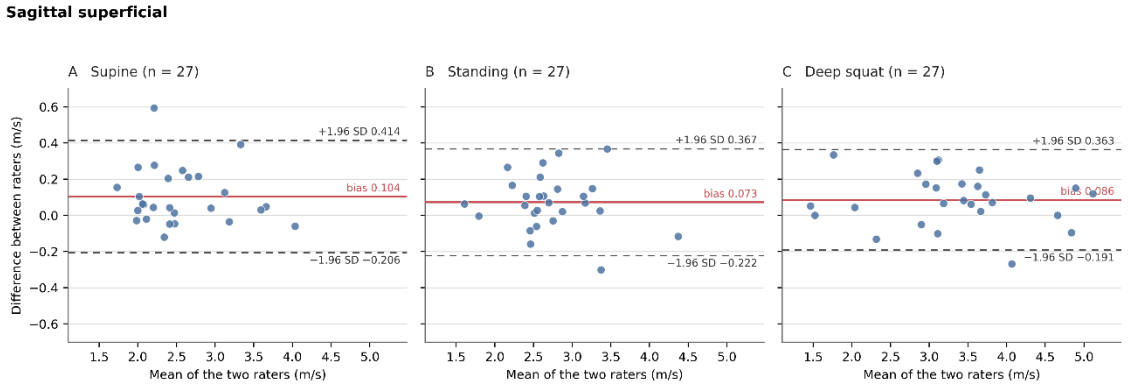


Figure S 1. Bland–Altman plots representing the inter-rater agreement for the median shear wave velocity (m/s) of the perineal complex imaged in the sagittal plane at the superficial region of interest, with the participant in (A) supine (n = 27; bias +0.104 m/s; 95% limits of agreement −0.206 to +0.414 m/s), (B) standing (n = 27; bias +0.073 m/s; 95% limits of agreement −0.222 to +0.368 m/s) and (C) a deep squat (n = 27; bias +0.086 m/s; 95% limits of agreement −0.191 to +0.363 m/s). Solid line = bias; dashed lines = 95% limits of agreement. All three panels share a common vertical and horizontal scale.

Sagittal deep

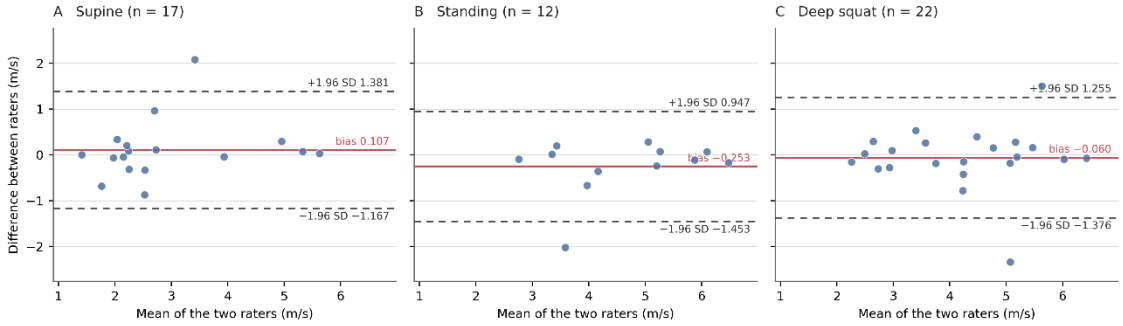


Figure S 2. Bland–Altman plots representing the inter-rater agreement for the median shear wave velocity (m/s) of the perineal complex imaged in the sagittal plane at the deep region of interest, with the participant in (A) supine (n = 17; bias +0.107 m/s; 95% limits of agreement −1.167 to +1.381 m/s), (B) standing (n = 12; bias −0.253 m/s; 95% limits of agreement −1.453 to +0.947 m/s) and (C) a deep squat (n = 22; bias −0.060 m/s; 95% limits of agreement −1.376 to +1.255 m/s). Solid line = bias; dashed lines = 95% limits of agreement. All three panels share a common vertical and horizontal scale. The estimate obtained in standing is based on a low effective sample size (n = 12).

Transverse

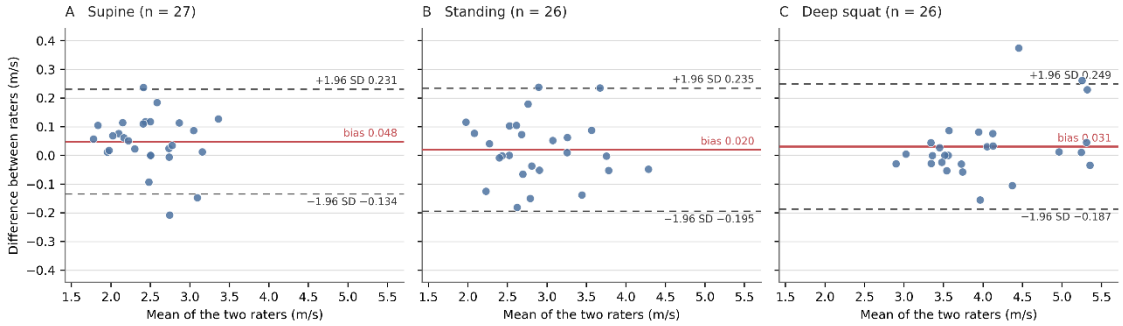


Figure S 3. Bland–Altman plots representing the inter-rater agreement for the median shear wave velocity (m/s) of the perineal complex imaged in the transverse plane, with the participant in (A) supine (n = 27; bias +0.048 m/s; 95% limits of agreement −0.134 to +0.231 m/s), (B) standing (n = 26; bias +0.020 m/s; 95% limits of agreement −0.195 to +0.235 m/s) and (C) a deep squat (n = 26; bias +0.031 m/s; 95% limits of agreement −0.187 to +0.249 m/s). Solid line = bias; dashed lines = 95% limits of agreement. All three panels share a common vertical and horizontal scale.